Fall 2020

TUNING SURFACE PROPERTIES OF TITANIUM DIOXIDE FOR CARBON MONOXIDE OXIDATION OVER COPPER-TITANIUM DIOXIDE

Guoqiang Cao
University of New Hampshire, Durham

TUNING SURFACE PROPERTIES OF TITANIUM DIOXIDE FOR CARBON MONOXIDE OXIDATION OVER COPPER-TITANIUM DIOXIDE

BY

GUOQIANG CAO

Baccalaureate Degree, Mineral Processing Engineering,
China University of Mining and Technology, Beijing, China, 2012
Master of Science, Mineral Processing Engineering,
China University of Mining and Technology, Beijing, China, 2015

DISSERTATION

Submitted to the University of New Hampshire
in Partial Fulfillment of the Requirements for the Degree of

Doctor of Philosophy

in

Chemical Engineering

September, 2020

This dissertation has been examined and approved in partial fulfillment of the requirements for the degree of Doctor of Philosophy in Chemical Engineering by:

Dissertation Director, Dr. Nan Yi
Assistant Professor of Chemical Engineering, UNH

Dr. Xiaowei Teng
Professor and Chair of Chemical Engineering, UNH

Dr. Nivedita Gupta
Professor of Chemical Engineering, UNH

Dr. Young Jo Kim
Assistant Professor of Chemical Engineering, UNH

Dr. Gonghu Li
Professor of Chemistry, UNH

On

July 24th, 2020

Original approval signatures are on file with the University of New Hampshire Graduate School.

TABLE OF COTENT

ACKNOWLEDGMENTS ..... **vii**

LIST OF TABLES ..... **ix**

LIST OF FIGURES ..... **x**

ABSTRACT ..... **xiv**

CHAPTER 1 INTRODUCTION **1**

1.1 CARBON MONOXIDE OXIDATION 1

1.2 CATALYSTS 4

1.2.1 METAL CATALYSTS 4

1.2.2 SUPPORTED METAL CATALYSTS 8

1.2.3 COPPER-METAL OXIDES 16

1.3 MECHANISM AND KINETICS 20

1.3.1 MECHANISM 20

1.3.2 KINETICS 22

1.4 RATIONALES AND OBJECTIVES 25

CHAPTER 2 EXPERIMENTAL METHODS **27**

2.1 SYNTHESIS OF CATALYSTS 27

2.1.1 SYNTHESIS OF Cu-TiO_2 CATALYSTS WITH INEQUAL HYDROXYL GROUPS 28

2.1.2 SYNTHESIS OF Cu-N-TiO_2 CATALYSTS WITH VARIOUS PHASES 29

2.1.3 SYNTHESIS OF Cu-TiO_2 CATALYSTS WITH DIFFERENT CALCINATION GAS 30
2.2 CATALYSTS CHARACTERIZATIONS 30
2.2.1 INDUCTIVELY COUPLED PLASMA ATOMIC EMISSION SPECTROSCOPY (ICP-AES) 30
2.2.2 X-RAY POWDER DIFFRACTION (XRD) 31
2.2.3 BRUNAUER-EMMETT-TELLER SURFACE AREA (BET) 31
2.2.4 LASER RAMAN SPECTROSCOPY (RAMAN) 31
2.2.5 COPPER DISPERSION 32
2.2.6 TEMPERATURE PROGRAMMED SURFACE REACTION (TPR & TPSR) 33
2.2.7 X-RAY PHOTOELECTRON SPECTROSCOPY (XPS) 34
2.2.8 IN-SITU DIFFUSE REFLECTANCE INFRARED FOURIER TRANSFORM SPECTROSCOPY (IN-SITU DRIFTS) 35
2.3 CATALYTIC PERFORMANCE 35

CHAPTER 3 EFFECT OF HYDROXYL GROUPS ON CARBON MONOXIDE OXIDATION OVER COPPER-TITANIUM DIOXIDE CATALYSTS 37

3.1 INTRODUCTION 37
3.2 CARBON MONOXIDE OXIDATION ACTIVITY OVER Cu-TiO_2 CATALYSTS 39
3.3 CHARACTERIZATION OF Cu-TiO_2 CATALYSTS 43
3.3.1 PHYSICAL PROPERTIES 43
3.3.2 REDOX BEHAVIOURS 45
3.3.3 CHEMICAL STATES ANALYSIS 48
3.3.4 IN-SITU DRIFTS 51

3.4 SUMMARY 53

CHAPTER 4 EFFECT OF PRETREATMENT ON COPPER-TITANIUM DIOXIDE CATALYZED CARBON MONOXIDE OXIDATION 55

4.1 INTRODUCTION 55

4.2 CARBON MONOXIDE OXIDATION ACTIVITY OVER Cu-TiO_2 CATALYSTS CALCINED IN DIFFERENT GAS ATMOSPHERE 56

4.3 CHARACTERIZATION OF PRETREATED Cu-TiO_2 CATALYSTS 58

4.3.1 PHYSICAL PROPERTIES 58

4.3.2 REDOX BEHAVIOURS 59

4.3.3 CHEMICAL STATES ANALYSIS 61

4.3.4 IN-SITU DRIFTS 65

4.4 SUMMARY 66

CHAPTER 5 EFFECT OF NITROGEN DOPING ON CARBON MONOXIDE OXIDATION OVER COPPER-TITANIUM DIOXIDE CATALYSTS 68

5.1 INTRODUCTION 68

5.2 CARBON MONOXIDE OXIDATION ACTIVITY OVER Cu-N-TiO_2 CATALYST 70

5.3 CHARACTERIZATION OF Cu-N-TiO_2 CATALYSTS 72

5.3.1 PHYSICAL PROPERTIES 72

5.3.2 CHEMICAL STATES ANALYSIS 74

5.3.3 REDOX PROPORTIES 79

5.3.4 IN-SITU DRIFTS 83

5.4 SUMMARY 84

CHAPTER 6 EFFECT OF TITANIUM DIOXIDE PHASES ON COPPER-NITROGEN-TITANIUM DIOXIDE CATALYZED CARBON MONOXIDE OXIDATION 87

6.1 INTRODUCTION 87

6.2 CARBON MONOXIDE OXIDATION ACTIVITY 89

6.3 CHARACTERIZATION OF Cu-N-TiO_2 CATALYSTS 91

6.3.1 PHYSICAL PROPERTIES 91

6.3.2 CHEMICAL STATES ANALYSIS 94

6.3.3 REDOX PROPORTIES 100

6.3.4 IN-SITU DRIFTS 105

6.4 SUMMARY 109

CHAPTER 7 CONCLUSIONS AND PERSPECTIVES 111

7.1 CONCLUSIONS 111

7.2 PERSPECTIVES 113

LIST OF REFERENCES 115

ACKNOWLEDGMENTS

This dissertation would not have been possible without the help and support of many people, to whom I would like to give my acknowledgment.

First and foremost, I would like to express my sincere gratitude to my advisor, Prof. Nan Yi, for his patience, his guidance, his continuous scientific and financial support, and endless help on every aspect. I will never forget his invaluable advice and the friendly cooperative atmosphere created by him. It is he, who opened the fascinating academic door of catalysis to me and immensely raised me up to a higher level. His motivation, optimism, and strong execution always inspiring me to devote myself to science career.

I would like to extend my appreciation to my dissertation committee: Prof. Xiaowei Teng, Prof. Nivedita Gupta, Prof. Young Jo Kim, and Prof. Gonghu Li for sharing their knowledge, providing their invaluable support and dedication on this dissertation.

I am very grateful to John Newell and Darcy Fournier. The majority of my experiments could not be accomplished smoothly without their tremendous support. By attributing to John's strong manufacturing skills, he helped me build the first thermal reaction system in our lab and provided countless consultations regarding troubleshooting on other instruments. Darcy is full of enthusiasm and always willing to giving me a hand. She helped me build our second thermal reaction system and new photocatalysis reaction system. Moreover, a newly designed and highly integrated gas supplier was created to support two reaction systems simultaneously with her help.

I would like to thank Mengyao Ouyang at Tufts University for performing the ICP-AES tests, which were of great help to my dissertation. I also appreciate Zhen Tian for training me to carry out the Raman Spectroscopy experiments. Special thanks to Willian T Paterson at the Connors Writing Center of UNH for helping me the improve dissertation's writing. Many thanks to Center

for Nanoscale Systems at Harvard University for providing the fantastic platform that allowed me to conduct XRD, XPS and TEM studies which gave a deep insight into the nature my catalysts.

Funding and fellowships for my research projects provided by Department of Chemical Engineering (Teaching Assistantship), the Graduate School (Summer Teaching Assistant Fellowship and Graduate Student Travel Grants) are greatly acknowledged.

Special thanks to my friends, group members and roommates for being part of my life at UNH. I am thankful for the time spent with them that enriched my time at UNH and made my life full of variety.

I also express earnest gratitude to my parents and my wife. My parents gave me unconditionally support as much as they could, to let me be myself, make my own decisions and pursue my dream firmly. Most of all, I appreciate the support of my beloved, patient wife. Her unwavering encouragement, innumerable sacrifices promoted me to be a better self for my family. Without her continuous support behind me, I will not be possible to be here.

Last but not least, to the end of my student life, I would also like to thank the one who kept working hard and never gave up. It has been 15 years since I left home to chase my dream at the age of 15. This long journey is always full of hardships, uncertainty, and challenge. I am lucky enough to be in this place. It is the time to start a new journey to explore more possibilities.

At the end, in such an extraordinary period of COVID-19 pandemic, it is extremely stressful, and we all are experiencing a number of unpredictable conditions. I would like to sincerely wish all the best to everyone. I believe we will eventually overcome it and meet a bright future.

LIST OF TABLES

Table 3.1 BET surface area and copper concentration of Cu-TiO_2 samples..... 44

Table 3.2 Analysis of hydrogen-temperature programmed reduction (H_2-TPR)..... 46

Table 3.3 Analysis of carbon monoxide-temperature programmed surface reaction. 47

Table 3.4 Surface copper concentration and composition based on XPS results. 48

Table 4.1 BET surface area and Cu concentration of Cu-TiO_2 catalysts..... 58

Table 4.2 Analysis of hydrogen-temperature programmed reduction (H_2-TPR)..... 60

Table 4.3 XPS results analysis of Cu-TiO_2 catalysts. 62

Table 5.1 Physical properties of Cu-N-TiO_2 and Cu-TiO_2 catalysts..... 73

Table 5.2 XPS results analysis of Cu-N-TiO_2 and Cu-TiO_2 catalysts. 74

Table 5.3 H_2-TPR deconvolution analysis and H_2 consumption. 80

Table 6.1 Physical properties of Cu-N-TiO_2 and Cu-TiO_2 catalysts..... 91

Table 6.2 H_2-TPR deconvolution analysis and H_2 consumption results..... 101

LIST OF FIGURES

Figure 1.1 Mechanism of CO oxidation on Au/CeO_2 catalysts [49]. 9

Figure 1.2 Crystalline structures of TiO_2 in different phases: (a) anatase, (b) rutile, (c) brookite. [69]..... 13

Figure 1.3 A model of a supported metal particle, illustrating the effects of metal support interfacial interactions [79]..... 15

Figure 1.4 Three main reaction mechanisms: (a) Langmuir-Hinshelwood, (b) Eley-Rideal, and (c) Mars-van-Krevelen [107]..... 20

Figure 2.1 Typical synthetic pathway of copper modified titanium dioxide (Cu-TiO_2) catalysts. 29

Figure 3.1 Light-off curves of Cu-TiO_2 samples. Test condition: 1%CO/20%O_2/ Helium, flow rate 30 mL/min. 39

Figure 3.2 Arrhenius plot of activation energy of CO oxidation over Cu-TiO_2 catalysts. 41

Figure 3.3 Cyclic light-off curves of Cu-TiO_2-pH7 and Cu-TiO_2-pH14 (three trials for each sample)..... 42

Figure 3.4 XRD patterns of Cu-TiO_2-pH7, Cu-TiO_2-pH9, and Cu-TiO_2-pH14..... 43

Figure 3.5 (a) Hydrogen-temperature programmed reduction (H_2-TPR) profiles and (b) carbon monoxide-temperature programmed surface reaction (CO-TPSR) profiles for Cu-TiO_2-pH7/ Cu-TiO_2-pH9/ Cu-TiO_2-pH14..... 45

Figure 3.6 Cu XPS profiles for (a) Cu-TiO_2-pH14, (b) Cu-TiO_2-pH9, (c) Cu-TiO_2-pH7..... 49

Figure 3.7 Oxygen XPS profiles for (a) Cu-TiO_2-pH14, (b) Cu-TiO_2-pH9, (c) Cu-TiO_2-pH7... 50

Figure 3.8 In-situ DRIFTS profiles for (a) Cu-TiO_2-pH7 and (b) Cu-TiO_2-pH14. Test conditions: 10%CO/Helium. 51

Figure 4.1 Catalytic performance of pretreated Cu-TiO_2 catalysts in carbon monoxide oxidation. (a) Light-off curves, (b) Arrhenius plots, Test condition: 1%CO/20%O_2/ Helium, flow rate 30 mL/min. 56

Figure 4.2 H_2-TPR profiles of (a) Cu-TiO_2-H_2, (b) Cu-TiO_2-O_2, and (c) Cu-TiO_2-He catalysts. 59

Figure 4.3 XPS spectra of Cu 2p of (a) Cu-TiO_2-H_2, (b) Cu-TiO_2-O_2, and (c) Cu-TiO_2-He. 61

Figure 4.4 XPS Ti 2p of (a) Cu-TiO_2-H_2, (b) Cu-TiO_2-O_2, and (c) Cu-TiO_2-He. 63

Figure 4.5 XPS O 1s of (a) Cu-TiO_2-H_2, (b) Cu-TiO_2-He, (c) Cu-TiO_2-O_2. 64

Figure 4.6 In-situ DRIFT of (a) Cu-TiO_2-H_2, (b) Cu-TiO_2-O_2, and (c) Cu-TiO_2-He. Test condition: 1%CO, 20%O_2, balanced in Helium. 65

Figure 5.1 Light-off curves of Cu-N-TiO_2 and Cu-TiO_2 samples. Test condition: 1%CO/20%O_2/Helium, flow rate 30 mL/min. 70

Figure 5.2 Arrhenius plot of activation energy of CO oxidation over Cu-N-TiO_2 and Cu-TiO_2. 71

Figure 5.3 Raman spectra of Cu-N-TiO_2, Cu-TiO_2, N-TiO_2 and TiO_2 supports. 72

Figure 5.4 (a) XPS N 1s spectra over N-TiO_2 support, (b) interstitial nitrogen doping in TiO_2, (c) substitutional nitrogen doping in TiO_2 [165, 166]. 75

Figure 5.5 XPS O 1s spectra of N-TiO_2 support. 76

Figure 5.6 XPS Ti 2p spectra of (a) TiO_2 support and (b) N-TiO_2 support. 77

Figure 5.7 XPS Cu 2p spectra of (a) Cu-N-TiO_2 and (b) Cu-TiO_2. 78

Figure 5.8 Hydrogen-temperature programmed reduction (H_2-TPR) profiles for (a) Cu-N-TiO_2 and (b) Cu-TiO_2 catalysts. 79

Figure 5.9 Carbon monoxide-temperature programmed surface reaction (CO-TPSR) profiles for (a) Cu-N-TiO_2 and (b) Cu-TiO_2 catalysts. 81

Figure 5.10 Oxygen-temperature programmed reaction comparison of N-TiO_2 and TiO_2 supports 82

Figure 5.11 In-situ DRIFTS profiles of (a) Cu-N-TiO_2 and (b) Cu-TiO_2 under reaction conditions. Test condition: 1%CO, 20%O_2, balanced in Helium. 83

Figure 6.1 Catalytic performance of copper-based catalysts in carbon monoxide oxidation. (a) Light-off curves, (b) Arrhenius plots, Test condition: 1%CO/20%O_2/ Helium, flow rate 30 mL/min. 89

Figure 6.2 Raman spectra profiles of different TiO_2 supports and catalysts: (a) TiO_2 (A) based samples, (b) TiO_2 (R) based samples. 93

Figure 6.3 XPS N 1s profiles for (a) N-TiO_2 (A) support, (b) N-TiO_2 (R) support 94

Figure 6.4 XPS Ti 2p profiles of (a) N-TiO_2 (A) support, (b) N-TiO_2 (R) support. 96

Figure 6.5 XPS Cu 2p spectra over (a) Cu-N-TiO_2 (A), (b) Cu-N-TiO_2 (R), (c) Cu-TiO_2 (A), and (d) Cu-TiO_2 (R) 97

Figure 6.6 XPS O 1s spectra over (a) Cu-N-TiO_2 (A), (b) Cu-N-TiO_2 (R), (c) Cu-TiO_2 (A), and (d) Cu-TiO_2 (R) 99

Figure 6.7 H_2-TPR profiles of (a) Cu-TiO_2 (A), (b) Cu-TiO_2 (R), (c) Cu-N-TiO_2 (A), and (d) Cu-N-TiO_2 (R). 100

Figure 6.8 CO-TPSR profiles of (a) Cu-TiO_2 (A), (b) Cu-TiO_2 (R), (c) Cu-N-TiO_2 (A), and (d) Cu-N-TiO_2 (R). 102

Figure 6.9 O_2-TPR profiles of N-TiO_2 supports. 104

Figure 6.10 In-situ DRIFTS profiles over copper-based catalysts: (a) Cu-TiO_2 (A), (b) Cu-TiO_2 (R), (c) Cu-N-TiO_2 (A), and (d) Cu-N-TiO_2 (R), Test condition: 10% CO, balanced in Helium. 105

Figure 6.11 (a) In-situ DRIFTS profiles of anatase TiO_2 based supports and catalysts. Test condition: 10% CO, balanced in Helium; (b) In-situ DRIFTS profiles of N-TiO_2 (A)

tested in different conditions, Test condition: pure Helium and 10% CO, balanced in Helium. 106

Figure 6.12 In-situ DRIFTS profiles of: (a) Cu-TiO_2 (A), (b) Cu-TiO_2 (R), (c) Cu-N-TiO_2 (A), and (d) Cu-N-TiO_2 (R) Test condition: 1% CO, 20% O_2 balanced in Helium..... 108

ABSTRACT

TUNING SURFACE PROPERTIES OF TITANIUM DIOXIDE FOR CARBON MONOXIDE OXIDATION OVER COPPER-TITANIUM DIOXIDE

by

Guoqiang Cao

University of New Hampshire, September 2020

Besides being widely used as a probe reaction, carbon monoxide (CO) oxidation has been playing a crucial role in multiple industrial applications, including automotive emission elimination, chemical production, and abatement of toxic waste. Copper (Cu) based catalysts have been extensively investigated for CO oxidation, because of its low cost and comparable activity to precious metal-based catalysts. Meanwhile, the surface properties, such as the oxidation state of copper species and oxygen species, depend on the synthesis process. Surface properties would eventually impact the catalytic performance. Therefore, it is desirable to build the property-activity relationship to understand factors that can affect the performance of copper-based catalysts for carbon monoxide oxidation.

This dissertation applied different approaches to tune the surface properties of titanium dioxide (TiO_2) and understand how those surface properties affect reaction rate. The first project aimed at investigating the effect of surface hydroxyl groups on Cu-TiO_2 catalysts by adjusting pH values. Our results revealed enhanced catalytic performance could be achieved over Cu-TiO_2-pH7

catalyst, which contained less hydroxyl groups and Cu (I) species on the surface. The ratio between Cu (I) and hydroxyl groups correlated well with activity performance. The second project applied different pretreatment to tune surface properties of Cu-TiO_2 catalysts. Reductive treatment on Cu-TiO_2 improved copper dispersion, thus reinforced its catalytic performance. The third project focused on the impact of introduced nitrogen on the Cu-TiO_2 catalyst. Activity results indicated that the promotion effect existed through the addition of nitrogen to TiO_2 support. Interstitial nitrogen, which was identified as the dominant nitrogen species, contributed to the improved copper dispersion on the surface. The fourth project studied how TiO_2 phases (anatase and rutile) affect the surface properties of Cu-N-TiO_2 catalysts. Anatase TiO_2 facilitated CO oxidation with lower activation energy and higher reaction rate. Characterization results demonstrated the concentration of oxygen vacancies increased with the addition of nitrogen to TiO_2 (anatase).

This dissertation also proposes to consider the spectator species when building the property-activity relationship. As evidenced from four different projects, the consideration of the combined effect of Cu (I) species and surface oxygen species, emphasized the importance of balancing active and spectator species while exploring the catalytic performance.

CHAPTER 1

INTRODUCTION

1.1 CARBON MONOXIDE OXIDATION

Carbon monoxide exists in both natural and artificial environments. In industry, carbon monoxide is formed by the incomplete combustion of carbon-containing compounds when there is not enough oxygen to produce carbon dioxide. The incomplete combustion mainly occurs in transportation (vehicle emissions), power stations, and other industries. Carbon monoxide also plays a role in ground-level zone, which may react with oxygen to produce carbon dioxide and causes destruction of ground-level zone. To eliminate carbon monoxide in the air pollution treatments, oxidation of CO into CO_2 is a most commonly applied method. Despite the toxic and hazardous properties of carbon monoxide, it is valuable for chemical production. In different industrial scales, carbon monoxide is employed to produce chemicals like aldehydes, methanol, hydrocarbons, and hydrogen by hydroformylation, hydrogenation, Fischer-Tropsch process, and water-gas shift reaction, respectively [1].

Studies on CO oxidation reaction play a significant role in fundamentally serving as a probe reaction, practically lowering automotive emissions, and abating gaseous waste in industry.

Fundamentally, the CO oxidation reaction is one of the most extensively investigated probe reactions [2]. As a probe reaction, it could help investigate the course of the reaction and identify how the property of the catalysts affects the reaction [3]. Specifically, CO oxidation has been used as a probe reaction to investigate the surface properties of heterogeneous catalysts [4]. CO molecule is also applied as a probe molecule in spectroscopic study. Spectroscopy is a principle

technique for surface characterization [5]. Therefore, it provides an insight into the relationship between surface properties and catalytic performance. To characterize properties of Pt_1/FeO_x and understand the Pt atom efficiency [8], CO oxidation reaction was employed as a probe reaction to reveal the role of Pt. Results revealed single Pt atoms were isolated anchored to iron oxide surfaces, which provided excellent stability and high activity [6]. In-situ DRIFTS with CO as a probe molecule shown different band position of CO adsorption on Au sites of Au/TiO_2 catalyst [7]. Adsorbed CO helped to identify exposed Au coverage of the Au/TiO_2 catalyst and determined the success of ligand removal treatment [7]. By conducting CO adsorption, CO has also been reported to form stable carbonyls with unsaturated Cu^+, whereas it could not coordinate on Cu^{2+} [8].

Practically, CO oxidation is a critical reaction to reduce the amount of CO in automotive emissions. Automotive exhaust gas, which contains harmful CO, needs to be converted to inert gases by catalytic converters before emission [9]. In most commonly used catalytic converters, platinum group metals impregnated ceramic substrate coating is affirmed as a key part of catalytic converter [10]. Regarding the employed catalysts in catalytic converters, on account of the expensive cost of platinum group metals and deactivation caused by the agglomeration of active and inactive particles, advanced techniques or alternative materials are desired [11-12]. Recently study on single-atom Pt/CeO_2 produced a highly dispersed and thermally stable candidate [11]. This advanced technique could not only reduce the usage of Pt and cost, but also decrease the agglomeration.

Another critical application of CO oxidation is in the fuel cell industry. Fuel cell powered system, as a high fuel efficiency and low environmental impact technique, has arouse great interest [13-15]. Proton exchange membrane fuel cell (PEMFC) fueled with hydrogen is always facing the challenge of CO poison, which comes from the impurity of hydrogen feed [13-16]. Therefore,

preferential oxidation of carbon monoxide (PROX) in H_2 was investigated to eliminate CO poison [17-18]. Selected catalysts have the ability to only promote CO oxidation and stay inert towards H_2 oxidation in the CO/H_2 mixed feedstock. Atomically dispersed $Fe_1(OH)_x$ on silica-supported Pt nanoparticles by atomic layer deposition (ALD) was reported has the ability to remove 100 % CO from the mixture CO and H_2 at the temperature range of -75 to 105 ^oC [17]. Fe doped Cu/CeO_2 catalysts exhibited a 400 hrs stability time for PROX reaction [18]. The incorporation of Fe into CeO_2 lattice generated more oxygen vacancies by forming Fe-O-Ce structure. Along with more oxygen vacancies, it could enhance the interaction between Cu and Ce and release more subsurface lattice oxygen to supply reactive oxygen.

Beyond the previously mentioned application of CO oxidation reaction, CO is also valuable in chemical production. In Fisher-Tropsch process, CO is mixed with hydrogen to produce liquid hydrocarbons. Cobalt-based and iron-based catalysts were reported to highly active towards the F-T process. In the production of light olefins via F-T process, the biggest challenge would be the wide product distribution of hydrocarbons. Only 58 % of C_2-C_4 hydrocarbons were synthesized [19]. Jiao reported a bifunctional catalysts Oxide-Zeolite which could achieve 94 % for C_2-C_4 selectivity [19]. Water gas shift reaction is another important application of CO in industry to produce hydrogen. WGS could also be combined with coal gasification to produce hydrogen and therefore expand the use of coal resources. Gold-ceria catalysts have been recognized as the most active catalysts for WGS since 2003 [20]. Most recent research carried out through in situ characterization and isotopic tracing techniques, suggested that bridged -OH on the surface oxygen vacancies is dominant to the reactivity [21]. Methanol production by CO hydrogenation is also one of the significant CO applications. Studt studied the CO hydrogenation to methanol over Cu-Ni catalysts [22]. Their experimental and DFT results indicated the Cu-Ni catalysts performed a high

activity on CO hydrogenation. This is a comparable performance to the industrially used Cu, ZnO catalysts.

In summary, the oxidation of carbon monoxide plays an important role in fundamental studies and practical applications. On one hand, as a probe reaction provides information about surface properties to get insight into the function of newly developed heterogeneous catalysts. On the other hand, CO oxidation drops the automotive emission and boosts the fuel cell efficiency would benefit the economic growth and development of human society.

1.2 CATALYSTS

To perform carbon monoxide oxidation reaction, catalysts are necessary. Up to now, CO oxidation over unsupported metals and supported metals catalysts has been widely investigated. In comparison to unsupported metals, both metals and supports of the supported metal catalysts could affect the catalytic performance. Therefore, it deserves to conduct more studies in molecular level to understand what exactly occurs on the unsupported and supported metal catalysts.

Reviews of metals and metal-support catalysts are discussed. First, the catalytic performance of transition metals will be addressed and focused on Pt, Pd, Au, and Cu. Second, the effect of irreducible and reducible supports will be discussed, including Al_2O_3, SiO_2, CeO_2, and TiO_2. In addition, metal support interaction will be briefly introduced.

1.2.1 METAL CATALYSTS

Fundamental understanding of heterogeneous catalysts was gained from the simplified model catalysts [23]. Heterogeneous catalysis reactions mostly occur on metal and metal oxide surfaces. Transition metals are widely investigated because of the high dissociation probability and low adsorption energy [24].

1.2.1.1 GROUP VIII METALS - PLATINUM AND PALLADIUM

Adsorption of CO on VIII metals surface has been extensively studied, mainly attributed to its important industrial application [25]. It is commonly accepted that most group VIII metals could be active and efficient towards CO oxidation. Two VIII metals (Pt and Pd) were selected to be shortly reviewed. CO oxidation on Pt and Pd single crystal surfaces has also been developed as a model system for heterogeneous catalysis [26].

Yeo studied the sticking probabilities and adsorption energy of CO and O_2 on Pt (111) based on CO and O_2 coverage [25]. They suggested that CO tends to remain the same sticking probability regardless of CO coverage, whereas O_2 sticking probability declines as O_2 coverage increases. Additionally, the CO oxidation process occurs on the covered Pt (111) surface requires higher energy than that of CO on the clean Pt (111) surface. Grabow reported surface strain impacted bond-making and breaking steps on Pt (111), further affecting the energetics and consequently influencing the catalytic performance in terms of reaction rate [27]. Ackermann demonstrated the role of spontaneously formed surface oxides on Pt (110), which exhibited a much higher CO oxidation rate than metallic Pt surface [26]. By carrying out modeling and experiment comparison, Oertzen proposed that the formation of subsurface oxygen on the Pt (110) significantly impacted the properties and limited the CO conversion [28]. Hendriksen and Frenken firstly proposed the effect of gas phase existence on surface oxides on Pt (110) [23]. They claimed the surface oxides could be stabilized by gas phases at high pressure, while at low temperature, reversible switch occurs between the oxidic state and the metallic state.

Berlowitz conducted the kinetic study on Pd (110) and suggested strongly bound oxygen species was formed under highly oxidizing conditions [29]. Furthermore, deliberate oxidation decreased the reaction rate and kept the similar activation energy (between 22 and 33 kJ/mol). The

reduced reaction rate demonstrated the role of oxide was serving as a site blocker. Logan and Paffett measured the activation energy of 22 kcal/mol for CO oxidation over Pd (100) single crystal surfaces in a higher pressure/ultra-high vacuum system [30]. Adsorption heat variation on Pd (100) surfaces led to reaction order diminution for CO, and reaction order increased for O_2. Szanyi and Goodman investigated the CO coverage change on Pd (100) surface [31]. Their results demonstrated that CO coverage was the same with change in oxygen pressure. Uetsuka reported the presence of subsurface oxide layer on Pd (110) and suggested that either kinetics or the dynamics of CO oxidation on Pd (110) was not impacted by the surface oxide layer [32]. Szanyi and Goodman studied CO oxidation on Pd (111) shown activation energy is close to the CO heat of adsorption and illustrated the decrease of activation energy and adsorption heat at a lower temperature [33].

1.2.1.2 GROUP IB METALS - GOLD, SILVER, AND COPPER

In terms of electronic structure, Group IB metals have no unpaired d-electrons, whereas Group VIII metals have incomplete d-electron. The electron-deficiency is essential to reduce the free energy of reaction intermediates, such as *O, *OOH, $*O_2$. Meanwhile, it could help form strongly adsorbed oxygen species and improve thermodynamic stability [34]. Although Group IB metals do not have unpaired d-electrons, tremendous research had reported that group IB metals could provide appreciable catalytic performance on CO oxidation.

Outka and Madix investigated the CO oxidation on clean and oxidized Au (110) surface and illustrated that surface carbonate could not be generated from the reaction of CO_2 with oxygen adatom [35]. In addition, they evaluated the effective activation energy of 2 ± 1 kJ/mol and suggested that neither CO nor O_2 molecules could stabilize on the Au (110) surfaces. Gottfried conducted reactive thermal desorption measurements on Au (110) - (1×2) surface and reported the

maximum CO oxidation reaction rate achieved at -98 ^{o}C and started to decrease with temperature increase [36]. Min proposed that CO oxidation depended on the reaction temperature and oxygen overlayer characters on Au (111) surface [37]. The reaction temperature dependence was affected by the residence time of CO, size of Au-O complexes, and degree of oxygen layer order. In addition, three types of oxygen were identified as chemisorbed oxygen, surface oxide, and bulk oxide. Chemisorbed oxygen is more active and could be used as active oxygen to participate in the oxidation process. Gong revealed that the activated water or OH groups could directly participate in the CO oxidation process on oxygen pre-covered Au (111) surface, and CO_2 production was negatively affected by the oxygen pre-coverage [38].

Based on DFT calculation, Su reported that co-adsorbed water on Ag (111) surface induced the stabilization of reactants by an H bond and affected the transition states and intermediates, eventually resulted in the enhancement of CO oxidation reactivity [39]. Additionally, atomic oxygen on the Ag (111) surface reacted with adsorbed water and formed hydroxyl groups. Consequently, CO_2 was produced with CO. Biwker examined adsorption of CO on oxygen-dosed Ag (110) surface and reported that CO was oxidized rapidly to CO_2 during the adsorption process. Surface carbonate species were formed by CO_2 and oxygen surfaces. At 215 ^{o}C, surface carbonate species could decompose to release CO_2 and O_2 [40]. Barth and Zambelli examined the effect of molecularly adsorbed O_2 on the Ag (110) surface on CO oxidation. They proposed that single oxygen atoms played the role of the intermediate product in the reaction, and the course of oxidation readily occurred upon CO exposure [41].

Domagala and Campbell manipulated the temperature of gas phase CO to study CO oxidation over Cu (110) [42]. Results suggested that the reaction rate and activation energy were independent of CO gas phase temperature. They proposed the CO molecules were required to accommodate to

Cu (110) surface before reaction. Sueyoshi investigated the dissociate adsorbed oxygen on Cu (110) at -173 ^{o}C and indicated these oxygen adatoms performed 25 times higher CO oxidation reactivity than that of oxygen in the (2×1)-O phase [43]. Eren conducted a study on Cu (111) surface to reveal the chemical state of Cu during CO oxidation reaction [44]. During the reaction process, the Cu (111) surface was covered by chemisorbed CO. Meanwhile, a thin Cu_2O layer was formed on the surface under reaction conditions. An intermediate of $CO_2^{\delta-}$ was identified on Cu_2O, which suggested Cu_2O is most active for CO oxidation. Szanyi and Goodman demonstrated that oxidation of CO by molecular oxygen on Cu (100) surface was strongly dependent on the ratio of CO to O_2 [45]. CO oxidation activity increased along with CO/O_2 ratio increased and decreased rapidly under stoichiometric conditions.

As models, single crystals could provide a deep understanding of the effect of surface structure and composition on the CO oxidation process [46]. Whereas shortages are obvious, single crystals cannot be applied in a long-term flow system, and single crystals could not precisely represent metal particles. Besides, the investigation process requires extreme conditions, such as high vacuum, that are not suitable for atmospheric pressure reaction. Therefore, supported metal catalysts draws more attention.

1.2.2 SUPPORTED METAL CATALYSTS

Metal oxides supports help the metal dispersion. Therefore, more active sites could be exposed to reactant gases and offer more chances to adsorb the reactant. More exposure could result in surprisingly high activity for CO oxidation. In addition, the interaction established between metal and oxide supports impact the surface properties, such as oxygen vacancies and valences of supported metals. Eventually, the interaction could significantly elevate the catalytic performance.

Different supports, including Al_2O_3, SiO_2, CeO_2, and TiO_2, have been widely studied. Among these metal oxides, Al_2O_3 and SiO_2 are irreducible supports, where the oxygen supply most likely comes from O_2 dissociative adsorption on the metal particles [47]. Meantime, CeO_2 and TiO_2 are reducible supports, because they exhibit variable valence or oxidation states of the metal and can activate lattice oxygen to provide more active oxygen. In the meantime, molecular oxygen species could adsorb and dissociate on these supports [48]. The reaction pathway over Au-CeO_2 was proposed and shown in Figure1.1 to illustrate the effect of supports [49]. Oxygen species adsorbed on the CeO_2 support and dissociated at the Au/CeO_2 interface. CO adsorbed on the Au particles. The reaction would occur either on the metal particles or at the Au/CeO_2 interface. Reactive oxygen is supplied to involve in the reaction [50].

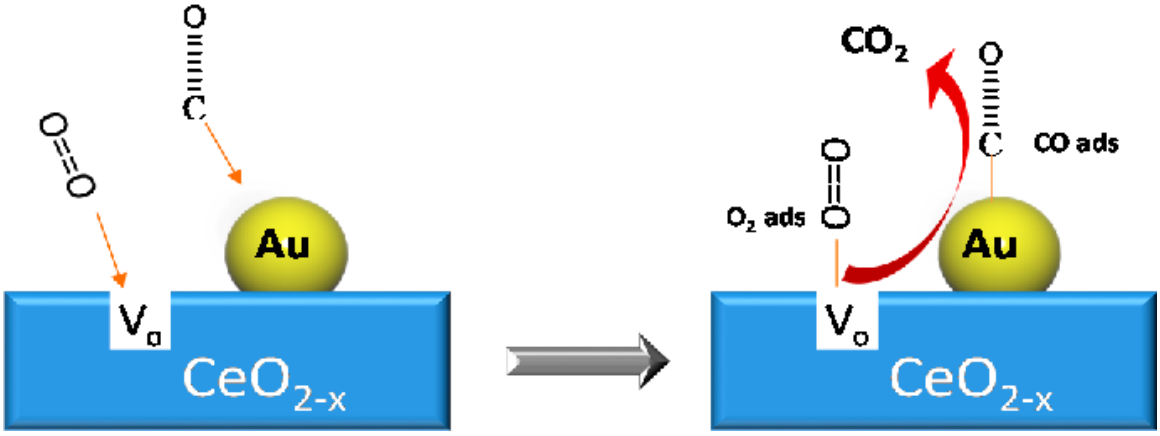

Figure 1.1 Mechanism of CO oxidation on Au/CeO_2 catalysts [49].

1.2.2.1 Alumina or silica-supported catalysts

γ-alumina (γ-Al_2O_3) is the most applied phase of Al_2O_3, as a catalyst and catalyst support in the application, such as CO oxidation [50-52]. The advantages of alumina could be attributed to its natural properties, such as large surface area, pore volume. γ-Al_2O_3 exhibits high chemical and hydrothermal stability [52].

Nibbelke performed the kinetic study of CO oxidation over $Pt/\gamma\text{-}Al_2O_3$. CO conversation rate was suggested to be approximately proportional to O_2 partial pressure, while inversely proportional to CO partial pressure [53]. CO is found to be fully covered on the Pt surface, and oxygen adsorption is rate-determined and potentially followed by instantaneous dissociation. In addition, the reaction rate could be enhanced by introducing stream. Pavlova identified adsorption and reactivity of adsorbed species on $Pd/\gamma\text{-}Al_2O_3$ surface through infrared spectroscopy studies [54]. At saturation coverages, both linear and bridge bonded CO adsorbed on Pd could be reactive. However, if O_2 was pre-adsorbed, the adsorbed O_2 decreased the relative intensity of linear form CO and resulted in a decrease of the initial CO oxidation rate. Gold supported on $\gamma\text{-}Al_2O_3$ and other supports were compared to understand the effect of support [55]. Au/Al_2O_3 presented the weakest oxygen storage capacity, which further confirmed the irreducible nature of Al_2O_3. After comparing with TiO_2 support, they proposed the chemical nature of the support (oxygen storage capacity, support reducibility) could affect the reaction, by impacting the ability to form and stand the active oxygen species on the surface. Silica has been considered as problematic support because silica is difficult to form strong interaction and well-disperse metal particles [56]. The inert property motivated researchers to develop advanced techniques to overcome the difficulty and expand the application of silica supported catalysts.

Kaul and Wolf were the first to conduct the kinetic study on Pt/SiO_2 [57]. To follow up their investigation of Pt/SiO_2, other metals such Sn was introduced to the structure to further promote the activity [58]. A core-shell structure was developed to provide high CO coverage without perturbing Pt chemical state. This core-shell structure exhibited a high CO conversion rate [59]. Li developed a single-step impregnation using $Pd(acac)_2$ as the Pd precursor to synthesize Pd/SiO_2, Pd was well dispersed on the support and, overall CO conversion occurred at 145 ^oC which is

much lower than Pd/SiO_2 prepared by other methods [60]. Qian synthesized Au/SiO_2 catalysts with Au nanoparticles around 3 - 4.5 nm, which provided effective CO chemisorption and was able to catalyze CO oxidation at room temperature [61].

1.2.2.2 Ceria-supported catalysts

The reducible oxide support is a promising candidate when comparing to the conventional oxide support [62]. The charge transfer in redox reactions is deemed to be an essential step for catalytic low temperature CO oxidation. CeO_2, known as a reducible support, has the advantage of being an effective support for CO oxidation due to its oxygen storage capacity (OSC). OSC is the ability to store oxygen under oxygen-rich conditions and release lattice oxygen under oxygen-lean circumstances. Additionally, it is convinced that CeO_2 supports could enhance catalysts activity by relying on its superior oxygen mobility via a redox reaction ($4\ CeO_2 \leftrightarrow 2\ Ce_2O_3 + O_2$) [62-64]. By far, lots of effects on introducing transition metal onto CeO_2 have tremendously extended its utilization.

Pt/CeO_2 catalysts were prepared for CO oxidation [65]. Their proposed reaction pathway clearly indicates that the chemisorbed CO on the Pt surface could react with the oxygen species. The oxygen species were provided at the Pt-CeO_2 interface on the CeO_2 support. Furthermore, large Pt particle size was suggested to accelerate the reaction because the large Pt particles and CeO_2 support formed the Pt-Ce-O solid solution and created oxygen vacancies. Bera synthesized Pt/CeO_2 catalyst by solution combustion method, and $Ce_{1-x}Pt_xO_{2-\delta}$ solid solution was formed [63]. Pt substituted Ce^{4+} ions to form the solid solution, and the substitution created oxide ion vacancies. The oxygen vacancies led to the strong interaction between Pt^{2+} and CeO_2 supports, which significantly improved catalytic activity. Oran and Under reported reaction orders of CO and O_2 over Pt/CeO_2 were -1.0 and 0.0, respectively [66]. The activation energy was around 70 kJ/mol.

Pd/CeO_2 catalysts could also be optional towards CO oxidation. Slavinskaya found two catalysts components of PdO nanoparticles and $Pd_xCe_{1-x}O_{2-\delta}$ solid solution in their Pd/CeO_2 catalyst [67]. TPR and XPS results suggested the palladium ions Pd^{2+} and palladium surface structures PdO_x(s)/Pd-O-Ce(s) in the $Pd_xCe_{1-x}O_{2-\delta}$ bulk phase. PdO_x(s)/Pd-O-Ce(s) played a significant role in promoting reaction as it contained high reactive oxygen. Widmann and Behm first experimentally verified the oxygen vacancies on Au/CeO_2 could enhance the CO oxidation reaction rate [68]. They underscored the critical role of oxygen vacancies in CO oxidation on Au/CeO_2 by obtaining a much higher activity after removing 0.07 ML surface oxygen species and released more oxygen vacancies.

1.2.2.3 Titanium-supported catalysts

Titanium dioxide (TiO_2), similar to CeO_2, has proven to be an alternative reducible support to improve catalytic CO oxidation performance. The advantages of TiO_2 support are low cost, high chemical, and thermal stability. Three crystalline phases, as shown in Figure 1.2, namely anatase, rutile, and brookite, have been extensively studied for their applications in chemical and physical sciences. All kinds of TiO_2 consist of TiO_6 octahedra [69], while the distortion of octahedron units is different. The difference in the TiO_2 structure leads to different densities and electronic band structures.

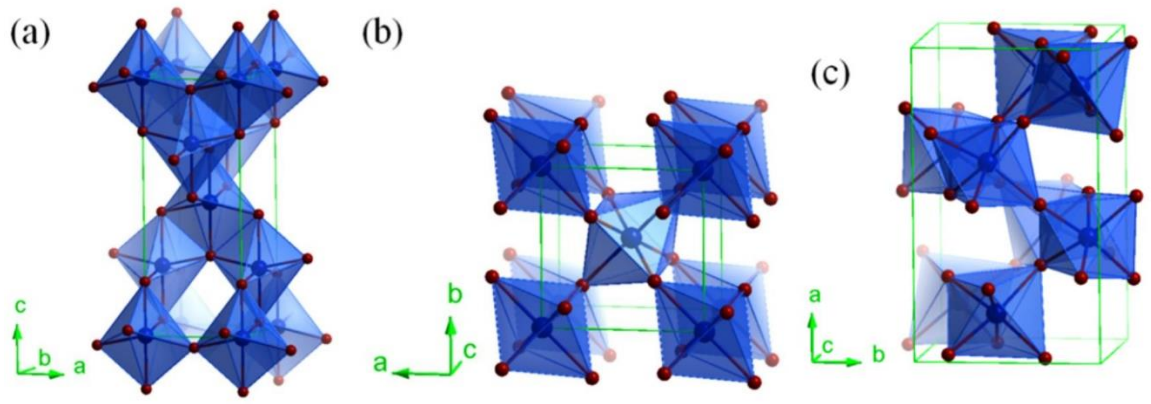

Figure 1.2 Crystalline structures of TiO_2 in different phases: (a) anatase, (b) rutile, (c) brookite. [69].

Thermodynamically, rutile is the most stable phase [69]. Anatase and brookite are merely stable at low temperature and could transform to rutile at higher temperature. Because of the phase transition, in most studies, synthesized TiO_2 supported metal catalysts could consist of different phases of TiO_2. Researches are mainly focused on the effects of the employed metals, the interaction between metal and supports, and morphology of TiO_2 supports. Au clusters in the range of 2.5-6.0 nm were deposited on TiO_2 thin film under an ultra-high vacuum. [70]. They proposed that the changes of electronic properties of Au mainly determined the pronounced structure sensitivity of CO oxidation on Au/TiO_2 catalyst. Bamwenda compared the effect of preparation methods on Pt/TiO_2 and Au/TiO_2 for CO oxidation [71]. CO oxidation over Au/TiO_2 was suggested to strongly dependent on the preparation method while insensitive for Pt/TiO_2. The different structure sensitivity could be attributed to the perimeter interface between Au particles and TiO_2 support. Taira investigated the support effect of Pt/TiO_2 on CO oxidation and concluded the high ratio of larger pores performed higher catalytic activity, whereas surface area, the crystal structure of TiO_2 have less effect [72]. Widmann reported a method to measure the amount of

active oxygen stored on Au/TiO_2 surface. In this method, CO/Ar and O_2/Ar were alternately introduced to peroxided catalysts to reveal the stability of adsorbed oxygen [73].

Despite the effects mentioned previously, in terms of TiO_2 itself, anatase and rutile are more chemically active as supports compared with brookite. Therefore, the crystalline phases themselves could also impact the catalytic performance of TiO_2 supported metal catalysts. Li carried out the study on Co_3O_4/TiO_2 catalysts with different crystalline structures of TiO_2 (anatase, rutile, and P25) [74]. Among these phases, rutile TiO_2 supported Co_3O_4 demonstrated the highest activity. Further analysis revealed that anatase TiO_2 contains the unstable state Ti^{3+} species. This defective structure exhibited good oxygen adsorption ability and led to the better redox property of anatase TiO_2 supported Co_3O_4. Di focused on different TiO_2 phase supported Au catalysts and reported an anatase-to-rutile ratio of 4:6 exhibited the highest performance on CO conversion [75]. They proposed the phase transformation of TiO_2 and preferential deposition of Au on rutile TiO_2 led to the high active performance. In addition, they also emphasized the improved surface area and generated oxygen vacancies were beneficial to catalytic performance.

1.2.2.4 Metal-support interaction

Metal-support interaction plays an essential role in improving catalytic performance. The metal-support interaction has been studied by various surface sciences techniques to reveal the surface properties at the atomic level. Understanding surface properties help to explain the mechanism of CO oxidation reaction [76].

In 1978, Tauster first came up with the concepts of strong metal-support interaction (SMSI) [77]. SMSI commonly exists at the interface between metal and supports, especially when reducible supports, such as TiO_2 and CeO_2, are employed [78]. Initially, electron transfer between support and metal, and intermediate phases were employed to explain SMSI [79-81]. Recent

researches have indicated that interfacial and transport phenomena, along with charge redistribution in the course of interface formation [79]. Sasahara studied three types of sites on rutile TiO_2 (110) surface to anchor Pd atoms. Three types of sites are Ti atom rows, O atom rows, and oxygen vacancies [82]. They claimed most Pd adatoms were observed on Ti atoms, however only the adatoms in oxygen vacancies are stable while adatoms on O and Ti atom rows are mobile. Furthermore, due to the contact of Pt atoms with Ti atoms at the oxygen vacancies, the electron transfer has been enhanced.

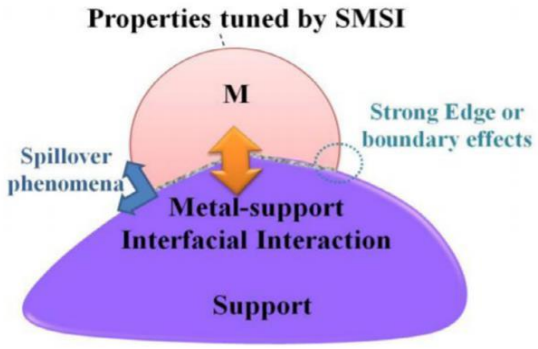

Figure 1.3 A model of a supported metal particle, illustrating the effects of metal support interfacial interactions [79].

As shown in Figure 1.2, Pan discussed the major effects on SMSI, including electronic, geometric, and bifunctional [79]. The effects of electronic properties mainly comes from the interaction between metal clusters and oxide supports [79, 83]. The effect of geometric could be attributed to the active sites were blocked [79, 84-85]. The bifunctional effect could be understood as the formation of dual active sites at the perimeter and enhanced the catalytic performance [79, 86].

Theoretical studies, especially density functional theory (DFT) studies have been included to further explain the SMSI between metal and supports. Prestianni proposed that co-adsorbed CO and O_2 on adjacent Au sites lead to a synergic electronic rearrangement, while CO oxidation did

not occur unless CO and O_2 were interacting with the same Au sites [87]. Liu and Hu conducted DFT study and revealed that O_2 dissociation on Au surfaces could not happen at low temperature [88]. They claimed that the CO oxidation occurred at the interface would follow a two-step mechanism: $CO + O_2 \rightarrow CO_2 + O$, $CO + O \rightarrow CO_2$. Zhang studied the Ru/TiO_2 and demonstrated the electronic interaction that occurred at the $Ru\text{-}TiO_2$ interface, and electron transfer significantly reduced the activation barrier [89].

1.2.3 COPPER-METAL OXIDES

As stated previously, precious metals, such as Pt, Pd, and Au have been reported to be highly active for CO oxidation. Although the precious metals present notable catalytic performance for CO oxidation, the application of the precious metals is still restricted to a great extent, due to the high cost. Therefore, less expensive transition metals were investigated to reduce the cost. Copper is a promising candidate and has been extensively studied for not only CO oxidation, but also water-gas shift reaction and NO_x elimination [90].

Unsupported copper oxide is thought to be unstable because the oxidation state of copper varies in the reaction process [91]. Regardless of the starting materials, Cu^{2+}, Cu^{+} and Cu^{0} are probably coexisting and each could be the active site under different reaction conditions. As early as 1952, Garner et al. [92] reported the tremendous catalytic performance of Cu_2O in CO oxidation at room temperature. The performance could be attributed to the propensity of Cu_2O towards valence variations. The propensity made Cu_2O able to seize or release surface lattice oxygen. Therefore, Cu_2O was able to improve catalytic performance than Cu and CuO. Jennings presented a detailed study of the oxygen chemisorption kinetics over the cuprous oxide [93]. The chemisorption was irreversible and could proceed to several monolayers. The activation energy for the formation of the first monolayer is 29 kJ/mol and increased for other monolayers. The increased activation

energy was controlled by space charge, which was formed from oxygen vacancies. White synthesized nearly monodisperse Cu_2O nanoparticles, which revealed improved activity toward CO oxidation [94]. More than 99.5 % CO conversion was obtained and could last for over 12h at less than 250 ^oC. CO pretreated $CuO/\gamma\text{-}Al_2O_3$ catalysts promoted the CO conversion, and CO could be fully converted to CO_2 under 200 ^oC [95]. Furthermore, they proposed that the CO pretreatment process led to the reduction of crystalline CuO to Cu^0, and dispersed Cu^{2+} was partially reduced to Cu^+. The promotion of CO pretreated Cu catalysts is attributed to the presence of Cu^+. Huang and Tsai compared Cu, Cu_2O, and CuO powder catalysts in both oxygen rich and oxygen lean conditions [96]. Regardless of the reaction conditions, Cu_2O is the only active site at 140 ^oC. They concluded that Cu_2O has the ability to seize or release surface lattice oxygen more easily, enabling Cu_2O to exhibit higher activities.

In contrast to the proposed promotion effect of Cu^+, a number of works have been carried out to reveal the role of Cu^0 or Cu^{2+} for CO oxidation [97-99]. In the work of Jernigan and Somorjai, a well-defined thin film of Cu^0, Cu_2O, and CuO was investigated to promote CO oxidation between 200 ^oC to 350 ^oC [97]. Metallic copper was completely oxidized to Cu^{2+} within 1 hour in the stream of CO and O_2 at a CO/O_2 partial pressure ratio of 66: 33. Metallic copper was suggested to be more active than Cu_2O and CuO. Activation energies were reported as 37, 70, and 57 kJ/mol for Cu^0, Cu_2O, and CuO, respectively. Chen synthesized highly active supported Cu catalysts by wet impregnation method. They claimed that the remarkable catalytic performance was determined by Cu^{2+} [98]. H_2-TPR results indicated the reduction of small CuO particles while larger Cu particles remained the same oxidation state. Therefore, Cu^{2+} is decided as the main factor. Luo applied a surfactant-templated method to synthesize high-surface area nanosized CuO catalysts. H_2-TPR results revealed the coexist of highly dispersed CuO, the Cu^{2+} in the support lattice, and bulk CuO

[99]. Highly dispersed CuO was removed by acid treatment, which resulted in reduced catalytic activity. Thereby they concluded that CuO species are the active sites under the reaction condition.

In addition to the effect of the chemical state of Cu on CO oxidation, oxide supports could improve metal dispersion, provide oxygen vacancies, form metal-support interaction, and modify the surface acidity. The characteristics of oxide supports are considered to facilitate the activity significantly. Therefore, oxide supports are also critical to boosting the catalytic performance. Both irreducible (Al_2O_3, SiO_2) and reducible (CeO_2, TiO_2) supports have been investigated. Among the studies on effects of support, most researches had been presented toward CO oxidation over Cu supported on reducible supports. This is because of the strong interaction and oxygen vacancies were mostly reported on reducible supports.

Liu and Flytzani-Stephanopoulos claimed that Cu-Ce-O catalysts could perform high activity, which is several orders of magnitude higher than conventional Cu/Al_2O_3 catalysts [100, 101]. Strong Cu-Ce-O interaction was thought to be vital to the CO conversion. In addition, O_2 adsorbed on the support could form oxygen vacancies. The CO adsorbed on Cu_2O could react with lattice oxygen. Mock investigated CeO_2 nanorod-supported CuO_x catalysts and identified the abundance of surface defects. The surface defects could be critical to the strong interaction between CuO_x and CeO_{2-x} supports [102]. This strong interaction resulted in improving CO oxidation reactivity. Lykaki revealed the significant influence of copper-ceria interaction towards stabilizing the Cu^+ species on the surface of catalysts [103]. They suggested the weakly bund oxygen species, the relative quantity of Cu^+/Ce^{3+}, along with abundant oxygen vacancies, worked collaboratively to determine the catalytic performance.

Chen carried out the study on Cu/TiO_2 for CO oxidation and claimed that Cu/TiO_2 catalysts are highly active [104]. Catalytic performance strongly depends on the formation of Cu^+ species

and a strong electron interaction between highly dispersed CuO particles and Ti^{3+} ion. This strong interaction resulted in the charge transferred reaction ($Cu^{2+} + Ti^{3+} \rightarrow Cu^{+} + Ti^{4+}$) and in turn generate more Cu^{+} species. Kang synthesized CuO/TiO_2 catalysts with various compositions of anatase and rutile phase and suggested the rutile phase of TiO_2 is crucial to CO conversion [105]. The rutile phase interacts weakly with the CuO particles, and Cu^{2+} species were readily reduced to Cu^{+} and Cu^{0}. Therefore, CuO supported on rutile phase was able to provide a large amount of oxygen to participate in the reaction.

Because of the cost-effective property and comparable catalytic activity, copper-based catalysts have the potential to be a promising candidate for low temperature carbon monoxide oxidation. Meanwhile, the supports for copper also play a significant role in boosting the catalytic performance of copper-based catalysts. Among different supports, TiO_2 is considered to be more suitable. This is not only because of the low price, but also attributed to the reducible characteristics and various phases of TiO_2. These characteristics of TiO_2 offered more probability to serve as oxide support for Cu towards CO oxidation. Nonetheless, the excellent opportunities that are created by Cu-TiO_2 along with challenges. The oxidation states of copper, which is complicated, the argument is still ongoing regarding the active sites. Besides, the formation and intensity of the interaction between copper and TiO_2 support various under different conditions. Therefore, Cu-TiO_2 catalysts are still attractive and deserve investigation nowadays. Further investigation could help to get insight into the determinative copper state and contribution from TiO_2 supports.

1.3 MECHANISM AND KINETICS

1.3.1 MECHANISM

Investigations on CO oxidation mechanisms over metals and supported metal catalysts have been extremely performed. Three forms of reaction mechanism, namely Langmuir-Hinshelwood (LH), Eley-Rideal (ER), and Mars-van Krevelen (MvK), have been proposed [106] based on how the adsorption occurs. In the course of investigation, infrared spectroscopy is considered a highly valuable tool to identify the chemical nature of adsorbed surface species, their interaction strength and geometry.

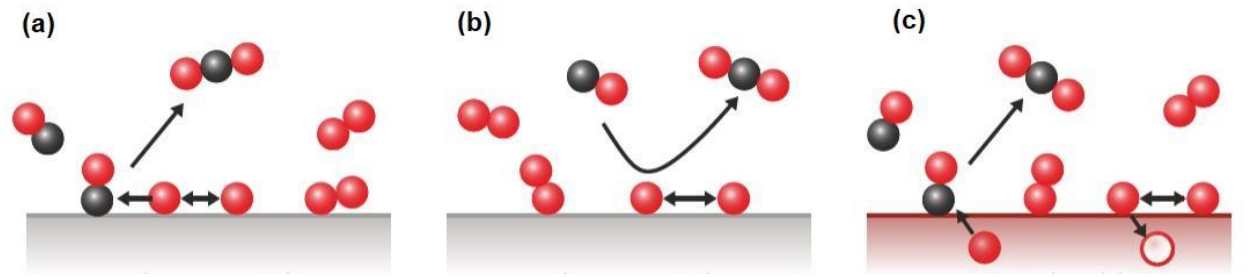

Figure 1.4 Three main reaction mechanisms: (a) Langmuir-Hinshelwood, (b) Eley-Rideal, and (c) Mars-van-Krevelen [107].

LH mechanism is a model of bimolecular chemical reaction on solid surfaces [108]. Two molecules are adsorbed on the neighboring sites on the surface, and reaction happens between adsorbed molecules [109]. As shown in Figure 1.4 (a), in the CO oxidation process under the LH mechanism, CO and O_2 molecules both adsorbed on the catalysts surface, constituting a three-step reaction to produce CO_2. ER mechanism proposed that one molecule is adsorbed on the surface and the other reactant joins the reaction directly from gas phase [110]. In specific for the CO oxidation reaction shown in Figure 1.4 (b), ER mechanism is demonstrated to have O_2 pre-adsorbed on the surface and directly react with gas phase CO molecule. Another mechanism shown

in Figure 1.4 (c), known as MvK mechanism, proposed to adsorb CO on the surface and O_2 is adsorbed to oxygen vacancies. The adsorbed CO reacts with lattice oxygen species to produce CO_2.

Tremendous investigation has been carried out to understand the CO oxidation mechanism over metal catalysts and supported metal catalysts. However, there is always controversy as reaction mechanisms are complicated. Up to now, LH is regarded as the most acceptable mechanism for low temperature CO oxidation [24]. Domagala performed the kinetics study of CO oxidation over Cu (110) by tuning the CO gas phase temperature [111]. Their results indicated the CO oxidation activation energy depends on CO pressure, while independence upon oxygen coverage and CO gas phase temperature. Therefore, CO oxidation was suggested to proceed through LH mechanism under their conditions. Choi performed kinetics study for CO oxidation over Cu/Al_2O_3 via in-situ IR measurements [112]. Their results indicated that CO conversion was not obtained until the CO band was detected at 2118 cm^{-1} on the surface. Besides, the CO conversion increased simultaneously with the increase of CO band peak. In addition, they reported the activity increased along with the decrease of O_2 partial pressure during the reaction process. These results suggested the CO oxidation occurred following the LH mechanism. Liu investigated the kinetics of CO oxidation over Cu atoms embedded in hexagonal boron nitride (h-BN) [113]. First-principle investigation revealed the formation of a peroxide-like complex on the surface. This peroxide-like complex is formed from the reaction of adsorbed CO and O_2. Therefore, the oxidation process was proposed to be instructed by LH mechanism.

Whereas, along with the rapid development of new materials and advanced synthesis methods, more work has been reported that the reaction could take place under ER or MvK mechanism. Furthermore, the CO oxidation reaction could also be co-affected by an arbitrary combination of the three mechanisms. Lu presented the kinetics study on CuO/CeO_2 by modifying CO and O_2

partial pressures [114]. CO was stabilized on the catalysts and shown in DRIFT results. In DRIFT results, peak at 2112 cm^{-1} represented chemisorbed CO on Cu^{+}. The characteristic band at 1230-1566 cm^{-1} confirmed the CO would further react with lattice oxygen in the CeO_2 support to form carbonates. Therefore, the reaction between chemisorbed CO with lattice oxygen was suggested to follow the Mvk mechanism. Wang computed the mechanism on supported Cu_n or Cu_nO (n=6, 7) clusters surfaces, to evaluate which is preferred between ER and LH mechanism [115]. The results indicated either ER or LH could be favorable under different conditions, which is determined by O_2 activation. Cu_6, Cu_7 and Cu_6O prefers the ER mechanism, while Cu_7O follows the LH mechanism. Sun investigated the CO oxidation reaction mechanism over Cu_2O (111) via DFT calculation [116]. Both ER and LH mechanisms are viable. In their reports, ER mechanism was determined to have a moderate barrier of 60.22 kJ/mol. This value is appropriate to make CO oxidation occur. LH mechanism was calculated with a relatively higher barrier than ER mechanism, while LH mechanism is also viable towards CO oxidation. Furthermore, the barrier of MvK mechanism was calculated as 600 kJ/mol, which is too large to make the reaction occur.

1.3.2 KINETICS

Kinetics study is fundamentally significant in investigating the CO oxidation reaction mechanism. Kinetics study of CO oxidation generally presented by individually identifying the effect of CO partial pressure and O_2 partial pressure on reaction rate. Thereafter CO oxidation reaction orders could be determined by plotting partial pressure with reaction rate. CO oxidation reaction rate equation could be expressed as Equation 1.1,

$$r = k \{CO\}^a \{O_2\}^b \quad (1.1)$$

where constant k is the reaction rate constant, a and b are partial orders of the reaction for CO and O_2, respectively.

Determining the reaction rate equation and reaction order of CO oxidation could help to identify the CO oxidation mechanisms. The relationship between previously depicted mechanisms and reaction rate equation of CO oxidation could be generally summarized as [114]: 1) LH mechanism would lead to a reaction rate equation with reaction order between 0 and 1 on O_2 partial pressure; 2) in an ER mechanism, this requires the O_2 reaction order of 1; 3) the Mvk mechanism results in reaction order of 0 on O_2 partial pressure.

Lu reported the reaction rate expression of CO oxidation over 5 wt% CuO/SiO_2 and 5 wt% CuO/TiO_2 are $r = 1.77\times10^{-7}P_{CO}^{0.85}P_{O_2}^{0.22}$ and $r = 1.62\times10^{-7}P_{CO}^{0.65}P_{O_2}^{0.19}$, respectively [114]. The results indicated that CO oxidation over CuO/SiO_2 and CuO/TiO_2 follows the LH mechanism. These are because the reaction orders O_2 are between 0 and 1, which are consistent with the LH mechanism. In the meantime, Lu also determined the reaction rate equation of CO oxidation over 5 wt% CuO/CeO_2, which is $r =1.77\times10^{-7}P_{CO}^{0.7}P_{O_2}^{0}$. The result indicated the CO oxidation over 5 wt% CuO/CeO_2 would follow a MvK mechanism. Paldey reported the CO oxidation over $Cu_{1.5}Mn_{1.5}O_4$ with the order of 0.85 with respect to CO and 0 order on O_2 [117]. Therefore, the reaction would be proceeded through the MvK mechanism.

Elementary reaction steps provide deeply understand of reaction mechanisms. Scheme 1.1 depicts the sequence of elementary steps for CO oxidation under the Langmuir-Hinshelwood mechanism.

$$CO + * \overset{K_1}{\leftrightarrow} CO^* \tag{1.2}$$

$$O_2 + * \overset{K_2}{\leftrightarrow} O_2^* \tag{1.3}$$

$$O_2^* + * \overset{k_3}{\leftrightarrow} 2\,O^* \tag{1.4}$$

$$CO^* + O^* \overset{k_4}{\rightarrow} CO_2^* \tag{1.5}$$

$$CO_2^* \xrightarrow{k_5} * + CO_2 \quad (1.6)$$

Scheme 1.1 Typical elementary steps of CO oxidation follow Langmuir-Hinshelwood mechanism. (* represents a vacant active site and X* denotes as the adsorbed species)

Steps shown in equation 1.2 and 1.3 represent the quasi-equilibrated non-dissociative adsorption steps for CO and O_2 [118]. Equation 1.4 presented the O-O bond activation. The next step in equation 1.5 indicated the reaction between chemisorbed CO and O molecules to produce CO_2. Thereafter, CO_2 is dissociated from the catalysts surface, and active site becomes available for CO and/or O_2.

$$O_2 + * \overset{K_1}{\leftrightarrow} O_2^* \quad (1.7)$$

$$O_2^* + * \overset{k_2}{\leftrightarrow} 2\ O^* \quad (1.8)$$

$$CO + O^* \xrightarrow{k_3} CO_2^* \quad (1.9)$$

$$CO_2^* \xrightarrow{k_4} * + CO_2 \quad (1.10)$$

Scheme 1.2 Typical elementary steps of CO oxidation follow Eley-Rideal mechanism. (* represents a vacant active site and X* denotes as the adsorbed species)

As shown in Scheme 1.2, equation 1.7-1.10 depicts the elementary steps of CO oxidation under ER mechanism. O_2 is adsorbed on the active sites first to form adsorbed oxygen species (equation 1.7-1.8). CO gases in the reactant stream would directly react with adsorbed oxygen species O^*. The produced CO_2 will eventually be dissociated from the surface.

$$CO + * \overset{K_1}{\leftrightarrow} CO^* \quad (1.11)$$

$$CO^* + [O] \xrightarrow{k_2} CO_2 + [] + * \quad (1.12)$$

$$O_2 + [] \xrightarrow{k_3} 2\ [O] \quad (1.13)$$

Scheme 1.3 Typical elementary steps of CO oxidation follow Mars-van-Krevelen mechanism. (* represents a vacant active site, X* denotes as the adsorbed species and [] is assigned as oxygen vacancies)

Scheme 1.3 demonstrated the elementary steps follow Mvk mechanism. The adsorbed CO would react with oxygen species, which was presented in the oxygen vacancies to produce CO_2. Oxygen vacancies were released to catch O_2 in the gas phase and could participate in the following reaction with adsorbed CO molecules.

1.4 RATIONALES AND OBJECTIVES

Catalytic oxidation of carbon monoxide (CO) over copper-based catalysts has drawn a great deal of persistent attention, attributed to the importance of CO oxidation itself and the high activity of copper. Titanium dioxide (TiO_2) has been widely used as a support because of its reducible and stable properties. In specific to CO oxidation over Cu-TiO_2 catalysts, research efforts usually considered the effect of Cu (I) species as the active species to improve reaction. However, it is notable that other species, especially different oxygen species, are presented along with copper species on the surface of Cu-TiO_2 catalysts. More or less, those oxygen species would affect the catalytic performance but gained less attention. This dissertation focused on building the property-activity relationship for carbon monoxide reaction over copper modified titanium oxide catalysts. Different approaches were applied to study how surface properties would impact surface properties of copper species and titanium dioxide. The following studies were studied to address the research goal.

(1) To control the concentration of surface hydroxyl groups. Cu-TiO_2 catalysts were synthesized through a direct one-step approach. The concentration of the surface hydroxyl

group was adjusted through the washing step. The relationship among copper species, surface hydroxyl group concentration, and reaction rate were studied.

(2) To investigate the effects of pretreatment atmosphere on surface properties. Cu-TiO_2 catalysts were pretreated under different gases, specifically H_2, O_2, and He. The concentration and oxidation state of surface copper species and different oxygen species were identified.

(3) To study the effect of the addition of nitrogen to TiO_2 support. Nitrogen modified TiO_2 (N-TiO_2) support was synthesized. The concentration and chemical status of nitrogen atoms in the N-TiO_2 support was determined.

(4) To evaluate the effect of TiO_2 phases. Anatase and rutile TiO_2 were used to prepare Cu-N-TiO_2 catalysts. The difference among surface properties was investigated, including the concentration of copper species and surface oxygen species, the existential state of nitrogen, and the presence of oxygen vacancies.

CHAPTER 2

EXPERIMENTAL METHODS

2.1 SYNTHESIS OF CATALYSTS

Supported copper catalysts for CO oxidation have been synthesized via different methods and each catalyst could be produced by different routes. The most commonly applied methods are precipitation and impregnation [119]. Other methods have also been reported include photodecomposition, sol-gel synthesis, microwave synthesis, ion exchange, atomic layer deposition, and anchoring/grafting. In both precipitation and impregnation methods, a copper precursor is required, such as $Cu(NO_3)_2$, $CuCl_2$, $CuSO_4$, and $Cu(OAc)_2$. In the process of precipitation synthesis, the supersaturation of Cu precursor solution could result in the nucleation and growth of Cu particles, which would restrict the dispersion of Cu particles and possibly impede the CO oxidation reaction [119]. The impregnation method is the simplest method and contains low waste streams [120]. In the process of impregnation synthesis, the concentration of the Cu precursor solution needs to below the supersaturation to prevent premature deposition [119]. Therefore, the impregnation method reduces the usage of Cu precursors and would be more suitable for our research.

The majority of impregnation synthesis processes and other synthesis methods require calcination step to anchor Cu species on the surface of supports. However, the reaction between copper (II) acetate and sodium hydroxide allowed the formation of copper (II) oxide in a single step without calcination [121]. Because of its convenient and energy-efficient characters, copper (II) acetate was selected as the Cu precursor to synthesize our as-designed catalysts. In practice, the stoichiometric amount of sodium hydroxide was doubled to guarantee the full conversion of

the copper precursor to copper oxide. Given this, the additional hydroxyl groups brought the concern that if the hydroxyl groups will have an impact on the CO oxidation reaction. Therefore, it is critical to address this concern before applying this synthesis method to investigate the effects of other aspects on the catalytic CO oxidation reaction.

2.1.1 SYNTHESIS OF Cu-TiO_2 CATALYSTS WITH INEQUAL HYDROXYL GROUPS

Copper modified titanium dioxide (Cu-TiO_2) catalysts were prepared by wet impregnation method. Copper loading was designed as 10 weight% (10 wt%). In a typical synthesis process (Figure 2.1), designed amount of Copper (II) acetate (Aldrich, 98 %) and 0.5 g TiO_2 (Aldrich, P25, 99.5 %) support were mixed in 50 mL D. I. water and stirred for 5 minutes at room temperature, 10 mL sodium hydroxide (Fisher Chemical, 98.8 %) aqueous solution (1 mol/L) was added to the mixture dropwise. Continued stirring for 1 h, followed by centrifugal separation. pH value of the centrifugal liquid was measured by pH testing strips, the obtained sample was labeled as Cu-TiO_2-pH14. Part of the sample (Cu-TiO_2-pH14) was taken out and separated into two centrifugal tubes, and each was washed by D. I. water, followed by centrifugal separation until the pH values of all those two samples were decrease to 9 and 7, respectively. All Cu-TiO_2 precipitations were dried overnight in vacuum at 50 ^oC. Obtained samples were denoted as Cu-TiO_2-pH9, Cu-TiO_2-pH7, respectively.

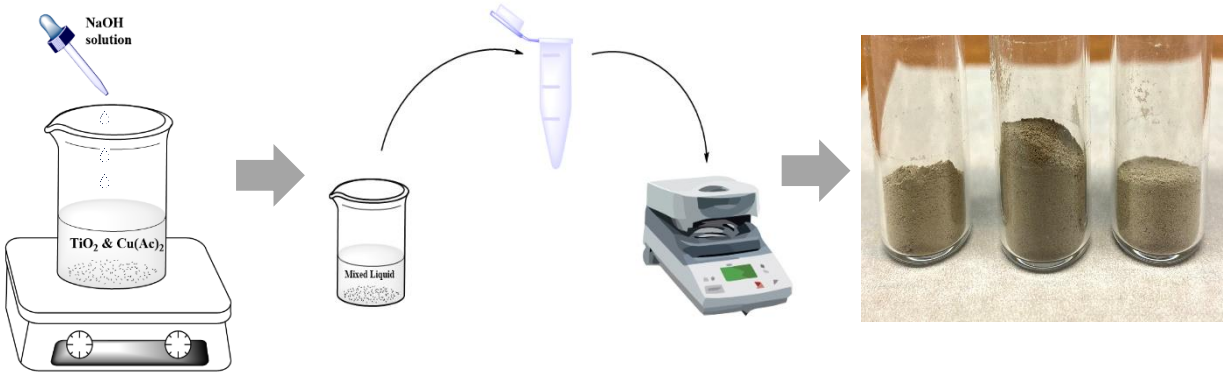

Figure 2.1 Typical synthetic pathway of copper modified titanium dioxide (Cu-TiO_2) catalysts.

2.1.2 SYNTHESIS OF Cu-N-TiO_2 CATALYSTS WITH VARIOUS PHASES

Cu-N-TiO_2 catalysts were synthesized using a two-step process. Nitrogen modified TiO_2 (N-TiO_2) supports were synthesized at first. Typically, TiO_2 (Anatase (Cristal ACTiV^{TM} G5, 99.7 %), Rutile (Alfa Aesar, 99.8 %), or P25 (Aldrich, 99.5 %)) and Urea (Sigma-Aldrich, 99.0 % - 100.5 %) were physically mixed with fixed mass ratio of TiO_2 and urea as 1:5. The mixture was vacuum dried overnight under room temperature to remove apparent moisture. Vacuum dried mixtures were heated up to 550 ^oC with 5 ^oC/ min heating rate in an open-air environment and kept for 15 hours. Calcined samples were labeled as N-TiO_2, N-TiO_2 (A), and N-TiO_2 (R), respectively representing nitrogen modified P25 TiO_2, anatase TiO_2, and rutile TiO_2.

Copper loading for Cu-N-TiO_2 samples was designed as 10 weight% (wt%). The typical process follows the procedure in synthesizing Cu-TiO_2 samples. The as-prepared samples at pH 14 were further washed by D. I. water until the pH value of centrifugal liquid reaches 7. All Cu-N-TiO_2 precipitations were dried overnight in vacuum at 50 ^oC. Obtained samples were denoted as Cu-N-TiO_2, Cu-N-TiO_2 (A), and Cu-N-TiO_2 (R), respectively, based on the supports type.

Cu-TiO_2 samples with various types of TiO_2 (P25, anatase, or rutile) were synthesized as references following the same procedure as Cu-N-TiO_2 samples. To eliminate the effect of the

calcination process, TiO_2 (P25, anatase, or rutile) was calcined at 550 ^oC for 15 hours prior to loading copper. Samples were labeled as Cu-TiO_2, Cu-TiO_2 (A), and Cu-TiO_2 (R).

2.1.3 SYNTHESIS OF Cu-TiO_2 CATALYSTS WITH DIFFERENT CALCINATION GAS

Cu-TiO_2 catalysts calcined under different gas atmospheres were synthesized using a two-step process. At first, Cu-TiO_2 samples were synthesized following the procedure detailed in section 2.1.1, while pH value was controlled at 7. Vacuum dried Cu-TiO_2 samples were respectively calcined within 30 % H_2/Helium, 10 % O_2/Helium, and pure Helium at 400 ^oC and stood for 3h (gas flow rate 30 mL/min). Catalysts were names as Cu-TiO_2-H_2, Cu-TiO_2-O_2, and Cu-TiO_2-He.

2.2 CATALYSTS CHARACTERIZATIONS

2.2.1 INDUCTIVELY COUPLED PLASMA ATOMIC EMISSION SPECTROSCOPY (ICP-AES)

Inductively coupled plasma atomic emission spectroscopy (ICP-AES) is a spectral method to precisely determine the elemental composition and quantify the elemental concentration of given samples. High-energy plasma from an inert gas like argon was employed to burn analytes rapidly. Elements were identified based on the color emitted from the analytes. The intensity of the spectral signal indicates the concentration of elements. ICP-AES measurements were conducted on a Leeman Labs PS1000 instrument. Before each measurement, the samples were digested in an aqua regia solution (2 - 3 mL) overnight and then diluted by deionized water to obtain the desired concentration of the metal in a neutral pH solution.

2.2.2 X-RAY POWDER DIFFRACTION (XRD)

X-Ray powder diffraction (XRD) serves as a rapid analytical technique to identify phases present in the analytes and provide information on grain size and texture. When conditions satisfy Bragg's law (Equation 2.1), constructive interference and diffracted rays are produced by samples and incident rays. These diffracted X-rays are then detected, processed, and counted to determine phases in the samples.

$$2d\sin\theta = n\lambda \tag{2.1}$$

where d is lattice distance, θ is incident wave angle, n is a positive integer and λ is the wavelength.

The XRD tests were performed on a Bruker D2 Phaser desktop X-ray diffractometer equipped with a Cu X-ray source, and scans were set for a 2θ-range from 15^{o} to 80^{o}.

2.2.3 BRUNAUER-EMMETT-TELLER SURFACE AREA (BET)

The Brunauer -Emmet-Teller (BET) theory is normally enrolled as an important analysis technique to measure the specific surface area of materials. The quantitative surface area is determined by measuring the adsorption and desorption amount of employed gaseous adsorbate. Nitrogen is commonly used as the probing gases when it does not chemically react with solid surfaces. BET test was performed on a Micromeritics AutoChem II 2920 equipped with a thermal conductivity detector. Prior to the experiment, samples were pretreated with pure Helium at 200 °C for 1.5 h. Isotherms of N_2 adsorption-desorption were measured based on the acquisition of N_2 adsorption isotherm at -196 ^{o}C.

2.2.4 LASER RAMAN SPECTROSCOPY (RAMAN)

Raman spectroscopy is a spectroscopic technique to identify molecule vibration modes based on inelastic scattering of photons, furthermore, provide structure information, and determine

specific molecules. Laser light illuminates on samples, energy change of the laser photons reflects molecular vibration modes. Raman spectra were carried out with an NT-MDT Raman spectrometer using a diode laser beam. An excitation wavelength of 532 nm was used. The Raman spectra were collected by co-adding ten scans of 2 s and the laser power of 22 ± 2 mW under ambient conditions.

2.2.5 COPPER DISPERSION

Copper dispersion is a crucial fundamental characteristic of copper-based catalysts because only copper atoms exposed on the surface could be employed in a catalytic reaction. The copper dispersion represents the fraction of copper atoms present on the surface. Copper dispersion and the specific surface area of metallic copper of catalysts are measured by dissociative N_2O oxidation and H_2 titration. Typically, 25 mg catalysts were first pretreated in a Helium flow at 200 °C for 1.5 h and cooled to room temperature to remove moisture and impurities that may remain on the surface. Then catalysts were reduced in a 10 % H_2/Ar mixture at a flow rate of 30 mL/min until 200 ^oC. The hydrogen consumption in this reduction process was assigned as A_1. Pure Helium (30 mL/min) was purged into the reactor and cooled down to 50 ^oC. The surface Cu was oxidized by 10 % N_2O/He (30 mL/min) at 60 ^oC for 0.5 h. Subsequently, the sample was flushed with pure Helium (30 mL/min) for 0.5 h to remove the residual N_2O. Finally, another reduction process was performed in 10 % H_2/Ar (30 mL/min), and hydrogen consumption was denoted as A_2. The dispersion and the specific surface area of metallic copper were calculated based on Van Der Grift's report [122], which are shown below:

Reduction of all Cu atoms, with hydrogen consumption A_1:

$$CuO + H_2 \rightarrow Cu + H_2O$$

Oxidation of surface Cu to Cu_2O:

$$2\ Cu + N_2O \rightarrow Cu_2O + N_2$$

Reduction of all surface Cu atoms, with hydrogen consumption A_2:

$$Cu_2O + H_2 \rightarrow 2\ Cu + H_2O$$

The dispersion of Cu (D, %) was calculated as Equation 2.2:

$$D = 2 \times A_2 / A_1 \times 100\ \% \quad (2.2)$$

The specific surface area of metallic copper (S, m^2/g) was calculated by Equation 2.3

$$S = 2 \times A_2 \times N_A / \left(A_1 \times M_{Cu} \times 1.4{\times}10^{19}\right) = 1353 \times A_2 / A_1 \quad (2.3)$$

where N_A is Avogadro's constant, M_{Cu} is the relative atomic mass of copper (63.46 g/mol), and 1.4×10^{19} is the number of copper atom of per square meter when the average surface area of copper atom is assigned as 7.11×10^{-2} nm^2.

2.2.6 TEMPERATURE PROGRAMMED SURFACE REACTION (TPR & TPSR)

Hydrogen temperature programmed reduction (H_2-TPR) was performed to investigate the surface reduction properties of catalysts. It was conducted on a Micromeritics AutoChem II 2920 equipped with a thermal conductivity detector. In a typical H_2-TPR experiment, 50 mg of the sample was placed in a U-shaped quartz tube. Prior to the experiment, the samples were pretreated in a Helium flow (30 mL/min) at 200 ℃ for 1.5 h and cooled to room temperature to remove moisture and impurities that may remain on the surface. The reduction profiles were collected using a ramp rate of 5 °C/min in the flow of 10 % H_2/Ar mixture with a flow rate of 30 mL/min from room temperature to 200 °C. The hydrogen consumption was calculated by the integrated area of TPR peaks, calibrated against a known amount of Ag_2O standard sample.

Carbon monoxide temperature programmed surface reaction (CO-TPSR) was performed in a fixed bed flow reactor. 50 mg of catalyst was filled in a quartz tube (I. D. = 10 mm). Reactant gas (10 % CO balanced with He) was passing through. Prior to the experiment, the same pretreatment was taken as H_2-TPR using pure Helium. The reaction profiles were collected using a ramp rate of

5 °C/min with a flow rate of 30 mL/min from room temperature to 400 °C. The reaction temperature was controlled by a shaft furnace. The CO concentration in the reactor effluent was analyzed using an MKS e-Vision 2 residual gas analyzer (RGA).

Oxygen temperature programmed reaction (O_2-TPR) is carried out to reveal the surface oxidation properties of catalysts. It is essential and helps to identify suitable materials applied as supports for post-treatment catalysis process. O_2-TPR test was conducted on a Micromeritics AutoChem II 2920 equipped with a thermal conductivity detector. Typically, 50 mg of the sample was placed in a U-shaped quartz tube. Prior to the experiment, the samples were pretreated in a Helium flow (30 mL/min) at 200 °C for 1.5 h and cooled down to room temperature to remove moisture and impurities that may remain on the surface. Then 10 % O_2/ He (30 mL/min) was purged into the reactor, and the TPR profiles were collected with a ramp rate of 5 °C/min from room temperature to 600 °C.

2.2.7 X-RAY PHOTOELECTRON SPECTROSCOPY (XPS)

X-ray photoelectron spectroscopy (XPS) was carried out on a Thermo Scientific K-Alpha system in the Center for Nanoscale System at Harvard University. Thermo Scientific K-Alpha system equipped with an Al source and a 180° double focusing hemispherical analyzer with a 128-channel detector at a pass energy of 50 eV for the analyses of the core level signals of Cu 2p, N 1s, Ti 2p, and O 1s. When processing the XPS spectra data, binding energy values were referenced to C 1s peak (284.8 eV) to eliminate the effect of surface adventitious contamination layer to correct the shift caused by the charge effect. XPS peak deconvolution was conducted by using XPS peak41 software.

2.2.8 IN-SITU DIFFUSE REFLECTANCE INFRARED FOURIER TRANSFORM SPECTROSCOPY (IN-SITU DRIFTS)

In-situ diffuse reflectance Fourier transform infrared spectroscopy (in-situ DRIFTS) experiments were performed using a Thermo Scientific Nicolet iS50 FT-IR equipped with a MCT detector and a KBr beam splitter. Praying Mantis reaction chamber was utilized to generate CO oxidation conditions. All copper-based samples were first pretreated under pure Helium for 90 minutes at 150 ^{o}C. A mixture of gas (1 % CO/20 % O_2 balanced in Helium or 10 % CO balanced in Helium) was then introduced to the chamber, temperature programmed heat up and tested under 25 ^{o}C, 80 ^{o}C, 100 ^{o}C, 120 ^{o}C, 140 ^{o}C, 160 ^{o}C, 180 ^{o}C, and 200 ^{o}C. All the background scans of the samples were collected under Helium prior to the reaction to remove contributions from the samples.

2.3 CATALYTIC PERFORMANCE

The carbon monoxide oxidation reaction light-off test was performed to evaluate catalytic performance in a fixed bed flow reactor equipped with a temperature controller. Typically, 50 mg of catalyst was filled in a quartz tube (I. D. = 10 mm). Reactant gas (1% CO, 20% O_2 balanced with Helium) was passing through. The total feed gas flow was 30 mL/min (gas hourly space velocity "GHSV" = 36,000 $mL \cdot h^{-1} \cdot g^{-1}$). The reaction temperature was measured with a K-type thermocouple reaching the top of the catalyst bed from room temperature to 200 ^{o}C. The samples were pretreated with pure Helium at 200 ^{o}C for 1.5 h before being passed through the reaction gas stream, the gas flow rate of the pretreatment was 30 mL/min (GHSV= 36,000 $mL \cdot h^{-1} \cdot g^{-1}$), and heating rate was 5 ^{o}C/min. CO conversion was calculated according to the change in CO

concentration between the inlet and outlet gases following Eq. 2.1. The CO concentration in the reactor effluent was analyzed online using a Gas Chromatograph (SRI 8160C).

$$X_{CO}(\%) = \frac{(C_{CO})_{in}-(C_{CO})_{out}}{(C_{CO})_{in}} \times 100 \quad (2.1)$$

The stability test was performed following the same procedure of the light-off test. After the first trial of the light-off test, pure Helium was introduced to replace reactant gases in the reaction system. Samples were cooled down to room temperature under pure Helium before starting the next light-off test. The same trial was repeated until CO conversion decreases at the same temperature, which indicates catalyst starts to deactivate.

The reaction rate was measured following the same procedure of the light-off test. In a typical test, CO oxidation reaction was restricted in the kinetic regime. The reaction occurred at the temperature that CO conversion is lower than 15 %. Ideal gas law was employed to calculate the reaction rate. The activation energy was determined by plotting the ln (rate) vs. 1000/Temperature.

Turnover Frequency (TOF) is a measure of the instantaneous efficiency of a catalyst [123], which quantifies the specific activity of catalytic site under reaction conditions. Typically, TOF is defined as the number of molecules of a specified product made per catalytic site and per unit time [124].

CHAPTER 3

EFFECT OF HYDROXYL GROUPS ON CARBON MONOXIDE OXIDATION OVER COPPER-TITANIUM DIOXIDE CATALYSTS

3.1 INTRODUCTION

Copper catalysts, either un-supported or supported on an oxide, have been explored for the carbon monoxide oxidation reaction for decades [125, 126]. Studies under high vacuum conditions suggested that low valence copper species, particularly Cu (I), demonstrated comparable reaction rates to those of precious metals [126]. However, identification of the copper oxidation states became challenging once copper species were supported on an oxide, especially reducible metal oxides, such as titanium dioxide and cerium oxide [100, 125]. Among those copper-reducible metal oxides system, copper oxides supported on titanium dioxides (Cu-TiO_2) have been extensively investigated because copper could be a replacement for precious metals-based catalysts, based on cost analysis regarding practical applications.

Highly dispersed copper species were suggested to be an essential factor for improved carbon monoxide conversion [104, 127, 128]. Therefore, the concept of well-dispersed active species embarked extensive studies focused on the development and understanding of the variety of synthesis strategies [129]. Taking copper oxides supported on titanium dioxides as an example, highly dispersed copper species were obtained either through the traditional deposition-precipitation method using copper salts and titanium dioxide [130] or through the sol-gel method using titanium complexes as the precursor [131]. In addition to the choice of synthesis methods,

pretreatment with hydrogen also proved to be an effective approach to tune the oxidation state of copper and to increase the concentration of Cu (I) on the surface. Both synthesis method optimization and the hydrogen treatment align with the goal of introducing a strong interaction between metal and supports (SIMS). The strong interaction between copper oxides and reducible oxides, TiO_2 in particular, is desirable because the changes in electronic and structural properties could facilitate the adsorption of carbon monoxide on the surface, therefore accelerating the carbon monoxide oxidation.

The calcination step is necessary for traditional approaches because it enables the formation of copper oxides through thermal decomposition of copper hydroxides. But post thermal treatment also leads to the reconstruction of surface properties. Herein, in this chapter, one direct approach would be reported to synthesize copper oxides supported on titanium dioxide without calcination. Copper oxide supported on titanium dioxides (Cu-TiO_2) catalysts were synthesized through the reaction between copper (II) acetate and sodium hydroxide. Unlike other copper precursors, copper (II) acetate allowed the formation of copper (II) oxide in a single step [121]. The stoichiometric amount of sodium hydroxide was doubled to guarantee the full conversion of the copper precursor to copper oxide. This one-step synthesis approach provides an uncalcined platform which enables us to elucidate how the concentration of surface hydroxyls affects the reaction rate in the carbon monoxide oxidation reaction.

3.2 CARBON MONOXIDE OXIDATION ACTIVITY OVER Cu-TiO_2 CATALYSTS

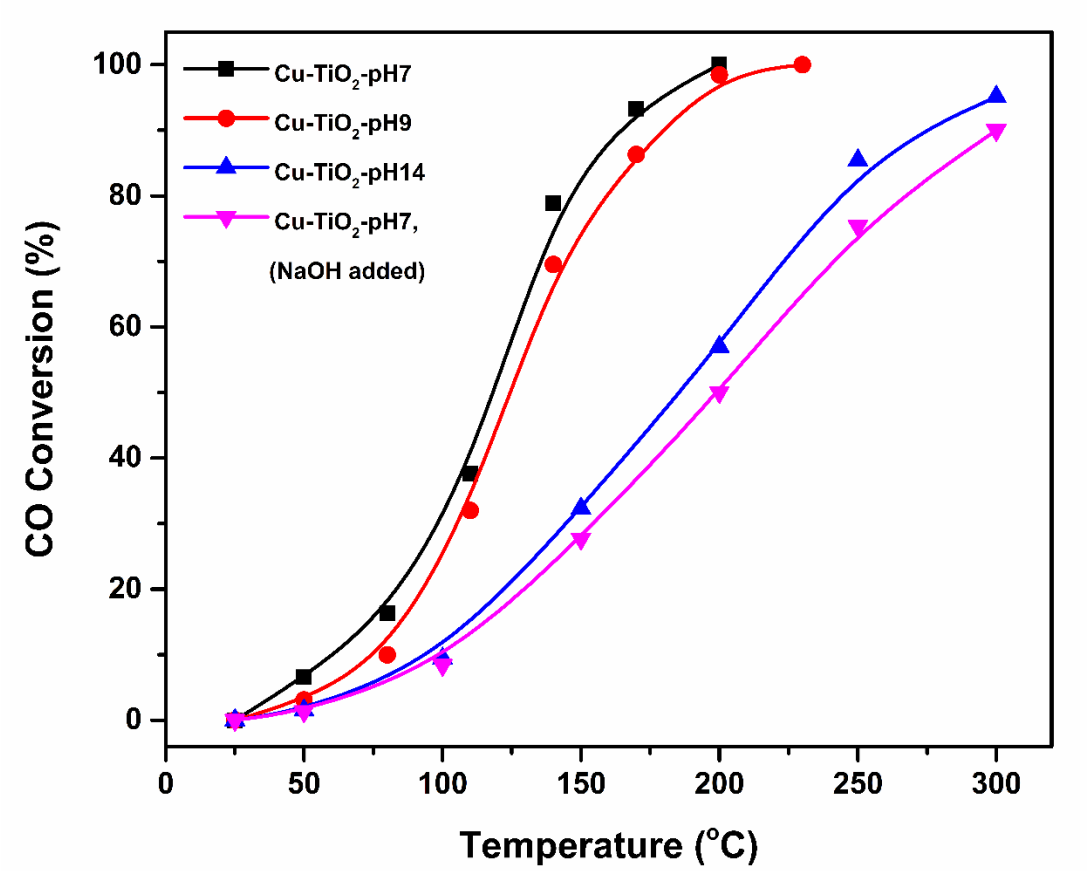

Figure 3.1 Light-off curves of Cu-TiO_2 samples. Test condition: 1%CO/20%O_2/ Helium, flow rate 30 mL/min.

Catalytic performance of Cu-TiO_2 catalysts was evaluated for carbon monoxide oxidation. The light-off activity tests results were shown in Figure 3.1. The activities of catalysts are potentially affected by the synthesis conditions, as it indicates that Cu-TiO_2 samples obtained from aqueous solution with lower pH values have much better activity performance under 200 ^oC. The activity performance over the Cu-TiO_2-pH7 catalyst is similar to that of the Cu-TiO_2-pH9 catalyst. Both catalysts achieved T_{50} (50 % CO conversion) around 125 ^oC and achieved full CO conversion

when the reaction temperature reached 200 ^{o}C. Meanwhile, the carbon monoxide conversion over Cu-TiO_2-pH14 only reached 50 % conversion at 185 ^{o}C. Cu-TiO_2-pH7 and Cu-TiO_2-pH14 have same as-designed Cu loading (10 wt%), and similar synthesis process, only pH values of centrifugal liquid is different. Therefore, the concentration of surface hydroxyl groups would be the primary difference among all catalysts. The different amount of surface hydroxyl groups results in discriminating catalytic performance of all catalysts.

To understand how hydroxyl groups could affect the activity, post-treatment was performed for the Cu-TiO_2-pH7 catalyst. Specifically, the Cu-TiO_2-pH7 catalyst was put into 1 M sodium hydroxide solution, and the solution was stirred for 1 hour, followed by filtration and vacuum dry at 50 ^{o}C overnight. As shown in Figure 3.1, with additional hydroxyl groups added to the catalyst surface, the post-treated Cu-TiO_2-pH7 catalyst exhibited similar performance to Cu-TiO_2-pH14. The CO conversion of post-treated Cu-TiO_2-pH7 is lower than that of the Cu-TiO_2-pH7 catalyst. The decrease in CO conversion indicated that treatment in sodium hydroxide solution impeded the activity in carbon monoxide performance. Therefore, it suggested that the surface hydroxyl groups would play an important role in achieving better activity performance.

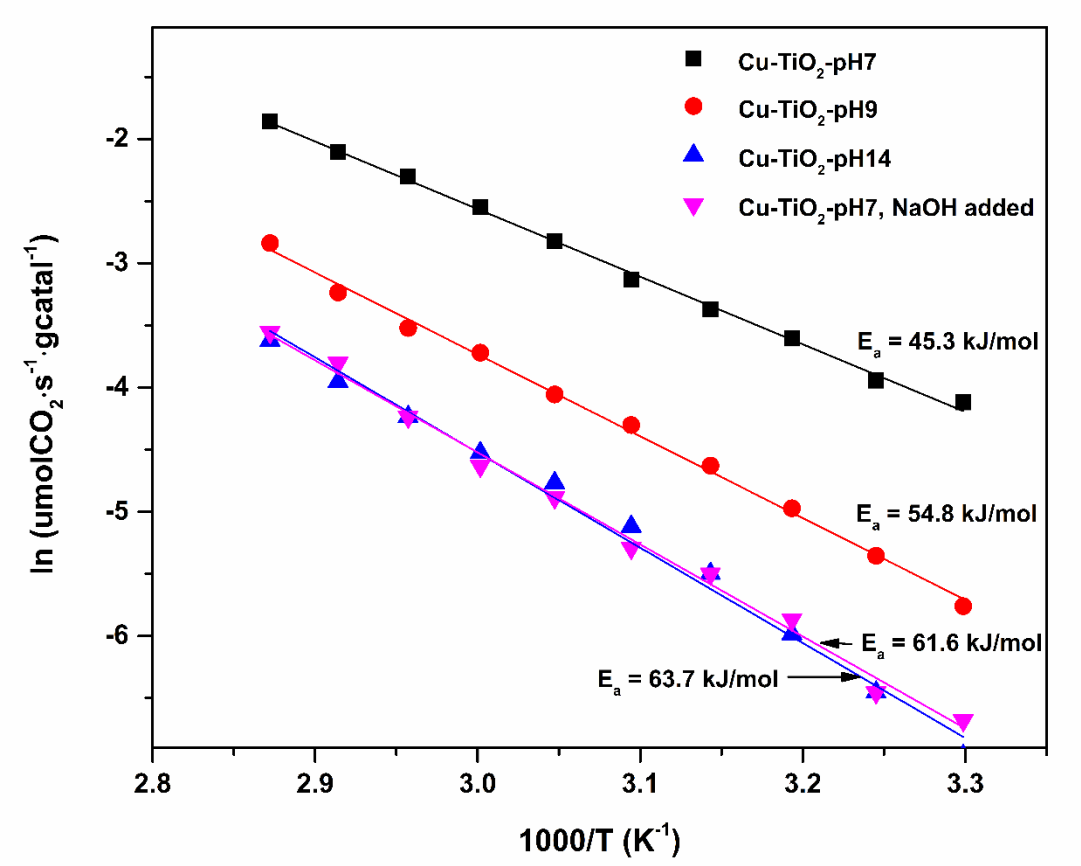

Figure 3.2 Arrhenius plot of activation energy of CO oxidation over Cu-TiO_2 catalysts.

To further evaluate the catalytic performance of Cu-TiO_2 catalysts, activation energy was determined by performing the reaction under 75 ^oC. As shown in Figure 3.2, the Cu-TiO_2-pH7 catalyst has the lowest activation energy as 45.3 kJ/mol. With the increase of pH values, higher activation energy was required to motivate the reaction. The comparison between Cu-TiO_2-pH7 catalyst and Cu-TiO_2-pH9 catalyst clearly indicates Cu-TiO_2-pH7 catalyst performed better than Cu-TiO_2-pH9 catalyst, even they have the similar trend of the light-off test. In the meanwhile, with additional hydroxyl groups introduced to Cu-TiO_2-pH7 catalyst, activation energy increased by 36 % to 61.6 kJ/mol. This is closed to the Cu-TiO_2-pH14 catalyst, which further confirmed the adverse effect of surface hydroxyl groups on catalytic performance.

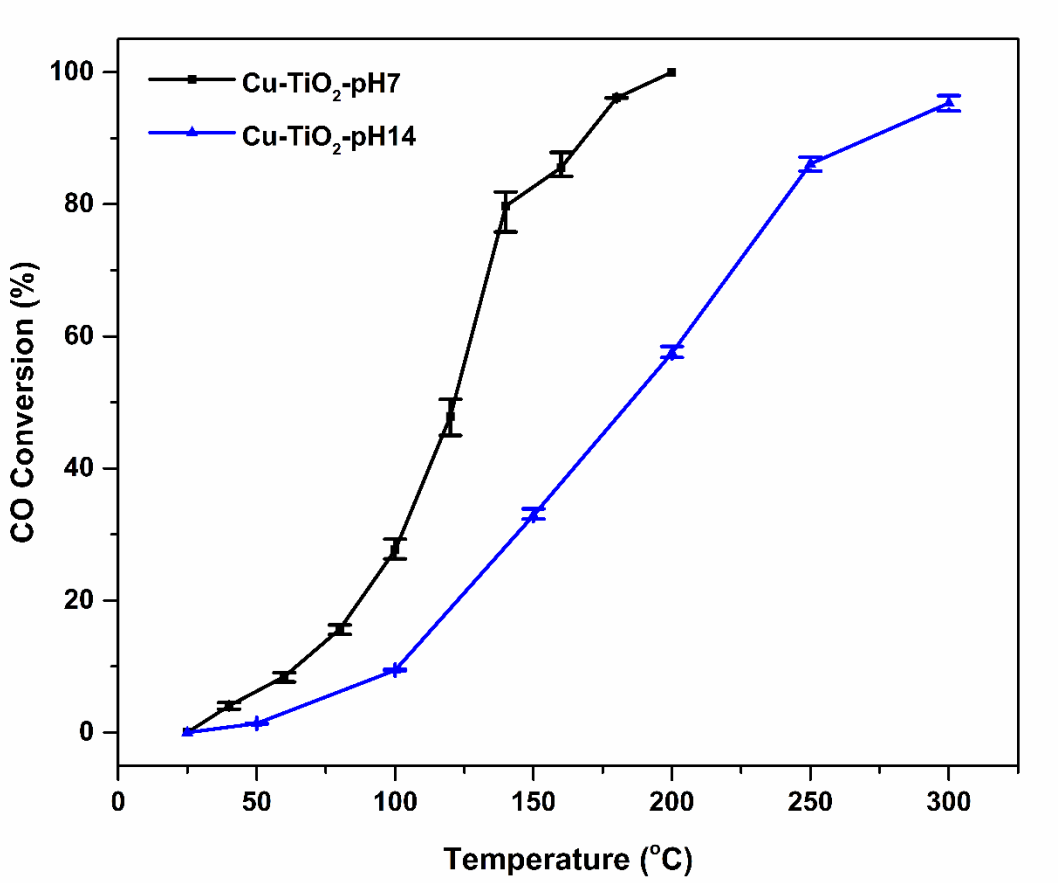

Figure 3.3 Cyclic light-off curves of Cu-TiO_2-pH7 and Cu-TiO_2-pH14 (three trials for each sample).

The stability of efficient catalysts is also critical to evaluate catalysts. Therefore, cyclic light-off tests were carried out to check whether active species on the surface are stable and to compare the stability of Cu-TiO_2-pH7 and Cu-TiO_2-pH14 catalysts. After the first run of reaction, the samples were cooled down to ambient temperature using pure Helium, and then cyclic activity tests were performed without further treatments. The cyclic light-off curves were shown in Figure 3.3, and it indicated light-off curves maintained the same trend for all samples after three runs. The results suggested that those active surface species are stable under the investigated conditions. Meanwhile, Cu-TiO_2-pH7 and Cu-TiO_2-pH14 catalysts have similar stability, although they performed differently regarding light-off tests.

3.3 CHARACTERIZATION OF Cu-TiO_2 CATALYSTS

3.3.1 PHYSICAL PROPERTIES

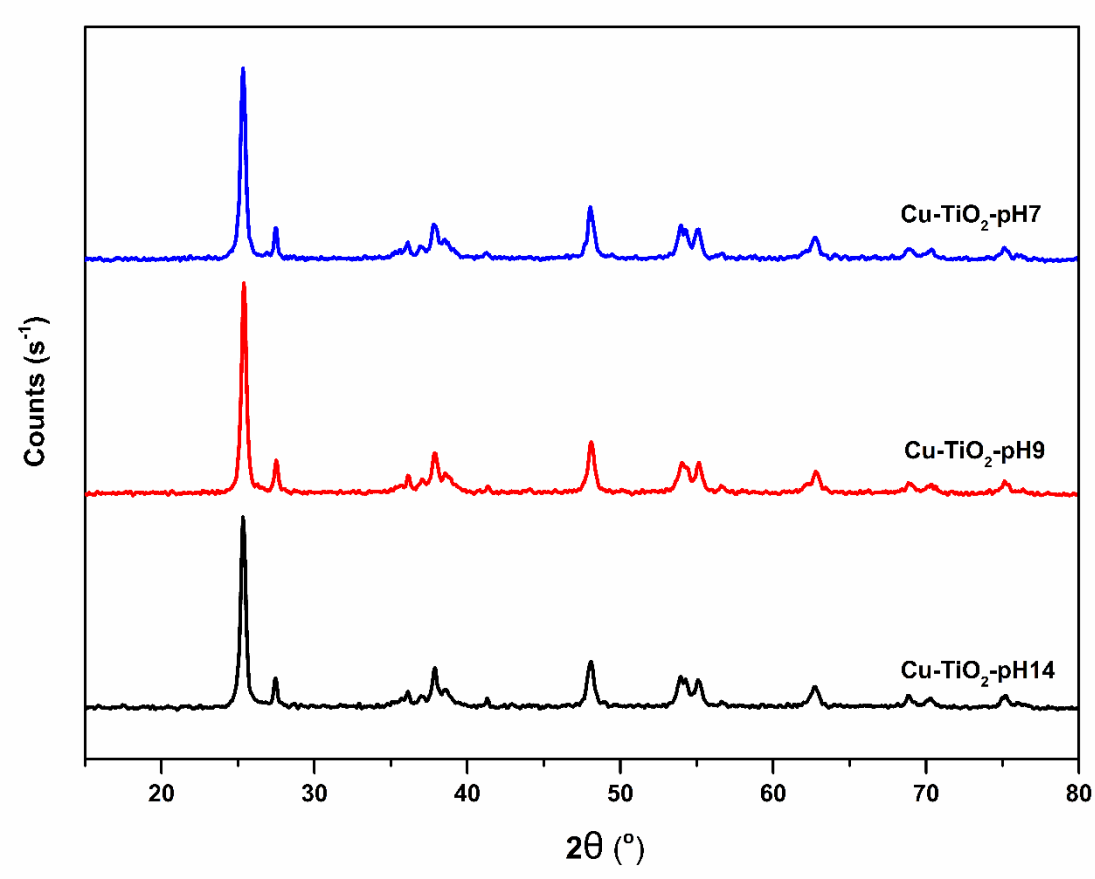

Figure 3.4 XRD patterns of Cu-TiO_2-pH7, Cu-TiO_2-pH9, and Cu-TiO_2-pH14.

XRD patterns of Cu-TiO_2-pH7, Cu-TiO_2-pH9, and Cu-TiO_2-pH14 were shown in Figure 3.4. Three samples have similar XRD profiles, and existing diffraction peaks represent for TiO_2. No diffraction peaks attributed to copper oxides were observed through XRD profiles, indicating that copper oxide species are highly dispersed on the surface and/or small clusters were formed and challenging to be detected by XRD [121]. The highly dispersed copper and/or small clusters could be attributed to the high surface area of TiO_2 supports, even though the addition of copper decreased the total surface area as compared to undoped titanium dioxide (not listed). When it

comes to the Cu-TiO_2 catalysts, as shown in Table 3.1, the surface area gradually increased when the pH value of the solution became close to 7. This increase in surface area may be explained by the fact that the washing step could remove extra sodium hydroxide from the pores of TiO_2. Therefore, more surface area became available after the washing step.

Table 3.1 BET surface area and copper concentration of Cu-TiO_2 samples.

Sample	Surface Area ($m^2/g \cdot catal$)	Copper Concentration		
		ICP (%) [a]	Dispersion (%) [b]	Surface Area of Cu atom (m^2/g) [b]
Cu-TiO_2-pH7	108	9.2	60.1	390
Cu-TiO_2-pH9	101	9.2	56.4	366
Cu-TiO_2-pH14	85	9.2	48.6	315

[a] Determined by Inductive Coupled Plasma. [b] Copper dispersion measured by N_2O titration.

Even though all catalysts have been designed with 10 wt% copper loading, the real loading might be different. Detecting the real loaded amount of copper on the catalysts surface could be helpful to understand the different light-off tests performance of all samples. ICP tests were presented, and results revealed the copper concentration was 9.2 wt% (Table 3.1) Cu-TiO_2-pH7, Cu-TiO_2-pH9 and Cu-TiO_2-pH14 have same copper concentration based on the ICP, indicating the washing steps by D. I. water will only remove surface hydroxyl groups and will not affect the amount of surface copper species. By applying N_2O titration, copper dispersion, and surface area of Cu atoms were determined. As shown in Table 3.1, three samples all contain relatively high Cu dispersion and high surface area of Cu atoms. Therefore, results from the ICP and Cu dispersion suggested the existence of highly dispersed copper species on TiO_2 surfaces and further explained the XRD profiles regarding no diffraction peaks attributed to copper oxides were detected. At the

same time, among all samples, Cu-TiO_2-pH7 has the highest Cu dispersion as 60.1 % and the highest surface area of Cu atoms. This would promote its catalytic performance.

3.3.2 REDOX BEHAVIOURS

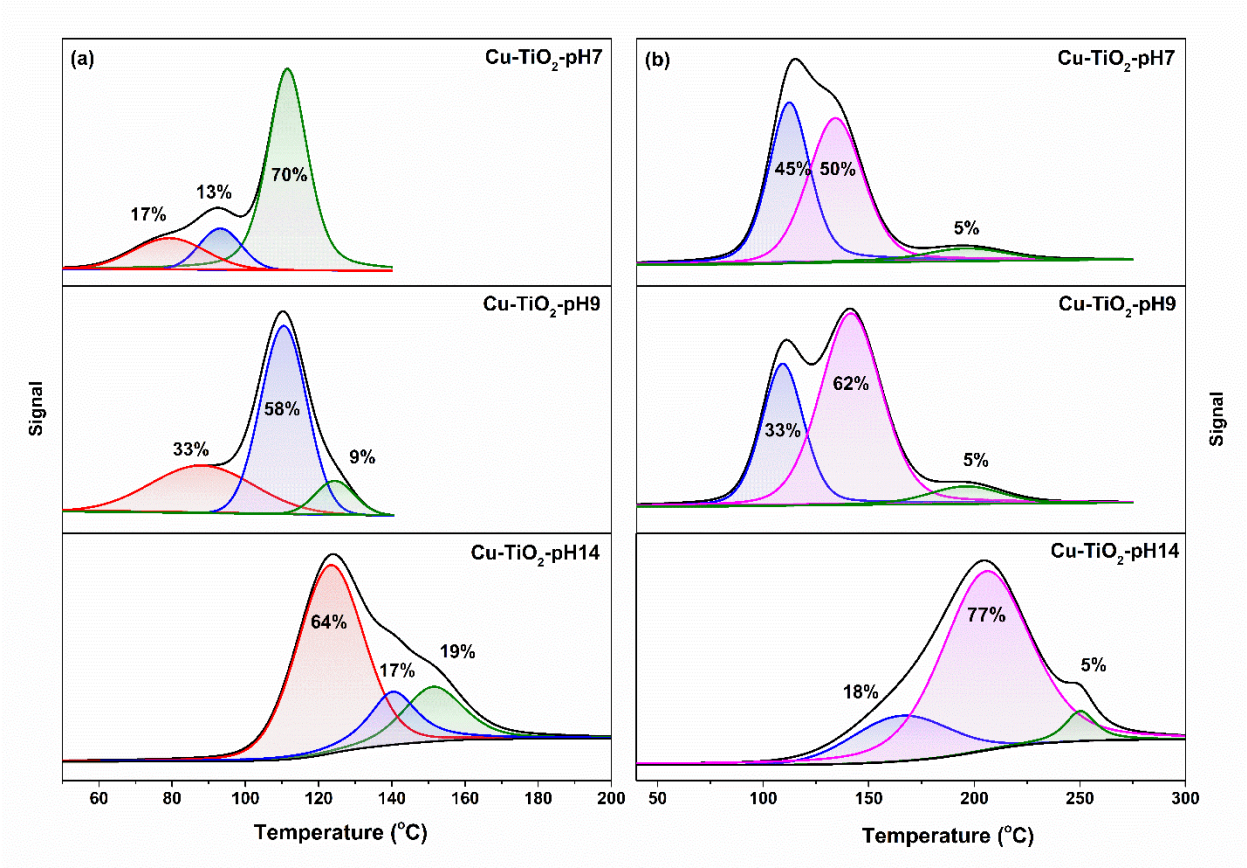

Figure 3.5 (a) Hydrogen-temperature programmed reduction (H_2-TPR) profiles and (b) carbon monoxide-temperature programmed surface reaction (CO-TPSR) profiles for Cu-TiO_2-pH7/ Cu-TiO_2-pH9/ Cu-TiO_2-pH14.

Table 3.2 Analysis of hydrogen-temperature programmed reduction (H_2-TPR).

Sample	Peak I		Peak II		Peak III	
	Temperature (^oC)	Area (%)	Temperature (^oC)	Area (%)	Temperature (^oC)	Area (%)
Cu-TiO_2-pH7	79	17	93	13	112	70
Cu-TiO_2-pH9	88	33	110	58	124	9
Cu-TiO_2-pH14	123	64	140	17	151	19

Hydrogen-temperature programmed reduction (H_2-TPR) was carried out to gain understandings of reducing properties and further reveal different copper species on the surface, as shown in Figure 3.5 (a). For both Cu-TiO_2-pH7 and the Cu-TiO_2-pH9, the reduction started as low as 60 ^oC and completed under 150 ^oC. The majority of reduction peaks occurred below 110 ^oC. Based on peak deconvolution analysis, it suggested there are three different copper states on the surface. The low temperature reduction peaks could be related to either surface oxygen species [101] or highly dispersed copper species located in the Cu-Ti interface area [132]. The overall un-symmetry peak shape indicated the involvement of the step-reduction of copper (II) oxides. The calculated hydrogen consumption corresponding to the step-reduction process decreased from 83 % for Cu-TiO_2-pH7 to 67 % for Cu-TiO_2-pH9 (Table 3.2). Meanwhile, the total hydrogen consumption above 100 ^oC was almost the same for both samples. It could explain why Cu-TiO_2-pH7 and Cu-TiO_2-pH9 have similar activity performance in low temperature ranges. For the Cu-TiO_2-pH14 catalyst, three reduction peaks indicated three different copper states on the surface, similar to other catalysts. However, the reduction reaction over the Cu-TiO_2-pH14 catalyst did not begin until 100 ^oC, and the majority of reduction occurred around 123 ^oC. Our calculations suggested that 36 % of hydrogen consumption over Cu-TiO_2-pH14 occurred at the temperature

above 125 ^{o}C. This high temperature reduction may be related to the reduction of crystalline copper oxide [133]. In summary, H_2-TPR results revealed that the surface copper species have different morphology and oxidation states. Therefore, the types and concentration of surface oxygen species are expected to be different.

Table 3.3 Analysis of carbon monoxide-temperature programmed surface reaction.

Sample	Peak I		Peak II		Peak III	
	Temperature (^{o}C)	Area (%)	Temperature (^{o}C)	Area (%)	Temperature (^{o}C)	Area (%)
Cu-TiO_2-pH7	112	45	134	50	197	5
Cu-TiO_2-pH9	109	33	141	62	196	5
Cu-TiO_2-pH14	165	18	205	77	250	5

CO-Temperature Programmed Surface Reaction (CO-TPSR) was applied to identify the differences among surface oxygen species, and the evolution of carbon dioxide was monitored. Based on peak deconvolution analysis shown in Figure 3.5 (b), three different types of surface oxygen species existed in different temperature ranges. Low temperature (Type I) oxygen species and medium temperature (Type II) oxygen species are dominant for Cu-TiO_2-pH7 and Cu-TiO_2-pH9. As shown in Table 3.3, the summary of area percentage of Type I and Type II species varied with the concentration of surface hydroxyl groups, but close to 95 % of oxygen species were detected under 150 ^{o}C. Type I and Type II oxygen species could be correlated to the high activity of those two catalysts in a lower temperature range. For Cu-TiO_2-pH7 and Cu-TiO_2-pH9, the third peak maintained 5 % contribution to overall reduction regardless of the sample. As a comparison, surface oxygen species were mainly available in the range above 150 ^{o}C for Cu-TiO_2-pH14. Although the first and second peaks for Cu-TiO_2-pH14 also prevailed compared to the third peak,

they appeared above 150 ^{o}C, compared to Cu-TiO_2-pH7 and Cu-TiO_2-pH9. The results from temperature programmed reaction using hydrogen and carbon monoxide as probe molecules confirmed three different active sites on the surface. Catalysts obtained from lower pH values have more active sites compared with the catalyst, which was obtained in high pH values.

3.3.3 CHEMICAL STATES ANALYSIS

X-ray photon spectroscopy (XPS) was employed to analyze the surface composition and oxidation state of copper species and to elucidate the types of oxygen species. As shown in Table 3.4, the surface copper concentration was determined by XPS. Regardless of the washing steps, the value for all Cu-TiO_2 samples was around 6.2 wt%. The similar amount of copper concentration indicated that the copper concentration does not significantly impact the catalytic performance under our reaction conditions. Therefore, the different oxidation states of copper species might be crucial to the reaction.

Table 3.4 Surface copper concentration and composition based on XPS results.

Sample	Copper Concentration		
	XPS [a]	(Cu^+/Cu^{2+}) [b]	(Cu^+/OH^-) [b]
Cu-TiO_2-pH7	6.4	30.8	1.10
Cu-TiO_2-pH9	6.2	36.6	1.09
Cu-TiO_2-pH14	6.2	42.3	0.96

[a] Determined by X-Ray Photon Spectrometry (XPS).

[b] Cu^+ represents the peak area covered by 932.4 eV; Cu^{2+} represents the peak area covered by 933.7 eV; OH^- represents peak area covered by 531.6 eV.

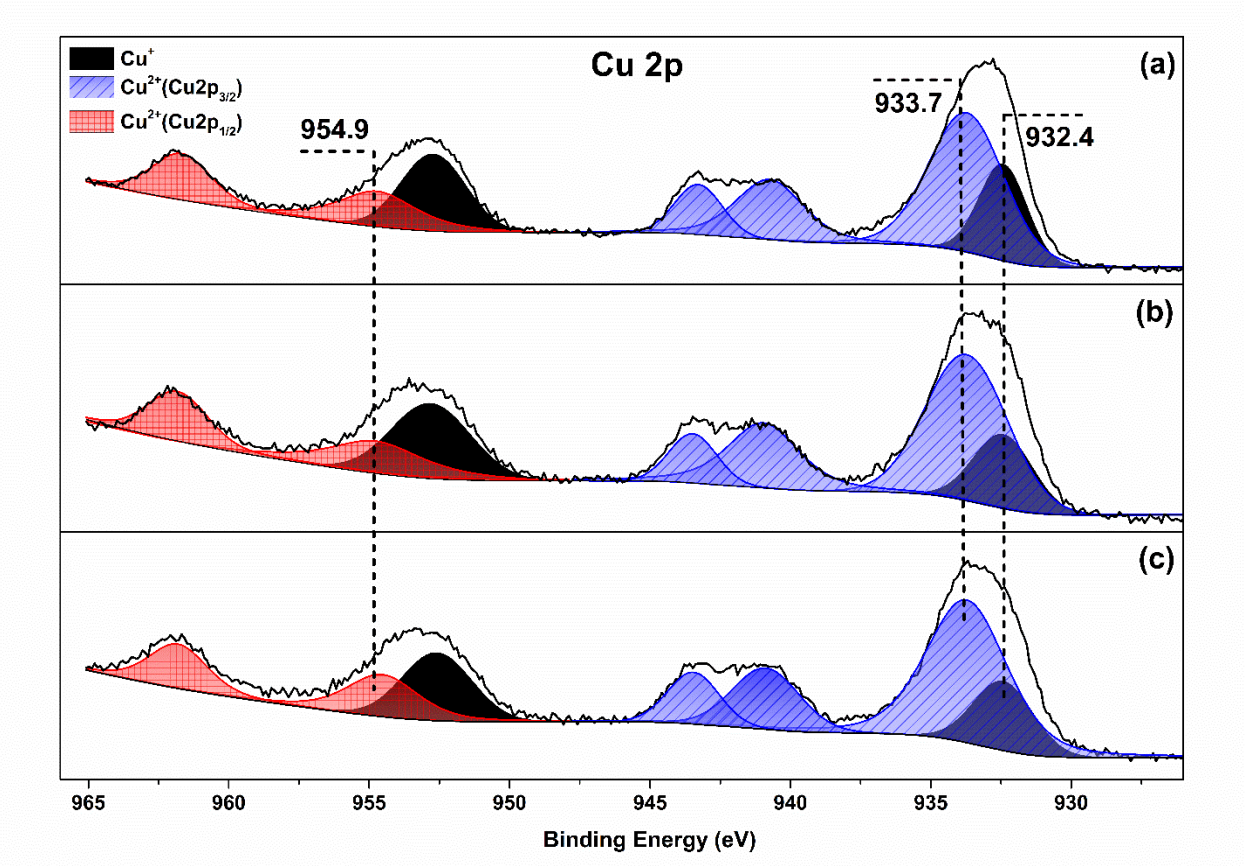

Figure 3.6 Cu XPS profiles for (a) Cu-TiO_2-pH14, (b) Cu-TiO_2-pH9, (c) Cu-TiO_2-pH7.

As shown in Figure 3.6, the XPS spectra of Cu 2p were deconvoluted into three pairs of peaks, which correspond to different copper oxidation states. Both Cu^{2+} and Cu^{+} were detected on the surface of all Cu-TiO_2 catalysts. The existence of Cu^{2+} was evidenced by the typical Cu $2p_{3/2}$ peak at 933.7 eV and two intensive shake-up satellites in the range of 938 - 945 eV [134]. The Cu $2p_{1/2}$ peak located at 954.9 eV and its shake-up satellites in the range of 960 - 965 eV, also attributed to Cu^{2+} [135]. Meanwhile, the existence of Cu^{+} was confirmed by the peak at 932.4 eV and its shake-up satellite peak located at 952.7 eV [136]. The relative ratio between two major copper species, namely 932.4 eV for Cu^{+}, and 933.7eV for Cu^{2+}, were calculated and listed in Table 3.4. The ratio suggested that copper (I) species are much more abundant for Cu-TiO_2-pH14 compared to Cu-TiO_2-pH7. Regarding copper oxides catalysts for CO oxidation, Cu^{+} has been considered as the

active species [104, 131]. In contrast, the Cu-TiO_2-pH7 catalyst presented the best catalytic performance with the least amount of Cu^+. Therefore, other surface species surrounding copper species might also affect the reaction and need to be considered.

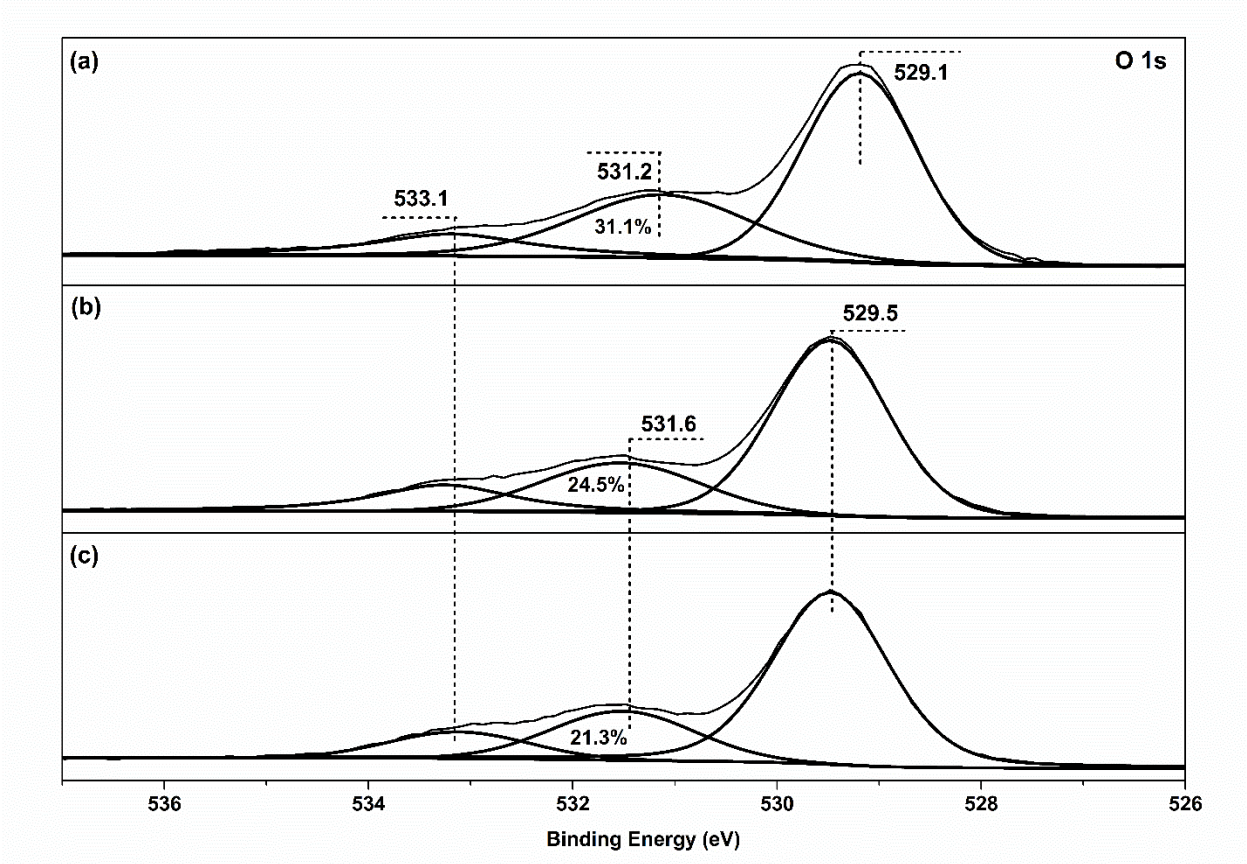

Figure 3.7 Oxygen XPS profiles for (a) Cu-TiO_2-pH14, (b) Cu-TiO_2-pH9, (c) Cu-TiO_2-pH7.

Figure 3.7 presented the O 1s XPS profiles of all catalysts. Three kinds of oxygen species were detected, which are in good agreement with CO-TPSR results. The peaks around 529 eV could be attributed to the lattice oxygen species from titanium dioxide support [137]. The deconvoluted results suggested that with the increase of pH value, the main O 1s peak was gradually shifted from 529.5 eV to 529.1 eV. Additionally, a weak shoulder peak is observed at 533.1 eV, which could be attributed to the oxygen of H-O-H bonds of the chemisorbed water [138]. It did not change at all, regardless of the pH value. We also observed a peak at 531.6 eV, which is related to bridging

surface hydroxyl groups. It increased with the increase of pH value and agreed with the fact that Cu-TiO_2-pH14 was prepared through the higher pH solution. On the surface of Cu-TiO_2-pH7, 21.3 % of oxygen species was hydroxyl groups, which is much lower than that of the Cu-TiO_2-pH14 catalyst. In the meantime, the highest CO conversion was achieved over the Cu-TiO_2-pH7 catalyst. Herein, hydroxyl groups were considered to block the reaction.

3.3.4 IN-SITU DRIFTS

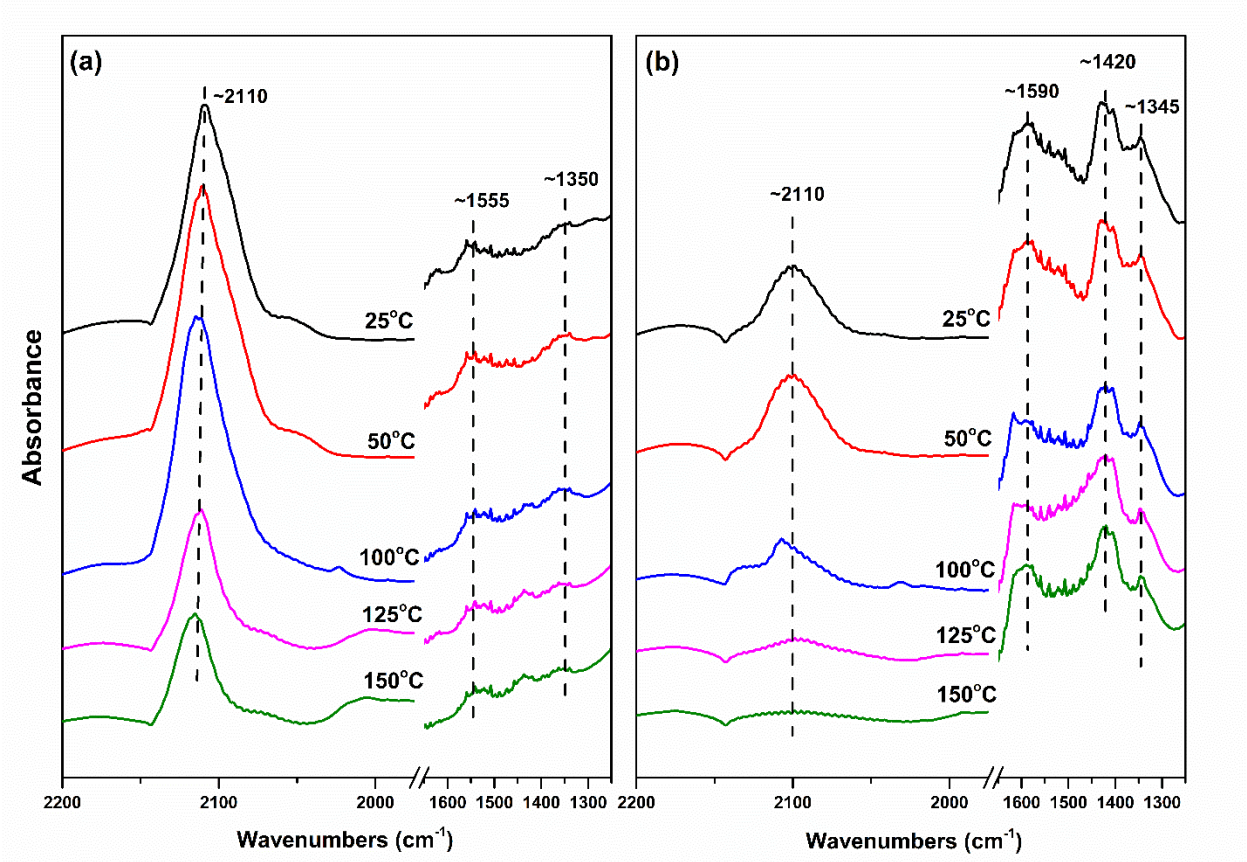

Figure 3.8 In-situ DRIFTS profiles for (a) Cu-TiO_2-pH7 and (b) Cu-TiO_2-pH14. Test conditions: 10%CO/Helium.

To further understand surface properties and the reaction process, in-situ DRIFTS was conducted using carbon monoxide as the probe molecule. The in-situ DRIFTS was recorded and

presented in Figure 3.8. Generally, adsorption of CO molecules on different copper species, such as Cu^{2+}, Cu^{+}, and Cu^{0}, would lead to various absorbance peaks located at 2220-2150 cm^{-1}, 2160-2080 cm^{-1}, and below 2130 cm^{-1}, respectively [139]. Cu^{+}-CO adsorption is the most stable. For the Cu-TiO_2-pH7 sample, the band located at 2110 cm^{-1} is dominant. This band could be assigned to the Cu^{+}-CO interaction [140]. The peaks of CO adsorption confirmed the presence of Cu^{+} on the surface, which in line with the XPS profile. With the increase of temperature, the peak intensities of Cu^{+}-CO increased to the maximum at 100 ^{o}C and then decreased. When the temperature increased, the Cu^{2+} species were reduced gradually to form Cu^{+}, which resulted in the increase of intensity of Cu^{+}-CO peaks. As the temperature continuously increased, Cu^{+} species were further reduced to form Cu^{0}. Along with the bands at 2110 cm^{-1}, weak bands at 1350 cm^{-1} and 1555 cm^{-1} were also observed. The band at 1350 cm^{-1} could be attributed to the poly- or monodentate carbonates [141]. The band at 1555 cm^{-1} is related to bidentate carbonates [142].

For the Cu-TiO_2-pH14 sample, the band around 2110 cm^{-1} was still observed. It suggested the existence of Cu^{+} species. However, the intensity is much lower compared with those observed from the Cu-TiO_2-pH7 sample. Lower intensity indicated less amount of Cu^{+} on the surface, which agreed with the XPS results and confirmed the abundant Cu^{2+} on Cu-TiO_2-pH14. Meanwhile, the bands between 1300 cm^{-1} and 1600 cm^{-1} were clearly dominant over Cu-TiO_2-pH14. The 1345 cm^{-1} bond is associated with v(OCO) of the carboxyl group (COOH) [143]. The band around 1420 cm^{-1} and 1590 cm^{-1} could be attributed to carboxylate (O-C-O) stretching [144, 145]. The surface of the Cu-TiO_2-pH14 catalyst was covered with a much higher concentration of hydroxyl group. Compared with the reaction of carbon monoxide and different oxygen species [101], the surface hydroxyl group would react faster with carbon monoxide. Therefore, the formation of carboxyl

species could explain why the carbon monoxide adsorbed on the surface is much lower compared with that of Cu-TiO_2-pH7 catalyst.

3.4 SUMMARY

In terms of CO oxidation over copper-based catalysts, Cu^+ has been considered the active species [104, 131]. To increase the Cu^+ concentration, a variety of strategies, including preparation methods and pretreatments before activity tests, have been extensively studied. It also explains why the majority of catalysts reported in literature to use the oxidation states of copper to correlate the catalytic performance. Although the variation of synthesis/operation variables could increase the concentration of Cu^+, it also complicated our understandings of the role of Cu^+, because copper species would change after the calcination and pretreatment.

Our approach to synthesize copper oxide is unique because highly dispersed copper oxide supported on titanium dioxide was synthesized through the direct route without calcination. XPS analysis revealed that copper species on the surface are the combination of Cu (I) and Cu (II) oxide. The relative ratio between two major copper species, namely 932.4 eV for Cu^+, and 933. 7eV for Cu^{2+}, suggested that copper (I) species are much more abundant for Cu-TiO_2-pH14. If we followed the traditional perspective to correlate activity with the concentration of Cu^+, it would be challenging because copper species is considered to be the only player in the crowded reaction arena. Meanwhile, Ti^{3+} was suggested to facilitate the formation of Cu^+ through the redox reaction between Cu^{2+} and Ti^{3+}. The alkaline solution promoted the increase of Cu^+ concentration [146]. Clearly, it is reasonable to consider the surroundings next to copper species and include other species while building the property-activity relationship. In our case, the abundance of surface hydroxyl groups is the major difference among different catalysts, besides the Cu^+ concentration. We calculated the ratio between copper (I) and hydroxyl groups and observed this ratio correlated

well with the activity performance. While taking into consideration the concentration of hydroxyl groups, we obtained a high ratio from Cu-TiO_2-pH7. It suggested that the particular reaction domain is controlled by all players in the reaction arena. It is important to balance the active and bystander species while exploring the reaction mechanism.

In conclusion, the synthesis of copper-titanium dioxide through the direct reaction between copper acetate and sodium hydroxide allowed us to identify the role of surface hydroxyl groups in carbon monoxide oxidation. Our results suggested that the activity can not only be determined by the surface abundance of copper (I) species but also the ratio between copper (I) and surface hydroxyl groups needs to be tuned for optimized carbon monoxide conversion.

CHAPTER 4

EFFECT OF PRETREATMENT ON COPPER-TITANIUM DIOXIDE CATALYZED CARBON MONOXIDE OXIDATION

4.1 INTRODUCTION

Copper-based catalysts have been demonstrated to be a potential alternate, attributed to its high activity on CO oxidation and the attention on copper catalysts, which have never diminished. The surface properties and catalytic performance were deeply affected by the synthesis process.

Preparation parameters, such as precursors, copper metal loading, support, calcination temperature, and atmospheres, immensely affected the catalytic behavior [147]. It is essential to perform the investigation with different factors in detail. Attempts have been devoted to tuning the amount of copper loading and modifying TiO_2 support to achieve better catalytic performance. Chen reported the CO oxidation activity over Cu-TiO_2 catalysts would be close to constant for the Cu loading in the range of 3.7 wt % to 10.3 wt % [98]. Kang deposited CuO on TiO_2 supports with the various compositions of anatase and rutile phase [105]. Rutile TiO_2 supported CuO catalyst was illustrated to offer large amounts of oxygen atoms, which resulted in better catalytic performance. Sun studied CO oxidation over CuO/CeO_2 to compare the effects of Cu precursors and calcination temperature [147]. The best activity was observed on CuO/CeO_2, which was prepared from copper acetate and calcined at 500 ^oC. Beyond these, it has been reported the pretreatment conditions are critical to catalytic performance of CO oxidation over other catalysts, such as Pt/TiO_2 and Au/Mn_2O_3 [148, 149], while the effect of calcination atmosphere on CO oxidation over Cu-TiO_2 catalysts has not been presented.

We carried out the CO oxidation over the Cu-TiO_2 catalysts, which were pretreated under oxidative, reductive, and inert gases, respectively. Cu-TiO_2 catalysts were characterized via a series of techniques to understand the composition and chemical states of copper. Furthermore, the effects of calcination atmosphere on the redox properties of copper species and CO oxidation activity were interpreted.

4.2 CARBON MONOXIDE OXIDATION ACTIVITY OVER Cu-TiO_2 CATALYSTS CALCINED IN DIFFERENT GAS ATMOSPHERE

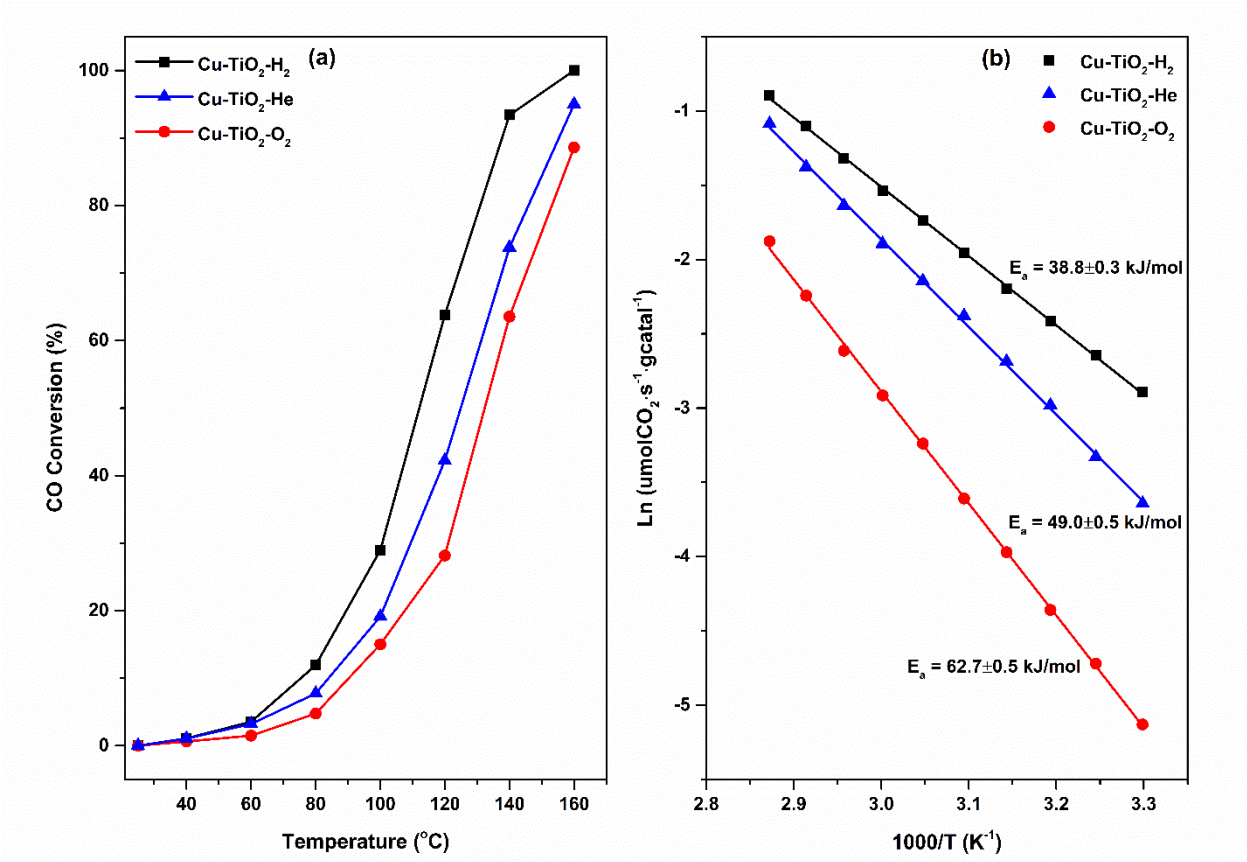

Figure 4.1 Catalytic performance of pretreated Cu-TiO_2 catalysts in carbon monoxide oxidation. (a) Light-off curves, (b) Arrhenius plots, Test condition: 1%CO/20%O_2/ Helium, flow rate 30 mL/min.

The oxidation of CO was employed as a probe reaction in order to reveal the impact of calcination gases on the catalytic performance of Cu-TiO_2 samples. Inert gas Helium treated Cu-TiO_2 sample was referred to as a reference to compare the difference between reduction and oxidation pretreatment. Figure 4.1 (a) presented the conversion of CO as a function of temperature for Cu-TiO_2 samples. It is clear that the activity of Cu-TiO_2 catalysts is sensitive to the pretreatment gases. The activity of catalysts is decreasing in the order of Cu-TiO_2-H_2 > Cu-TiO_2-He > Cu-TiO_2-O_2. Reduced Cu-TiO_2 sample (Cu-TiO_2-H_2), exhibited the best catalytic performance, which reached full CO conversion at 160 ^oC, while oxidized Cu-TiO_2 sample (Cu-TiO_2-O_2) presented an 88.6 % conversion at 160 ^oC, and less than that of Cu-TiO_2-He (95 %). This phenomenon suggested the calcination conditions in the pretreatment process played an important role in the catalytic CO oxidation, especially where the reductive treatment greatly promoted the reaction. The effect may attribute to the reduction or oxidation processes dramatically impact the surface properties of Cu-TiO_2 catalysts. In addition, activation energy and reaction rate were further investigated by performing the reaction in the kinetic regime. As shown in Figure 4.1 (b), reduced Cu-TiO_2 presented the lowest activation energy as 38.8 ± 0.3 kJ/mol, which is 38 % lower than that of Cu-TiO_2-O_2 sample (62.7 ± 0.5 kJ/). Reaction rate over Cu-TiO_2-H_2 at 50 ^oC is 0.14 $\mu mol \cdot s^{-1} \cdot gcatal^{-1}$ which is nearly five times higher than that of Cu-TiO_2-O_2 (0.03 $\mu mol \cdot s^{-1} \cdot gcatal^{-1}$). Cu-$TiO_2$-He presented a three times higher reaction rate than Cu-TiO_2-O_2. In terms of TOF, the highest TOF value was obtained for CO oxidation over Cu-TiO_2-H_2 which is 0.397 s^{-1}. In contrast, Cu-TiO_2-O_2 presented the TOF as low as 0.111 s^{-1}. The difference of activation energy, reaction rate, and TOF among pretreatment conditions, further confirmed the reductive treatment would improve the catalytic performance of CO oxidation over Cu-TiO_2 catalysts.

4.3 CHARACTERIZATION OF PRETREATED Cu-TiO_2 CATALYSTS

4.3.1 PHYSICAL PROPERTIES

BET surface area of Cu-TiO_2 catalysts are listed in Table 4.1. Among the three samples, Cu-TiO_2-H_2 exhibited the highest BET surface area, and more highly dispersed Cu species than Cu-TiO_2-O_2. ICP results suggested that copper concentrations on Cu-TiO_2 catalysts are close and all in the range of 9.1 % to 9.5 %. To investigate the Cu dispersion of Cu-TiO_2 catalysts, N_2O titration was carried out. As shown in Table 4.1, copper dispersion was 22.5 % on Cu-TiO_2-H_2, and a Cu atom surface area of 146 m^2/g was obtained. In the meantime, Cu-TiO_2-O_2 has the lowest dispersion and surface area of a Cu atom. The huge distinction of copper dispersion helped to explain the different surface area of Cu-TiO_2 catalysts. Furthermore, the larger copper dispersion and surface area of Cu-TiO_2-H_2, to some extent, facilitated the CO oxidation reaction and resulted in a higher reaction rate.

Table 4.1 BET surface area and Cu concentration of Cu-TiO_2 catalysts.

Sample	Surface Area ($m^2/g \cdot catal$)	Copper Concentration		
		ICP (%) [a]	Dispersion (%) [b]	Surface Area of Cu atom (m^2/g) [b]
Cu-TiO_2-H_2	78	9.3	22.5	146
Cu-TiO_2-O_2	64	9.1	15.7	101
Cu-TiO_2-He	69	9.5	19.5	126

[a] Determined by Inductive Coupled Plasma. [b] Copper dispersion measured by N_2O titration.

4.3.2 REDOX BEHAVIOURS

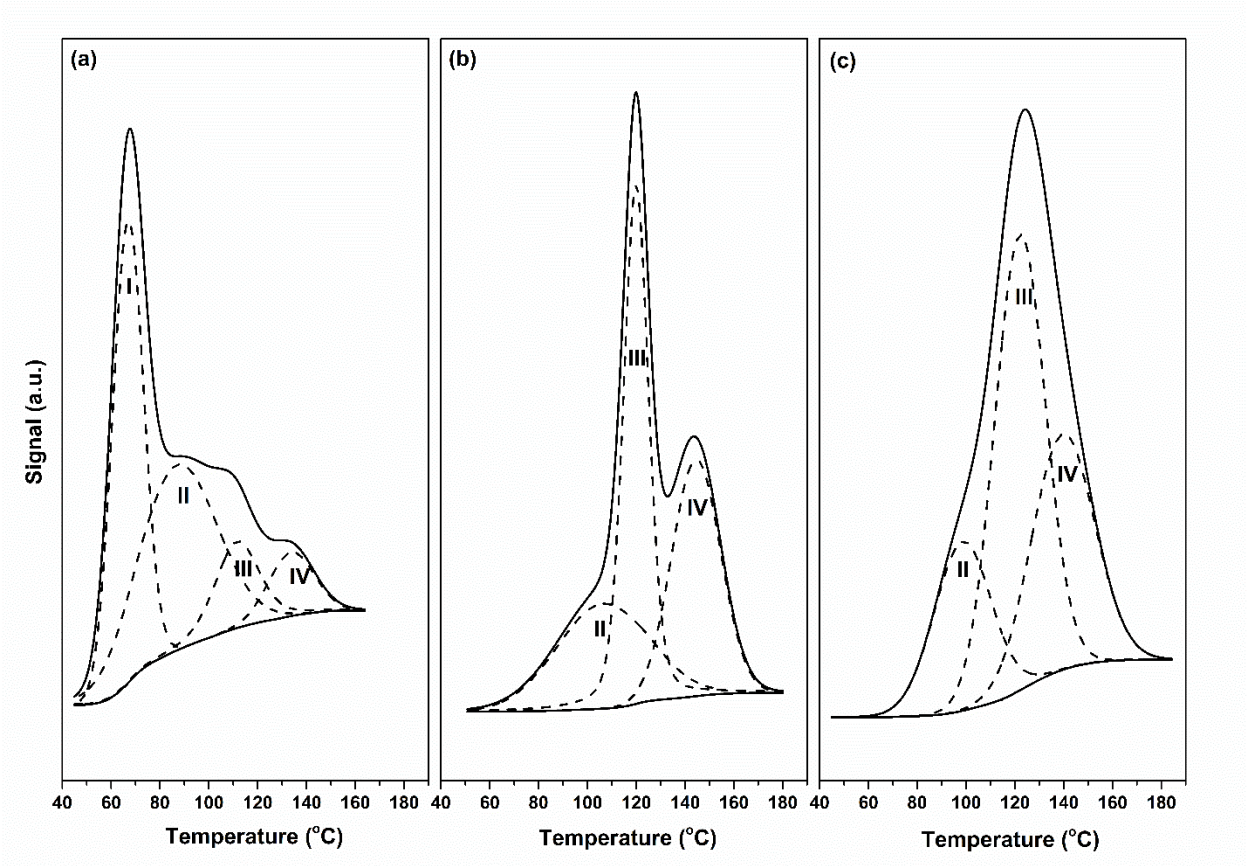

Figure 4.2 H_2-TPR profiles of (a) Cu-TiO_2-H_2, (b) Cu-TiO_2-O_2, and (c) Cu-TiO_2-He catalysts.

The reducing properties of the Cu-TiO_2 catalysts are characterized by hydrogen temperature programmed reduction (H_2-TPR). The H_2-TPR profiles of all three samples were shown in Figure 4.2. For Cu-TiO_2-H_2, the reduction started as low as 50 ^oC and completed around 160 ^oC. The majority of reduction peaks occurred below 100 ^oC. As a comparison, for Cu-TiO_2-O_2 and Cu-TiO_2-He, the reduction started around 60 ^oC and completed at 180 ^oC. These terminative temperatures are close to that of Cu-TiO_2-H_2. However, a large proportion of reduction peaks of Cu-TiO_2-O_2 and Cu-TiO_2-He occurred above 100 ^oC. To further investigate the different surface copper species, all TPR profiles are fitted with Gaussian function, and peak deconvolution results

were listed in Figure 4.2 and Table 4.2. Cu-TiO_2-H_2 has four individual reduction peaks, which represented four different copper states on the surface. Peak I was related to highly dispersed copper species on the surface [130, 150]. Peak II and Peak III can be assigned to step reduction of copper (II) oxides. Peak IV can be assigned to the reduction of crystalline CuO or copper species that have strong interaction with the support. On the contrary, Cu-TiO_2-O_2 and Cu-TiO_2-He only presented three reduction peaks, indicating none or a very small amount of highly dispersed copper species that existed on the surface.

Table 4.2 Analysis of hydrogen-temperature programmed reduction (H_2-TPR).

Sample	Peak I		Peak II		Peak III		Peak IV	
	Temp (^oC)	Area (%)	Temp (^oC)	Area (%)	Temp (^oC)	Area (%)	Temp (^oC)	Area (%)
Cu-TiO_2-H_2	67	40	87	40	112	12	134	8
Cu-TiO_2-O_2	--	--	106	27	120	41	145	32
Cu-TiO_2-He	--	--	99	20	122	49	140	31

In the meantime, as shown in Table 4.2, hydrogen consumption calculation provided intuitive comparison. The results indicated that 40 % of H_2 consumption occurred on highly dispersed copper species over Cu-TiO_2-H_2. More importantly, 92 % of hydrogen was consumed below 120 ^oC for Cu-TiO_2-H_2. However, only less than 30 % of hydrogen was consumed below 120 ^oC over Cu-TiO_2-O_2 and Cu-TiO_2-He. This consumption percentage is much lower than that of Cu-TiO_2-H_2. Meanwhile, peak IV indicated that more than 30 % of hydrogen consumption occurred on the crystalline CuO of Cu-TiO_2-O_2 and Cu-TiO_2-He. In summary, different kinds of surface copper species were identified by H_2-TPR. Highly dispersed copper species were identified on Cu-TiO_2-H_2 and more crystalline CuO on Cu-TiO_2-O_2. As a consequence, the reductive pretreatment process greatly affected the dispersion and morphology of surface copper species.

4.3.3 CHEMICAL STATES ANALYSIS

X-ray photon spectroscopy (XPS) was employed to explore the effect of pretreatment conditions on the oxidation state of copper species, oxidation state of titanium, and the types of oxygen species.

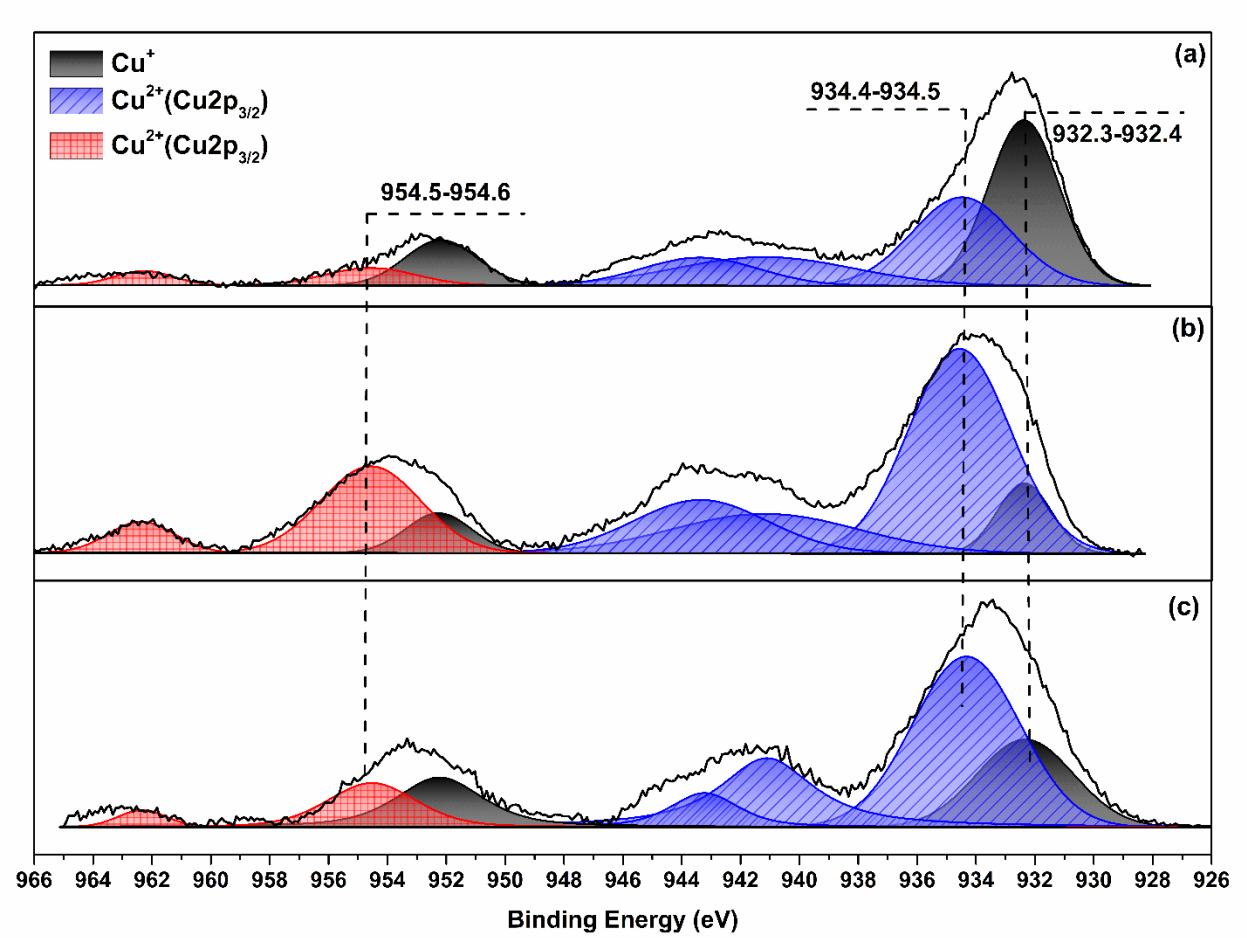

Figure 4.3 XPS spectra of Cu 2p of (a) Cu-TiO_2-H_2, (b) Cu-TiO_2-O_2, and (c) Cu-TiO_2-He.

The different pretreatment conditions could change the oxidation state of copper species. The XPS spectra of Cu 2p were deconvoluted and shown in Figure 4.3. Three pairs of peaks were identified and correspond to different copper oxidation states. The existence of Cu^+ was confirmed by a peak at 932.3-932.4 eV and its shake-up satellite peak located at 952.5 eV [136]. The Cu^{2+} was confirmed by typical Cu $2p_{3/2}$ peaks, which peak located at 934.4-934.5 eV and two intensive

shake-up satellites in the range of 938 - 946 eV, along with the Cu $2p_{1/2}$ peak located at 954.5-954.6 eV and its shake-up satellites in the range of 960 - 965 eV [135].

Table 4.3 XPS results analysis of Cu-TiO_2 catalysts.

Sample	$Cu^+/(Cu^+ + Cu^{2+})$, %	Ti^{3+}, %	$[O]_{surf}$, %	$Cu^+/[O]_{surf}$
Cu-TiO_2, H_2	62.7	11.3	13.9	4.51
Cu-TiO_2, O_2	19.3	--	58.4	0.33
Cu-TiO_2, He	43.3	7.1	16.6	2.61

Furthermore, we calculated the Cu^+ ratio based on the XPS spectra and listed in Table 4.3. Cu^+ ratios of Cu-TiO_2-H_2 and Cu-TiO_2-He are 62.7 % and 43.3 %, respectively. While Cu-TiO_2-O_2 only has 19.3 % of Cu^+ on the surface. The results indicated the pretreatment conditions greatly impact the oxidation states of copper. Reductive treatment by hydrogen promoted the reduction of copper species to Cu^+ and resulted in a higher fraction of Cu^+. However, in Cu-TiO_2-O_2, partial of Cu^+ was oxidized to Cu^{2+} and resulted in the least amount of Cu^+. It has been reported that Cu^+ is critical to the catalytic performance of CO oxidation over copper-based catalysts [104, 131]. Herein, XPS results accorded with the conclusion from light-off that Cu-TiO_2-H_2 is the best among all three catalysts.

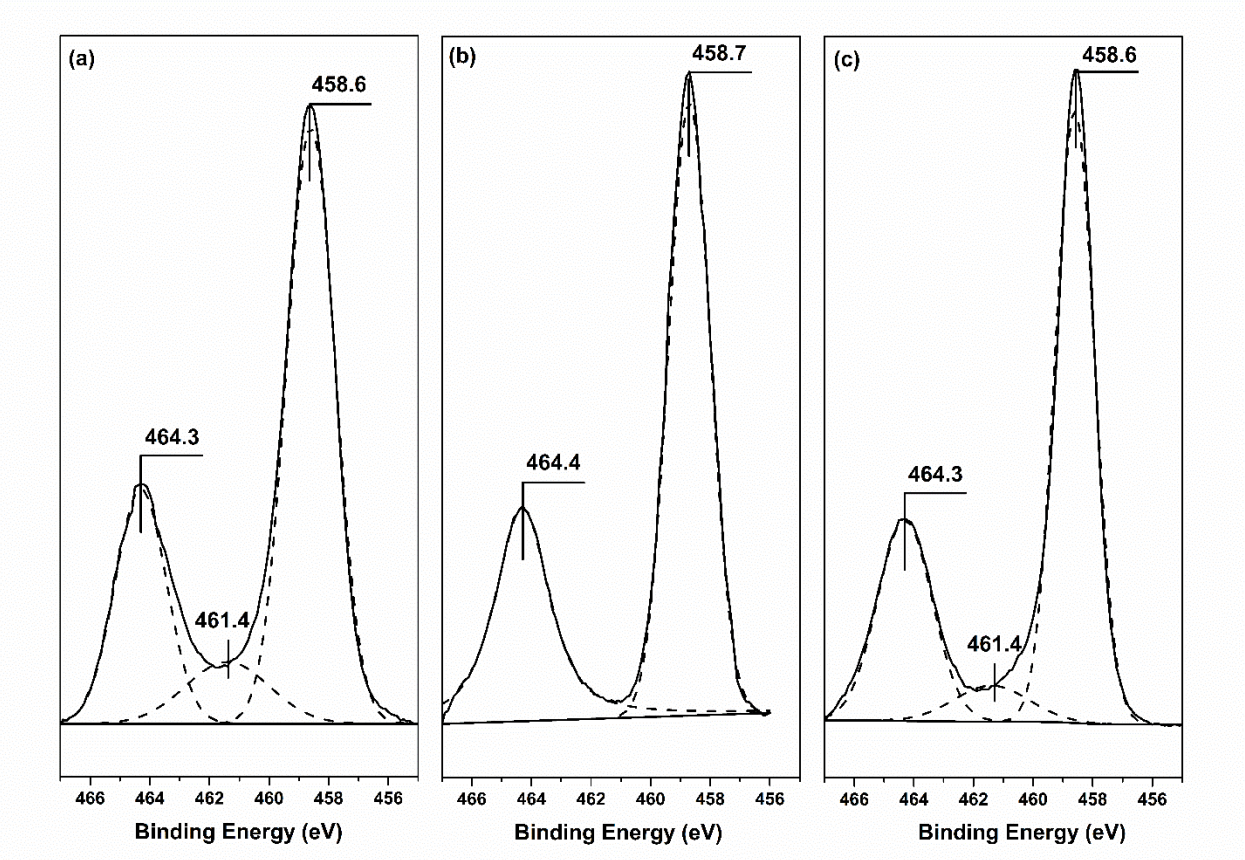

Figure 4.4 XPS Ti 2p of (a) Cu-TiO_2-H_2, (b) Cu-TiO_2-O_2, and (c) Cu-TiO_2-He.

The pretreatment process could affect the chemical state of titanium as well. XPS Ti 2p profiles were shown in Figure 4.4. Peaks located at 458.6 - 458.7 eV and 464.3 - 464.4 eV were attributed to Ti^{4+} [151, 152], which is the dominant oxidation state of titanium over TiO_2. These typical Ti^{4+} peaks were observed for all Cu-TiO_2 catalysts. Additionally, the pretreatment process, especially reductive pretreatment would possibly reduce the Ti^{4+} to Ti^{3+}. As shown in Figure 4.4 (a) an (c), presence of Ti^{3+} was revealed by the peaks occurred at 461.4 eV on Cu-TiO_2-H_2 and Cu-TiO_2-He [153]. This indicated the support was reduced in reductive condition. The pretreatment in inert gas was also able to affect the support by impacting the bonding between titanium atoms and oxygen atoms. However, Ti^{3+} was not detected on Cu-TiO_2-O_2. Ti^{3+} has been reported to be able to reduce Cu^{2+} to Cu^{+}. Apparently, pretreatment process has an impact on the oxidation state of titanium

which could further affect the oxidation state of copper, but the effect varies upon different pretreatment conditions. By calculating the amount of different types of titanium, the results shown in Table 4.3 suggested that the amount Ti^{3+} increased from 7.1 % to 11.3 % when pretreating the Cu-TiO_2 using hydrogen instead of Helium. The 60 % increase of Ti^{3+} is on account of the reduction of titanium when hydrogen was employed. Meanwhile, oxidatively pretreatment could restrain the formation of Ti^{3+} during the pretreating process by oxidizing the Ti^{3+} to Ti^{4+}. Therefore, there is no Ti^{3+} for Cu-TiO_2-O_2.

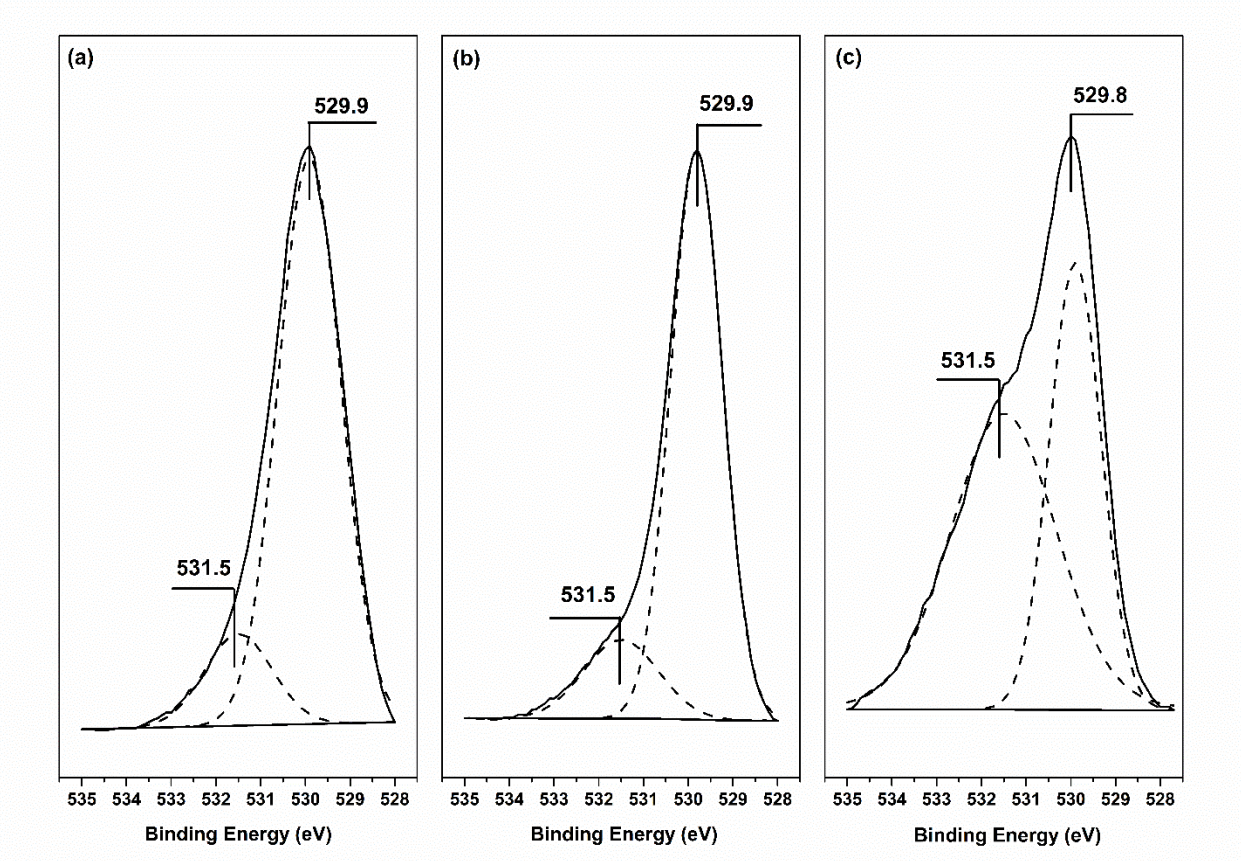

Figure 4.5 XPS O 1s of (a) Cu-TiO_2-H_2, (b) Cu-TiO_2-He, (c) Cu-TiO_2-O_2.

In addition to the chemical states of copper species and titanium, we compared the XPS O 1s profiles to understand the types of oxygen species as they are also crucial to catalytic performance. As shown in Figure 4.5, O 1s profile revealed two different oxygen species on the surface of all

three Cu-TiO_2 catalysts. The peak at 529.8 - 529.9 eV is assigned to the lattice oxygen related to the TiO_2 support [137]. The peak located at 531.5 eV is attributed to the surface-active oxygen ($[O]_{surf}$) [154]. The peak deconvolution results indicated the oxidatively pretreated Cu-TiO_2 has 58.4 % of surface-active oxygen species, which is much higher than that of the other two samples. It suggested the different pretreatment conditions affected the oxygen species.

4.3.4 IN-SITU DRIFTS

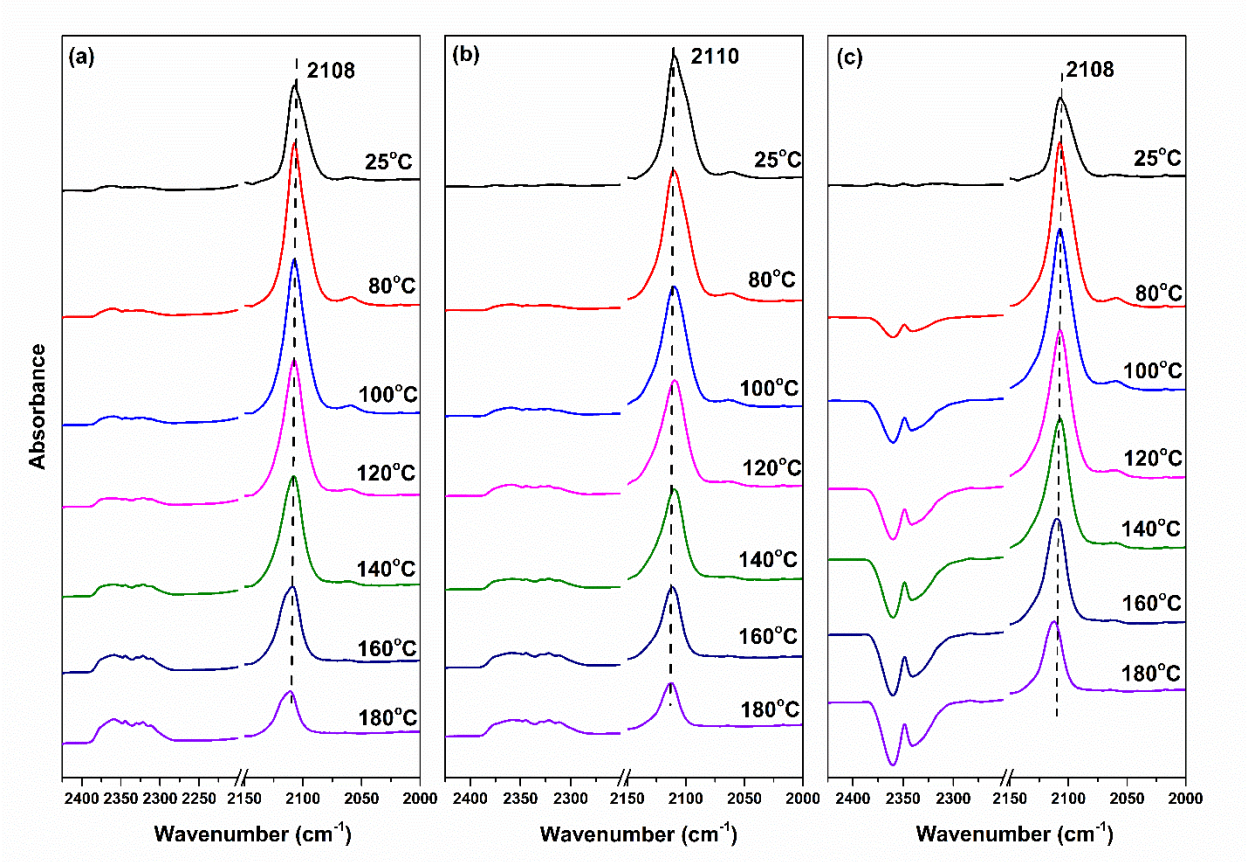

Figure 4.6 In-situ DRIFT of (a) Cu-TiO_2-H_2, (b) Cu-TiO_2-O_2, and (c) Cu-TiO_2-He. Test condition: 1%CO, 20%O_2, balanced in Helium.

To investigate the surface reaction process further, in-situ DRIFTS of CO and O_2 adsorption on Cu-TiO_2 catalysts were conducted under the reaction condition. The in-situ DRIFTS was recorded while temperature ranges from 25 ^oC to 180 ^oC and presented in Figure 4.6. The major

feature of those spectra is a broad band around 2108 - 2010 cm^{-1}. This vibration band is the characteristic band of Cu^{+}-CO bond [140]. The Cu^{+}-CO peaks confirmed the presence of Cu^{+} on the surface, which matched the XPS profiles. The intensity of this band is sensitive to the temperature. With the increase of temperature, the peak intensities of Cu^{+}-CO increased to the maximum at 80 ^{o}C and then decreased. Temperature-dependence trends are applied to all Cu-TiO_2 catalysts. Another apparent peak around 2340 - 2360 cm^{-1} was attributed to CO_2, which came from the CO oxidation [155]. The obvious increase on Cu-TiO_2-H_2 suggested the rapid reaction, which agreed with the light-off and reaction rate conclusion.

4.4 SUMMARY

In the case of Cu-TiO_2 catalyzed CO oxidation reaction, surface species played a significant role in determining catalytic performance. Surface Cu^{+} has been proposed as the active species toward CO oxidation [104, 131]. Meanwhile, it is well known that the high concentration of surface oxygen species is beneficial for the activity of catalytic oxidation [18]. Therefore, it is critical to understand how the pretreatment process affects the surface copper species and oxygen species while evaluating the effect of the calcination atmosphere on the catalytic performance.

As prepared Cu-TiO_2 catalysts were synthesized with the same copper precursor, support, and calcination temperature, and ICP results revealed similar copper concentration on the surface. These processes created an isolated space, which allowed us to focus on the effect of the calcination atmosphere. H_2-TPR results demonstrated a unique reduction peak on Cu-TiO_2-H_2 catalyst, which is correlated to finely dispersed copper species at low temperature. It also can be seen that the majority of reduction occurred at a lower temperature than that of Cu-TiO_2-O_2 and Cu-TiO_2-He. These results indicated the reductive pretreatment facilitated the reduction of copper to a great extent. Comparing the XPS spectra of Cu 2p, copper species presented in the form of

both Cu (I) and Cu (II) on all Cu-TiO_2 catalysts. Calculation on the concentration of Cu^+ suggested Cu (I) species are much more abundant on Cu-TiO_2-H_2 than Cu-TiO_2-He and Cu-TiO_2-O_2. Clearly, the reductive pretreatment was able to reduce the surface copper species to produce more Cu (I) species, which is a benefit to the catalytic performance. Further impact of different pretreatment conditions would be occurred on the TiO_2 support and eventually affect the surface properties. Ti^{3+} was considered to promote the reduction of Cu^{2+}, was only detected on the Cu-TiO_2-H_2 and Cu-TiO_2-He. In addition, XPS results indicated Cu-TiO_2-O_2 contained four times higher the amount of surface oxygen species than others. However, Cu-TiO_2-O_2 exhibited the worst catalytic performance, which is in contrast with the promotion effect of surface oxygen species. To correlate both the Cu (I) species and surface oxygen species to catalytic performance, a ratio between them was defined as $[Cu^+]/[O]_{surf}$. As listed in Table 4.3, it was determined as 4.51, 2.61, and 0.33 for Cu-TiO_2-H_2, Cu-TiO_2-O_2, and Cu-TiO_2-He, respectively. A positive relationship was established between the ratio and reaction rate, which suggested considering both Cu (I) and surface oxygen species to evaluate the catalysts.

In conclusion, we investigated the effect of calcination atmosphere on CO oxidation over Cu-TiO_2 catalysts and revealed the reductive pretreatment would greatly improve the copper dispersion and the formation of Cu (I) species. The promotion on reaction rates could be interpreted by the co-effect of Cu (I) species and surface oxygen species. The defined ratio of $[Cu^+]/[O]_{surf}$ precisely correlated to catalytic performance among all three catalysts.

CHAPTER 5

EFFECT OF NITROGEN DOPING ON CARBON MONOXIDE OXIDATION OVER COPPER-TITANIUM DIOXIDE CATALYSTS

5.1 INTRODUCTION

Copper-Titanium dioxide (Cu-TiO_2) catalyst has emerged as one of the robust catalysts to transform a variety of small molecules, including carbon monoxide, carbon dioxide, and methanol, into valuable chemicals [126, 127]. It is evident that enhanced interaction between nanosized copper oxide and titanium dioxide contributes to the increase in reaction rate [156]. The choice of synthesis strategy plays an important role in obtaining the nanosized copper oxides. Traditional wet-impregnation method using copper nitrate as precursor, which results in the copper particle size around 20 nm when the copper loading reached to 8 wt% [157]. However, copper particle sizes would be just around 6 nm through the photo-deposition method using copper nitrate in ethanol solution [158]. Tuning surface properties of titanium dioxide provides an alternative approach to enhance the interaction between copper and titanium dioxide [159]. Titanium dioxide has three different phases, namely anatase, rutile, and brookite. Those phases have different surface oxygen concentrations because of different arrangement of titanium atoms and oxygen atoms, especially on few layers near the surface. Copper supported on rutile phase TiO_2 demonstrated a higher reaction rate compared with that of anatase phase TiO_2 in CO oxidation [104]. The difference was suggested from TiO_2 phase also led to the variation of surface Ti^{3+} concentration, which would facilitate the formation of Cu^+ through the redox reaction, $Cu^{2+} + Ti^{3+} \rightarrow Cu^+ + Ti^{4+}$.

Besides choosing different TiO_2 phases, the addition of a third atom, such as hydrogen, nitrogen, and boron, provides another direction to optimize the surface oxygen vacancies [160, 161]. When it comes to the synthesis of nitrogen modified titanium dioxide, N-TiO_2, two approaches have been investigated. The first one is through in-situ approach, where nitrogen precursor was directly mixed with titanium precursors [162]. The second one is through the post-synthesis approach, where gaseous ammonia under high temperature was usually applied [163]. Both approaches could anchor nitrogen atoms on the surface of TiO_2. Meanwhile, the type nitrogen species and their concentrations varied with the choice of nitrogen sources. Here we adapted the urea pyrolysis approach to prepare N-TiO_2 and investigated its promotion effect as supports for copper catalysts in carbon monoxide oxidation.

5.2 CARBON MONOXIDE OXIDATION ACTIVITY OVER Cu-N-TiO_2 CATALYST

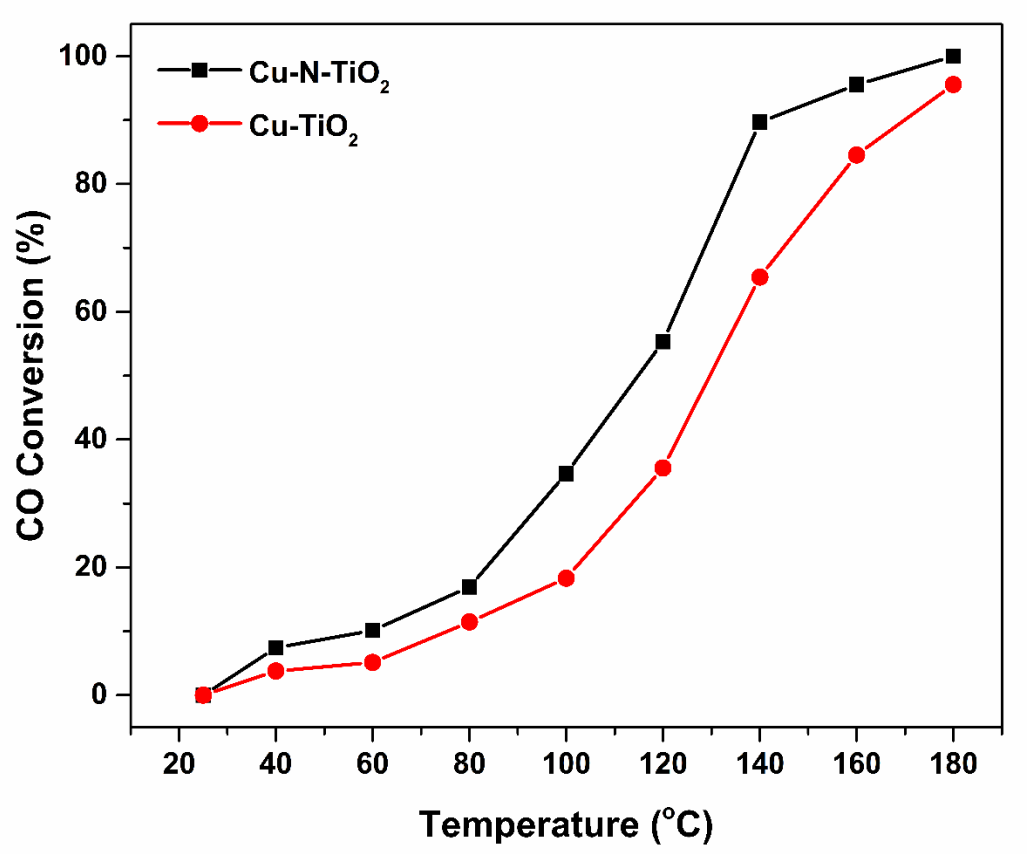

Figure 5.1 Light-off curves of Cu-N-TiO_2 and Cu-TiO_2 samples. Test condition: 1%CO/20%O_2/Helium, flow rate 30 mL/min.

Nitrogen modified Cu-TiO_2 catalyst was evaluated for carbon monoxide oxidation and compared with no nitrogen introduced Cu-TiO_2 catalyst. The light-off activity tests results were shown in Figure 5.1. The activities of catalysts are closely affected by the introduction of nitrogen to the support, as it indicates that the nitrogen modified Cu-TiO_2 sample has much better activity performance. Cu-N-TiO_2 achieved T_{50} at 113 ^oC and achieved full CO conversion when the reaction temperature reached 180 ^oC. Meanwhile, the carbon monoxide conversion over Cu-TiO_2 reached 50 % conversion at 130 ^oC, which is higher than Cu-N-TiO_2, and CO did not fully convert

at 180 °C. In the present work, the applied supports N-TiO_2 and TiO_2 both been calcined to reduce the effect of calcination process. Meanwhile, the same as-designed Cu loading (10 wt%) was used to eliminate the impact of copper concentration. Therefore, the introduction of nitrogen would be the primary factor to result in activity difference among all catalysts.

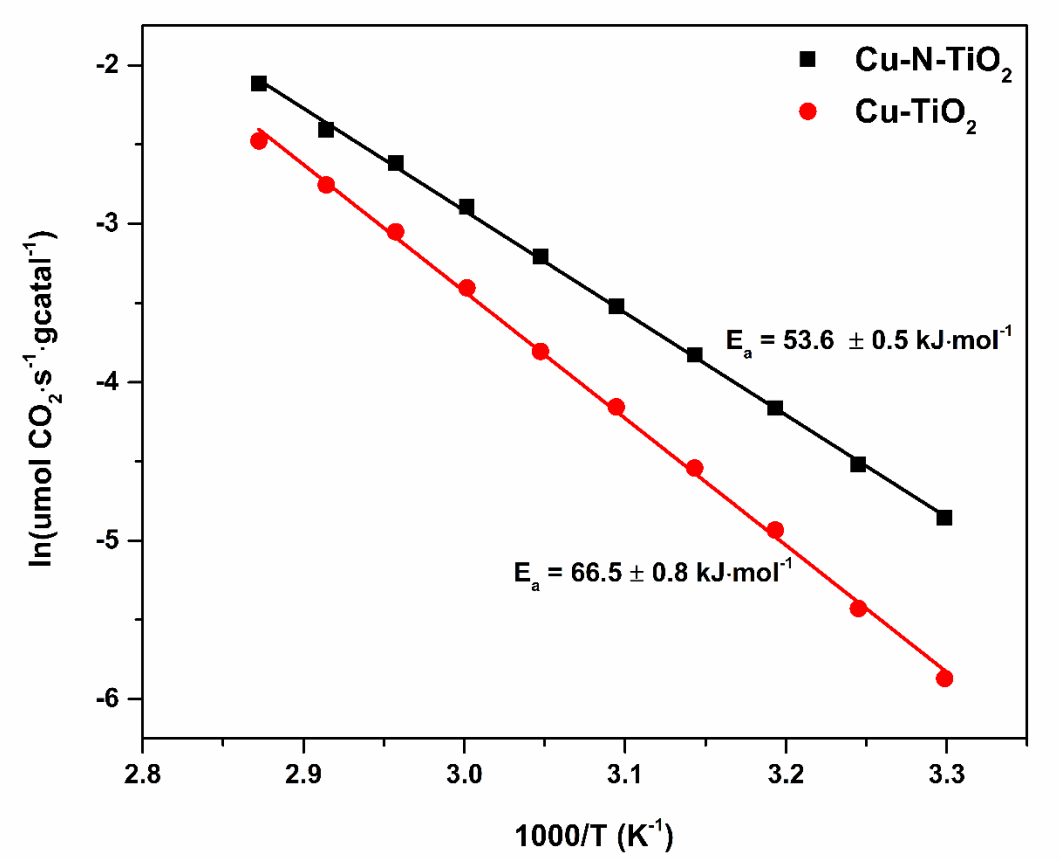

Figure 5.2 Arrhenius plot of activation energy of CO oxidation over Cu-N-TiO_2 and Cu-TiO_2.

Further catalytic evaluation was performed to identify reaction rate and activation energy over Cu-N-TiO_2 and Cu-TiO_2. Cu-N-TiO_2 catalyst prevailed over Cu-TiO_2 catalyst on CO oxidation. The reaction rate obtained at 70 °C is 0.098 μmol·s^{-1}·$gcatal^{-1}$ and 0.061 μmol·s^{-1}·$gcatal^{-1}$ for Cu-N-TiO_2 and Cu-TiO_2, respectively. Cu-N-TiO_2 presented 60 % faster of reaction rate than Cu-TiO_2. In terms of TOF, Cu-N-TiO_2 presented the value of 0.11 s^{-1}, which was higher than 0.065 of Cu-TiO_2. In the meantime, the Arrhenius plot and the activation energy of both catalysts were shown

in Figure 5.2. The activation energy values were calculated as 53.6 ± 0.5 kJ/mol for Cu-N-TiO_2 and 66.5 ± 0.8 kJ/mol for Cu-TiO_2 catalysts. These results agreed with the values of activation energy obtained over Cu-TiO_2 catalysts, which were synthesized through different approaches. The activation energy for copper over other supports (including CeO_2) ranges from 50 kJ/mol to 65 kJ/mol, depending on the choice of supports [110]. The activation energy was decreased by 20 % after nitrogen was introduced. Hence, nitrogen was critical to the facilitation of CO oxidation.

5.3 CHARACTERIZATION OF Cu-N-TiO_2 CATALYSTS

5.3.1 PHYSICAL PROPERTIES

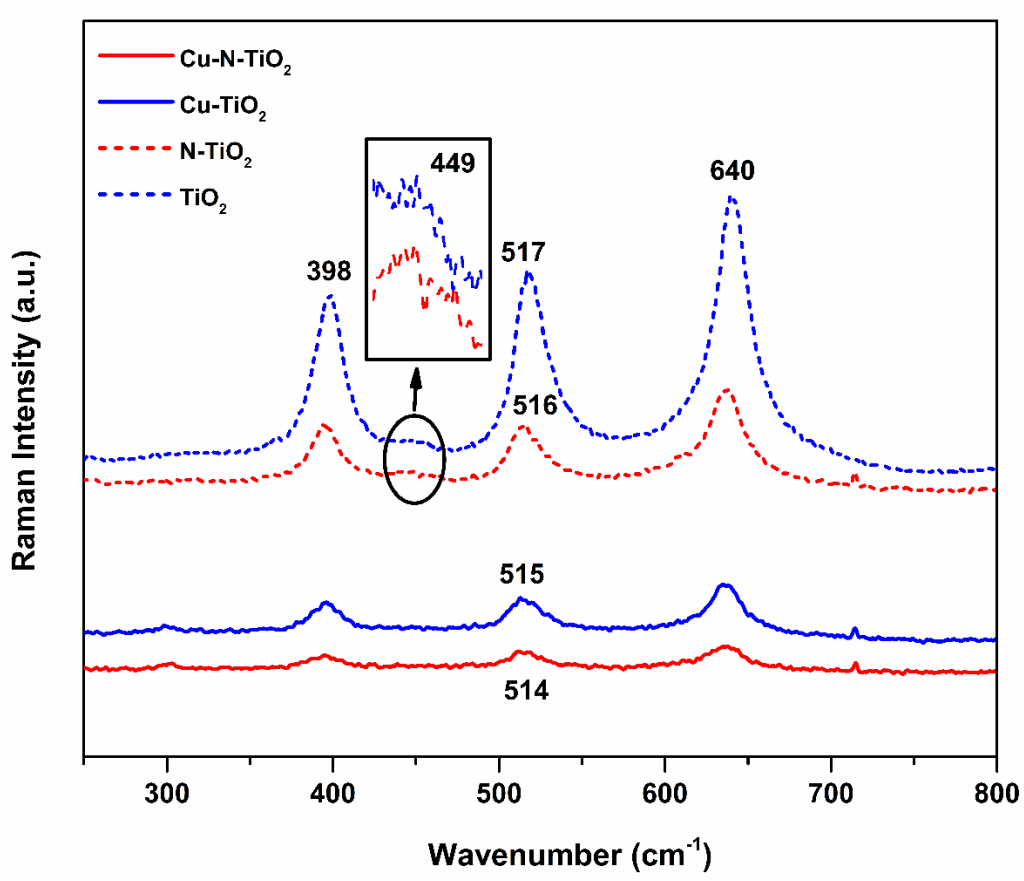

Figure 5.3 Raman spectra of Cu-N-TiO_2, Cu-TiO_2, N-TiO_2 and TiO_2 supports.

Raman spectroscopy was employed to gain structural information of supports and copper modified titanium dioxide catalysts. Raman spectroscopy results shown in Figure 5.3, confirmed that P25-TiO_2 is the mixture of anatase phase and rutile phase TiO_2. Three strong Raman bands located at 398 cm^{-1}, 517cm^{-1}, and 640 cm^{-1}, were observed over unmodified TiO_2 support. Those bands are assigned to the anatase phase TiO_2 [164]. One weak Raman band located at 449 cm^{-1}, which is associated with the rutile phase TiO_2 was also observed [164]. The overall Raman bands intensities were decreased with the introduction of nitrogen. All Raman bands corresponded to the anatase phase were still observed, but their intensities were decreased with further introduction of copper to supports (including TiO_2 and N-TiO_2). All characteristic bands also slightly shifted to the lower wavelength, which could be related to the adjustment of lattice structure with the nitrogen modification. Meanwhile, Raman bands related to the rutile phase disappeared. The decrease of Raman bands intensity and no observations of new bands would suggest that copper oxide may be well-dispersed on the surface.

Table 5.1 Physical properties of Cu-N-TiO_2 and Cu-TiO_2 catalysts.

Sample	Surface Area (m^2/g·catal)	Copper Concentration		
		ICP (%) [a]	Dispersion (%) [b]	Surface Area of Cu atom (m^2/g) [b]
Cu-N-TiO_2	96	9.4	62.5	423
Cu-TiO_2	85	9.1	58.8	398

[a] Determined by Inductive Coupled Plasma. [b] Copper dispersion measured by N_2O titration.

Detecting the real loaded amount of copper on the catalysts surface, helps to understand the different light-off tests performance of all samples. As listed in Table 5.1, ICP tests indicated Cu-N-TiO_2 and Cu-TiO_2 have the similar amount of copper, suggesting the introduced nitrogen will have less effect on the overall loaded amount of copper. By applying N_2O titration, copper

dispersion, and surface area of Cu atoms were determined. As shown in Table 5.1, highly dispersed Cu were obtained based on Cu dispersion and surface area of Cu atoms for Cu-N-TiO_2 and Cu-TiO_2. In comparison, Cu-N-TiO_2 presented higher Cu dispersion and larger surface area than that of Cu-TiO_2. This implied that the introduced nitrogen was able to facilitate the dispersion of Cu on the surface. Therefore, the ICP and Cu dispersion results suggested the existence of highly dispersed copper species on supports and further confirmed the decreasing of Raman bands intensity was attributed to well-dispersed copper species.

5.3.2 CHEMICAL STATES ANALYSIS

X-ray photon spectroscopy (XPS) was performed to analyze the surface composition, investigate the presence of nitrogen, reveal oxidation state of copper species as well as to elucidate the types of oxygen species.

Table 5.2 XPS results analysis of Cu-N-TiO_2 and Cu-TiO_2 catalysts.

Sample	N (%)	$Cu^+ / (Cu^+ + Cu^{2+})$ (%)	O / Ti	$Cu^+ / [O]_{surf}$
Cu-N-TiO_2	1.1	24.9	1.96	1.29
Cu-TiO_2	--	22.6	2.21	1.11

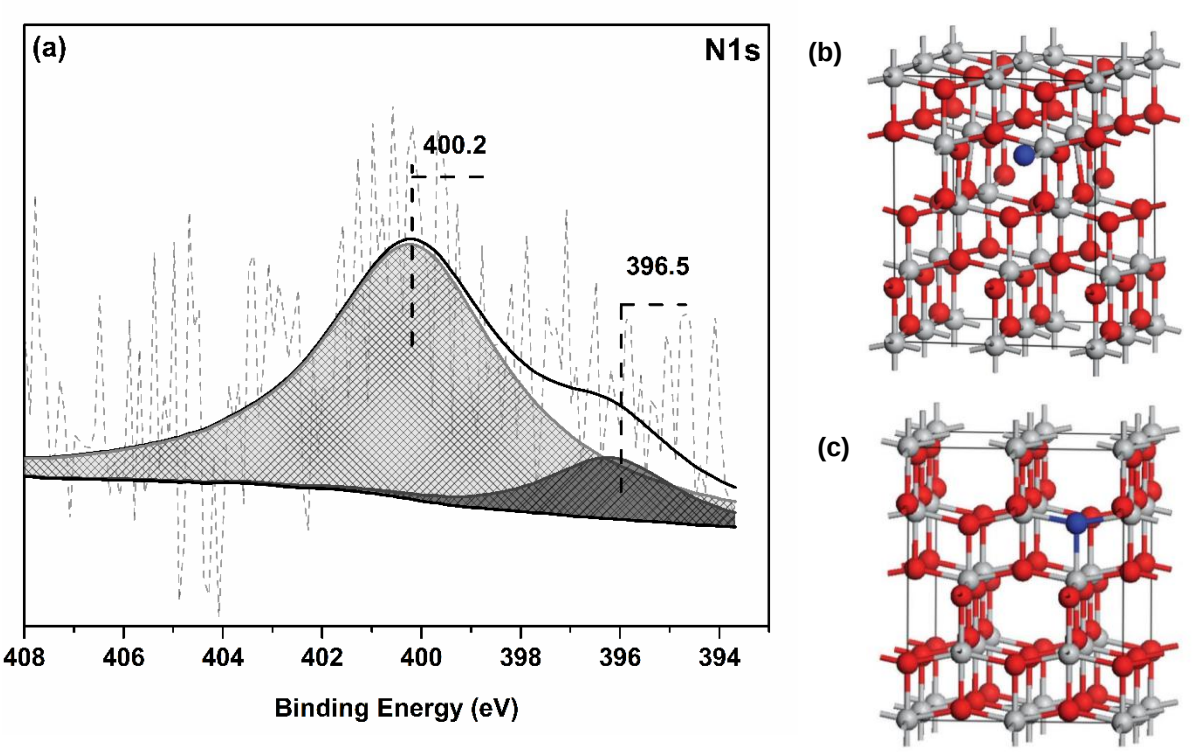

Figure 5.4 (a) XPS N 1s spectra over N-TiO_2 support, (b) interstitial nitrogen doping in TiO_2, (c) substitutional nitrogen doping in TiO_2 [165, 166].

In order to investigate if nitrogen was successfully introduced into TiO_2 support, XPS N 1s spectra of N-TiO_2 support was collected and presented in Figure 5.4. The results confirmed the success of introducing nitrogen to TiO_2, and the amount of nitrogen was 1.1 % (shown in Table 5.2). No nitrogen signals were detected for pure TiO_2 support. However, a broad N 1s profile was observed over N-TiO_2 support (shown in Figure 5.4 (a)). The peak deconvolution analysis revealed two different nitrogen states on the surface. 400.2 eV and 396.5 eV, which are assigned to interstitial nitrogen and substitutional nitrogen species, respectively [165, 166]. Figure 5.4 (b) exhibited the interstitial nitrogen in the crystal structure. Interstitial nitrogen occupied the space among Ti and O atoms. Figure 5.4 (c) shown how nitrogen was substituted into the TiO_2 crystal structure. Nitrogen atoms replaced the oxygen atoms and took up the position of O atoms. The percentages of interstitial nitrogen and substitutional nitrogen species were 86.7 % and 13.3 %.

Because oxygen replaced by nitrogen usually occurred in the high temperature (usually at least 600 ^{o}C) [167], it is convincing the majority of nitrogen species existed as interstitial status. The interstitial nitrogen affected the morphology of TiO_2 support itself and facilitate the copper dispersion on the surface.

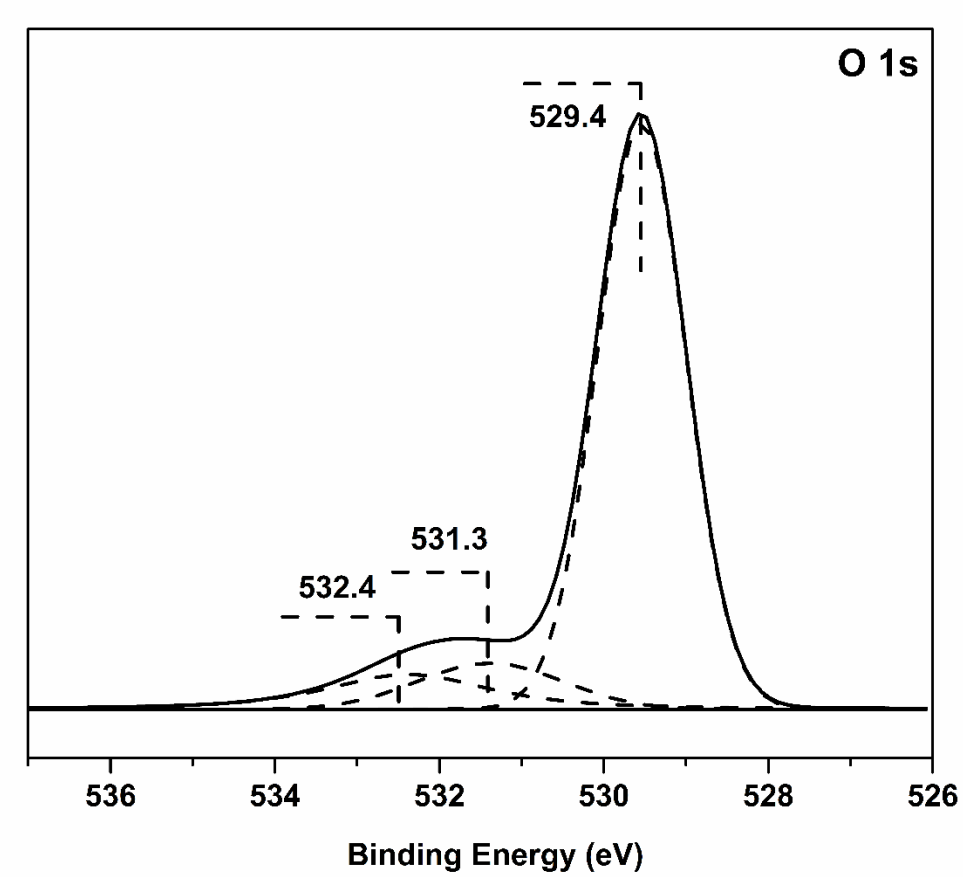

Figure 5.5 XPS O 1s spectra of N-TiO_2 support.

The O 1s XPS profile over N-TiO_2 (shown in Figure 5.5) revealed that three different oxygen species. Peak located at 529.4 eV is assigned to the lattice oxygen related to TiO_2 support. 531.5 eV is assigned to the surface-active oxygen. 532.5 eV could be possibly related to adsorbed oxygen species [137, 154]. It is worth to mention that the percentage of surface oxygen species was a 14.2 % increase compared with that of unmodified TiO_2. It suggested that the introduction of nitrogen

would affect the distribution of different oxygen species on the surface, but also increase the total surface oxygen concentration. Naturally, the improvement of copper dispersion was observed over N-TiO_2 support.

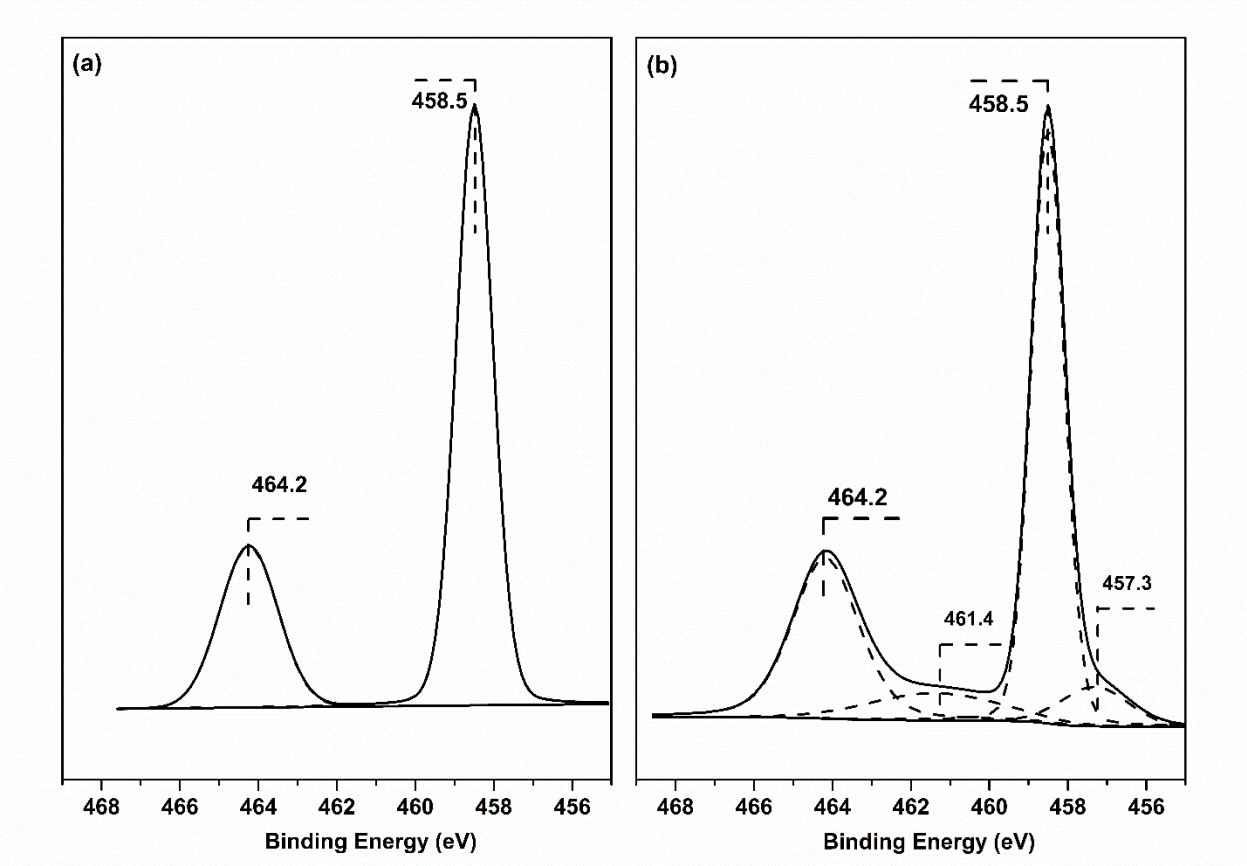

Figure 5.6 XPS Ti 2p spectra of (a) TiO_2 support and (b) N-TiO_2 support.

The addition of nitrogen would affect the oxidation state of titanium dramatically. XPS Ti 2p spectra of N-TiO_2 and TiO_2 supports were shown in Figure 5.6. Ti^{4+} characteristic peaks located at 458.5 eV and 464.2 eV were observed for both TiO_2 and N-TiO_2 [151, 152]. Ti^{4+} is the dominant oxidation state of titanium (Figure 5.6 (a)) over unmodified TiO_2. Meanwhile, the addition of nitrogen would affect the bonding between titanium atoms and neighbor oxygen atoms. Therefore, electron density around titanium atoms would be distributed differently. As shown in Figure 5.6 (b), the analysis of Ti 2p XPS spectra over N-TiO_2 also identified that the existence of a pair of

peaks centered at 457.3 eV ($Ti^{\delta+}$) and 461.4 eV (Ti^{3+}) [153]. The appearance of non-Ti^{4+} indicated that the possible replacement of oxygen atoms with nitrogen atoms occurred. This is in line with the presence of substitutional nitrogen in TiO_2 crystal structure. Table 5.2 listed the calculated ratio of the amount of oxygen atoms to that of titanium based on XPS analysis. The ratio values were 2.21 and 1.96 for TiO_2 and N-TiO_2, respectively. The lower value observed over N-TiO_2 indicated that oxygen atoms were partially replaced by nitrogen, thus generated oxygen vacancies. Clearly, additional nitrogen led to more impact on the chemical environment on the surface of catalysts.

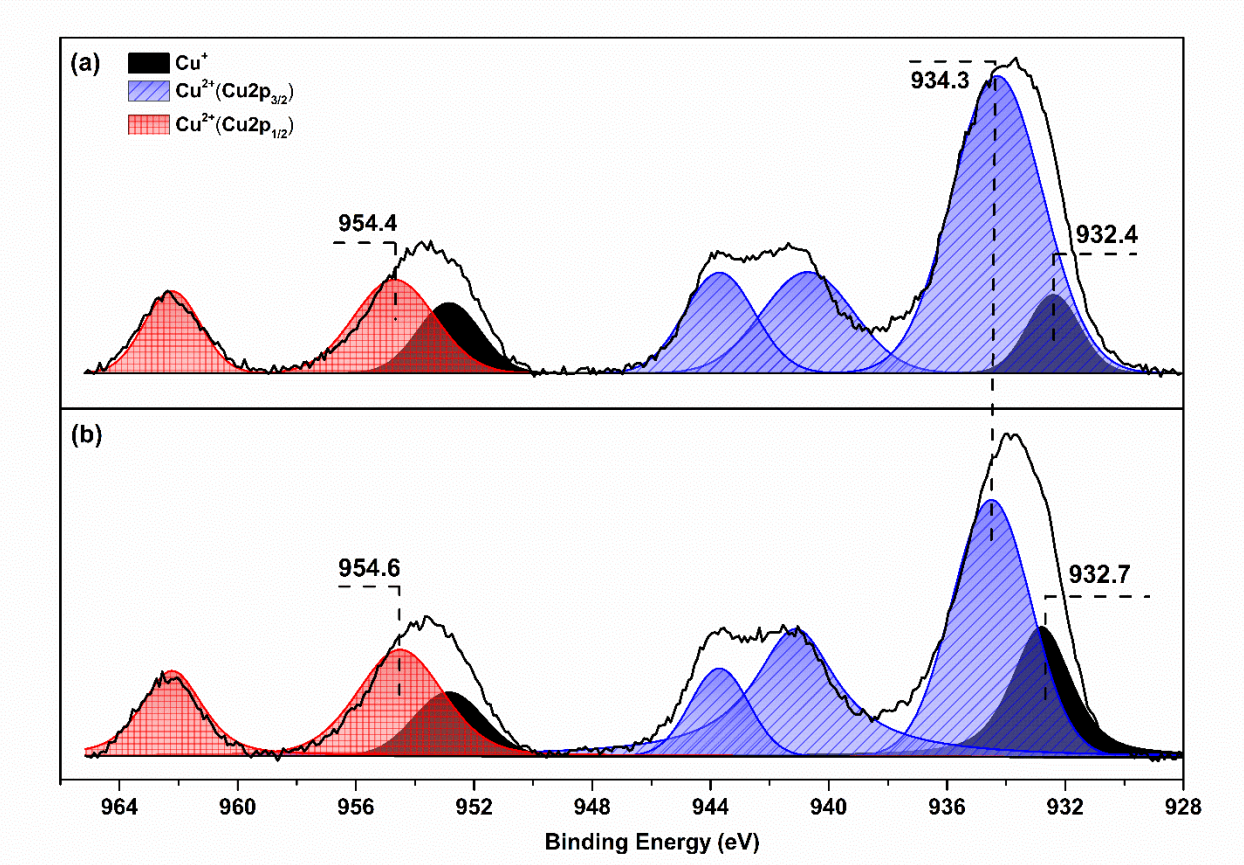

Figure 5.7 XPS Cu 2p spectra of (a) Cu-N-TiO_2 and (b) Cu-TiO_2.

In addition to the XPS spectra on N-TiO_2 and TiO_2 supports, XPS of Cu 2p was also applied to understand of chemical states of copper species. As shown in Figure 5.7, both characteristic Cu^+ and Cu^{2+} peaks were observed for Cu-TiO_2 and Cu-N-TiO_2. The existence of Cu^+ species was

confirmed by the peak located around 932.4 eV and its shake-up satellite peak located at 952.7 eV [134]. Meanwhile. 934.3 eV and 954.4 eV peaks were attributed to Cu^{2+} $2p_{1/2}$, and Cu^{2+} $2p_{3/2}$, respectively [135, 136]. The calculation of the $Cu^{+}/(Cu^{2+} + Cu^{+})$ was listed in Table 5.2. The ratio indicated 25 % of surface copper species of Cu-N-TiO_2 are Cu^{+}, and Cu-TiO_2 has 22 % Cu^{+} on the surface. Therefore, the Cu^{+} concentration suggested that introduction of nitrogen does not have a great effect on chemical states of copper.

5.3.3 REDOX PROPORTIES

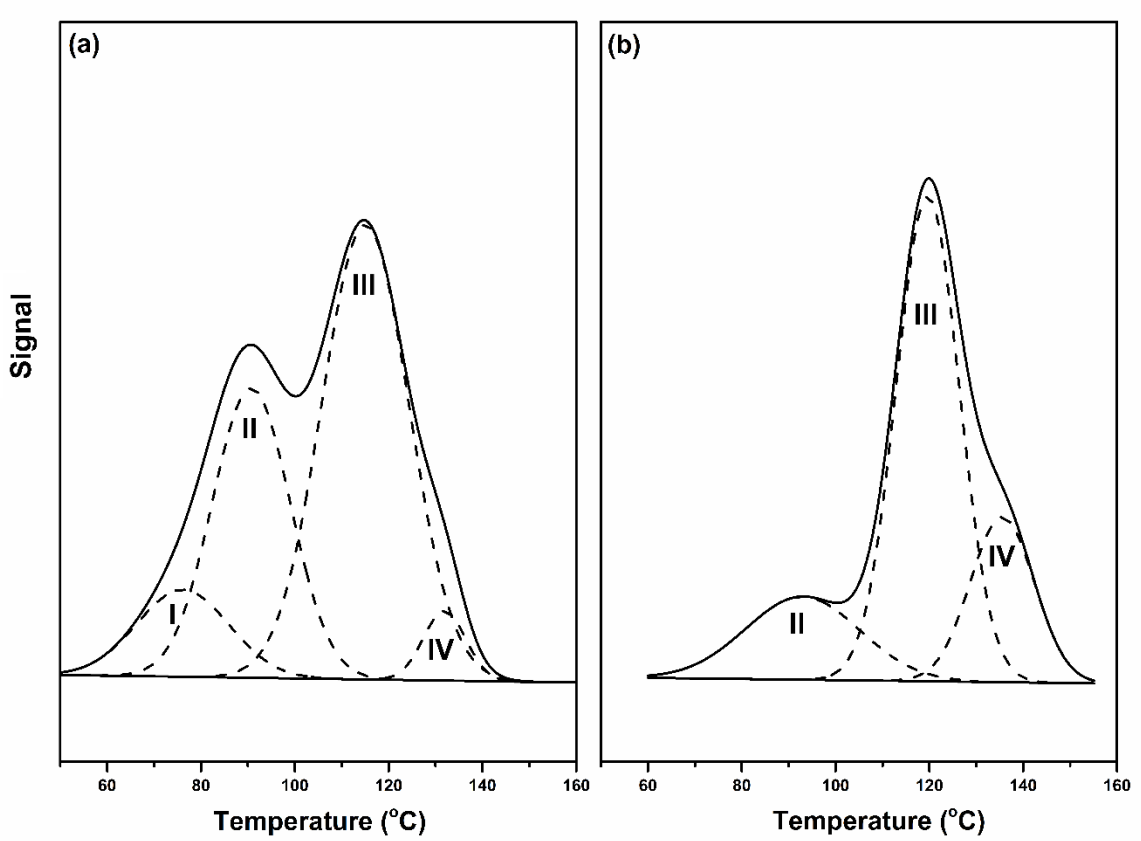

Figure 5.8 Hydrogen-temperature programmed reduction (H_2-TPR) profiles for (a) Cu-N-TiO_2 and (b) Cu-TiO_2 catalysts.

The reducing properties are characterized by hydrogen-temperature programmed reduction (H_2-TPR) to elucidate the surface copper states, as shown in Figure 5.8. The peak deconvolution

analysis indicated that there were four reduction peaks over the Cu-N-TiO_2 catalyst. Peak I is related to highly dispersed copper species on the surface [150]. Peak II and Peak III can be attributed to step reduction ($Cu^{2+} \rightarrow Cu^{+} \rightarrow Cu^{0}$) of copper (II) oxides. Peak IV could be assigned to the reduction of crystalline CuO or copper species that has strong interaction with the support [132]. Whereas only three reduction peaks were detected for Cu-TiO_2, suggesting that nitrogen promoted the copper dispersion.

Table 5.3 H_2-TPR deconvolution analysis and H_2 consumption.

Sample	Peak 1		Peak II		Peak III		Peak IV	
	T (^oC)	H_2 Consumption (μmol/g) (%)	T (^oC)	H_2 Consumption (μmol/g) (%)	T (^oC)	H_2 Consumption (μmol/g) (%)	T (^oC)	H_2 Consumption (μmol/g) (%)
Cu-N-TiO_2	76	186.0 (12.4)	90	431.1 (28.8)	115	735.4 (49.2)	132	142.1 (9.5)
Cu-TiO_2			93	270.2 (18.8)	120	829.4 (57.8)	136	334.6 (23.3)

The total hydrogen consumption was calculated for both catalysts and listed in Table 5.3. The results indicated that hydrogen consumption increased from 1434.2 μmol/g over Cu-TiO_2 to 1494.6 μmol/g over Cu-N-TiO_2. Most importantly, more than 90 % of the hydrogen consumption of Cu-N-TiO_2 resulted from lower temperature reduction (lower than 120 ^oC). At the same time, only 18.8 % of hydrogen was consumed under 120 ^oC for Cu-TiO_2 sample. Meanwhile, the reduction peaks were located at a slightly higher temperature range for Cu-TiO_2 catalysts. With more low temperature related hydrogen consumption, it indicated copper species on the surface of

Cu-N-TiO_2 were easier to be reduced. Consequently, Cu-N-TiO_2 presented a better catalytic performance than Cu-TiO_2.

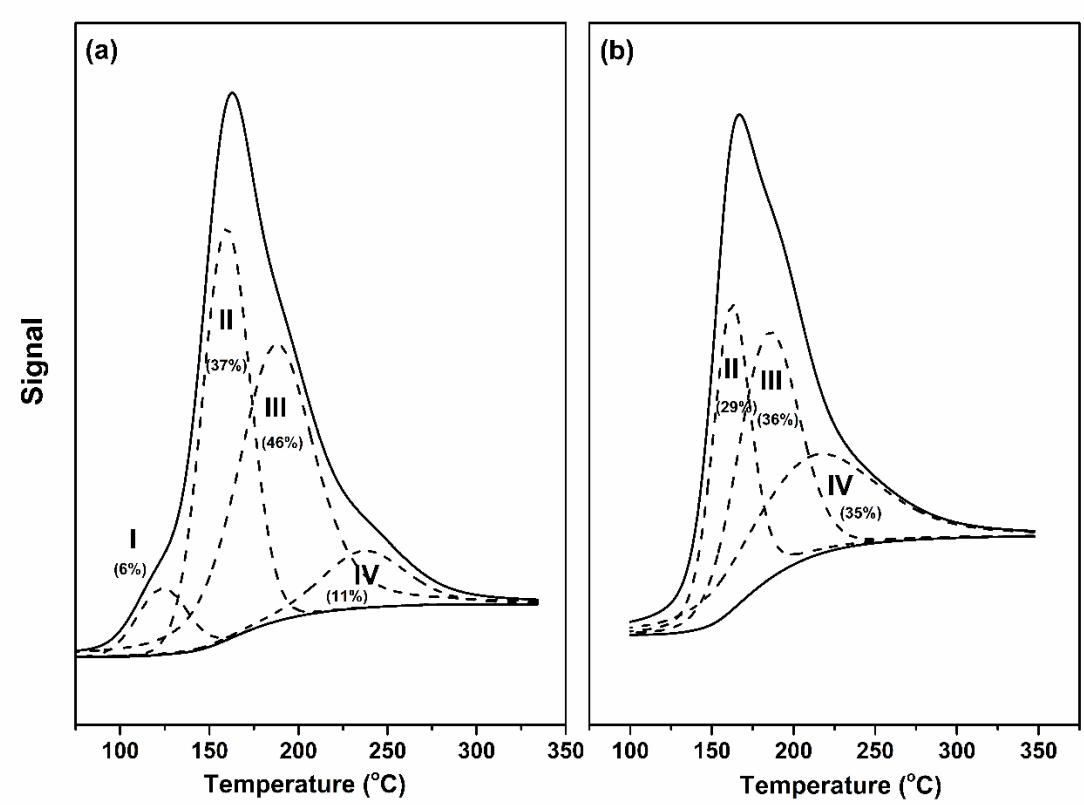

Figure 5.9 Carbon monoxide-temperature programmed surface reaction (CO-TPSR) profiles for (a) Cu-N-TiO_2 and (b) Cu-TiO_2 catalysts.

CO-TPSR was applied to identify the differences among surface oxygen species, and the evolution of carbon dioxide was monitored. Peak deconvolution analysis was shown in Figure 5.9. Four different types of surface oxygen species presence on Cu-N-TiO_2. Low temperature (peak I) oxygen species is unique for Cu-N-TiO_2 catalyst and occupied 6 % of overall CO consumption. This kind of oxygen species could be correlated to the high activity of Cu-N-TiO_2 catalysts in lower temperature range. Meanwhile, medium temperature (peak II and III) oxygen species are dominant for both Cu-N-TiO_2 and Cu-TiO_2 catalysts. The percentage of peak IV of Cu-TiO_2 catalyst located at high temperature (220 - 240 ^oC), is three times higher than that of the Cu-N-

TiO_2 catalyst. In the course of a reaction, the high temperature oxygen species are more difficult to be activated than low temperature oxygen species. The results from temperature programmed reaction using hydrogen and carbon monoxide as probe molecules confirmed different active sites on the surface of Cu-N-TiO_2 and Cu-TiO_2 catalysts. Nitrogen modified Cu-TiO_2 has more active sites compared with the unmodified Cu-TiO_2.

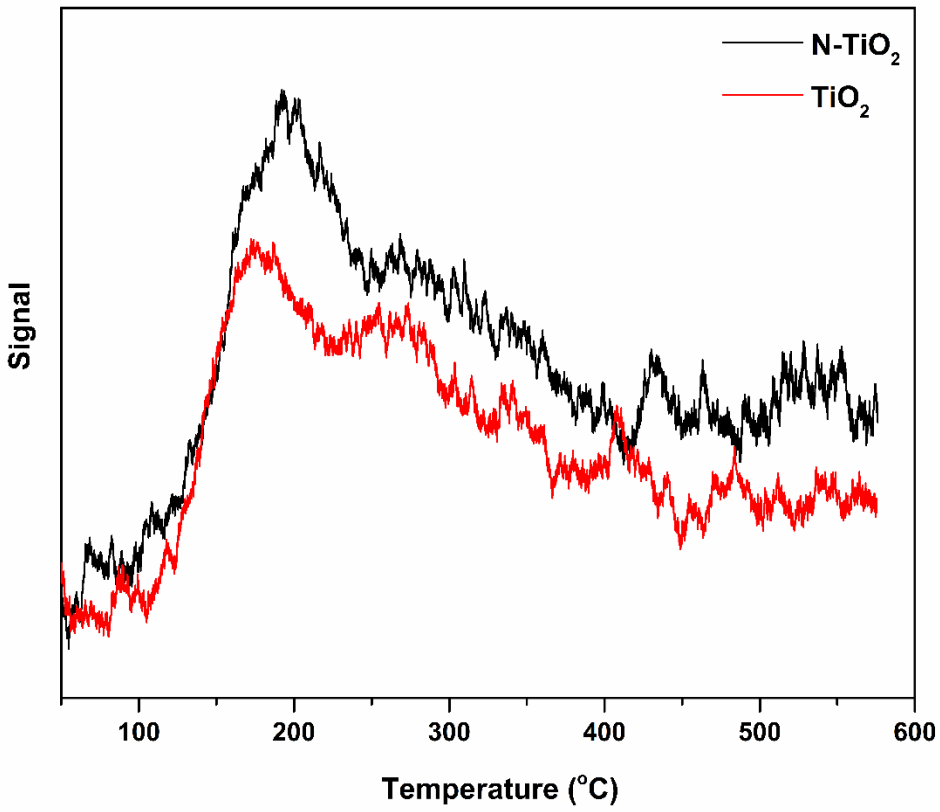

Figure 5.10 Oxygen-temperature programmed reaction comparison of N-TiO_2 and TiO_2 supports

The oxygen-temperature programmed reaction (O_2-TPR) experiment was performed on the supports to identify the ability to consume oxygen of the supports. Figure 5.10 presented the O_2-TPR comparison between nitrogen modified TiO_2 support and TiO_2 support. By calculation, the amount of oxygen consumed from supports, it demonstrated that N-TiO_2 has 28.9 % higher oxygen consumption than that of TiO_2. The oxygen consumption could be attributed to the oxidation of

Ti^{3+} species and oxygen vacancies. This demonstrated the presence of Ti^{3+} species and oxygen vacancies, which is in great agreement with XPS results. In N-TiO_2 supports, oxygen atoms were partially replaced by nitrogen, and therefore, oxygen vacancies were generated. When the N-TiO_2 support was exposed in an oxygen rich environment, oxygen vacancies were padded and resulted in a larger amount of oxygen consumption. Furthermore, this suggested that the introduction of nitrogen affected the distribution of different oxygen species on the surface, but also increased the total surface oxygen concentration. Naturally, the improvement of copper dispersion was observed over N-TiO_2 support.

5.3.4 IN-SITU DRIFTS

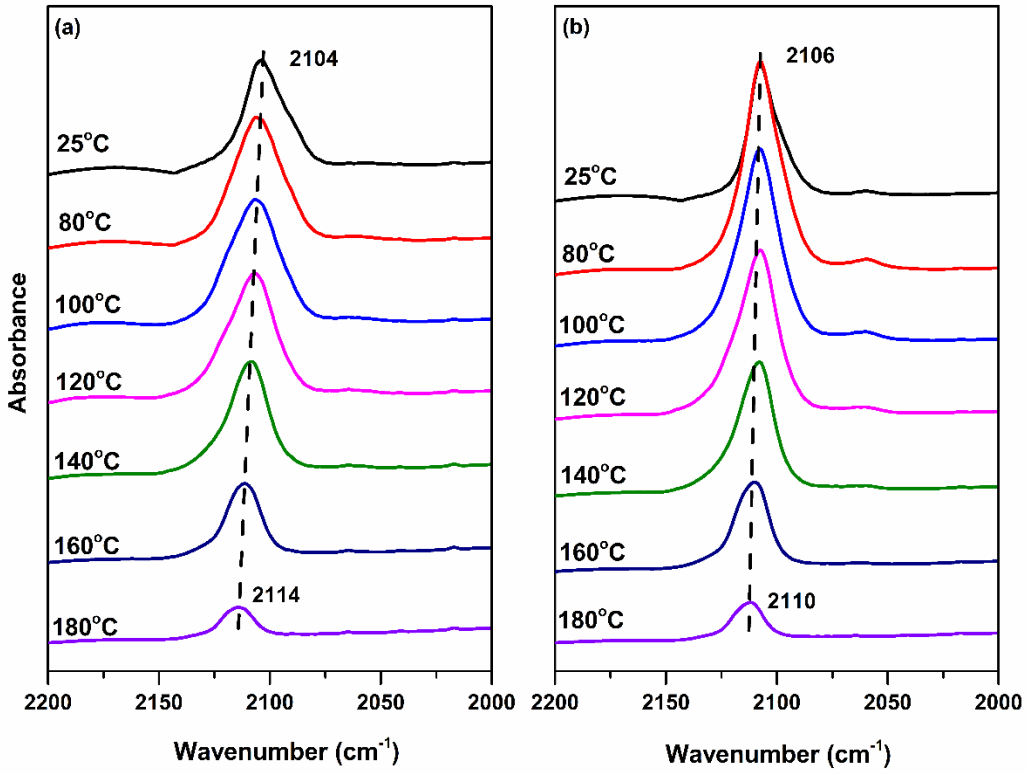

Figure 5.11 In-situ DRIFTS profiles of (a) Cu-N-TiO_2 and (b) Cu-TiO_2 under reaction conditions. Test condition: 1%CO, 20%O_2, balanced in Helium.

In order to investigate the surface reaction process further, in-situ DRIFTS of CO and O_2 adsorption on Cu-N-TiO_2 and Cu-TiO_2 were conducted under the reaction condition. The in-situ DRIFTS was recorded while temperature ranges from 25 ^oC to 180 ^oC and presented in Figure 5.11. As shown in Figure 5.11, the principal feature of those spectra was a broad band around 2104 cm^{-1}. This vibration band is the characteristic feature of Cu^+-CO bond [140]. The peaks of CO adsorption confirmed the presence of Cu^+ on the surface, which matched with the XPS profile. The intensity of this band is sensitive to the temperature. With the increase of temperature, the peak intensities of Cu^+-CO increased to the maximum at 80 ^oC and then decreased. In the meantime, the Cu^+-CO peaks shifted to a higher wavenumber. This could be attributed to the formation of Cu^+-$(CO)_2$ adsorption [133, 168], which could contribute to the activity of CO oxidation. Temperature-dependence trends are applied to both Cu-TiO_2 and Cu-N-TiO_2 catalysts. It is worth emphasizing that the shift appears more dominant over Cu-N-TiO_2. The shift for Cu-N-TiO_2 is almost twice larger than that of Cu-TiO_2. This agreed with the light-off results that the Cu-N-TiO_2 catalyst presented better catalytic performance.

5.4 SUMMARY

To build the property-activity relationship, a majority of effort focused on investigating the correlation between reaction rate and the surface concentration of copper (II) and/or copper (I) species on the surface [125]. In practice, copper species ultimately interact with other components/species on the surface, and those neighbor species would have impact on the reaction rate. Operation conditions, including the choice of pre-treatment approaches and a variety of gas compositions (particularly the ratio of carbon monoxide and oxygen), also make it challenging to identify the active copper species [44]. The consideration of species around the active copper species would clearly make it reliable to gain accurate information to elucidate the active species.

Copper species are sensitive to the variation of chemical environment. Copper-cobalt surface could alter carbon monoxide adsorption on the surface, then control the product distribution [169]. The stacking order of N-TiO_2 and Cu-TiO_2 double layer films led to different arrangements to saturate the surface defect, resulting in the photocatalytic performance of oxygenates differently [170].

Copper catalysts studied here did not undergo the calcination step. Before the activity test, all catalysts were only pre-treated at 200 ^oC with Helium to remove all moisture and other volatile impurities. Those treatments led to a unique reaction arena, where copper species and their surrounding species maintain intact before the stream of reactants being introduced to the reaction system. It enables us to gain understanding of how the addition of nitrogen affects the initial copper states (including oxidation states and morphology) differently. The XPS results revealed that both copper (II) and copper (I) species existed on both Cu-TiO_2 and Cu-N-TiO_2 catalysts. The surface copper(I) concentration over Cu-N-TiO_2 is 24.9 %, which is slightly higher than that of 22.6 % observed on Cu-TiO_2. Because the most abundant species besides copper on the surface are different oxygen species, the contribution of surface oxygen species should also be included while building the relationship between surface properties and the activity performance. The concentration of surface oxygen species was selected, which is corresponding to the 531.3 eV in XPS analysis to represent the oxygen species on the surface. The ratio between copper (I) and surface oxygen species was calculated (shown in Table 5.2). The values are 1.29 and 1.11 for Cu-N-TiO_2 and Cu-TiO_2, respectively. The results suggested that the positive correlation between the value of ($[Cu^+]/[O]_{surf}$) and the reaction rates. It is evident to take a comprehensive approach to evaluate the combined contribution from copper species and their vanities while building the property-activity correlation.

In summary, we report the promotion effect of nitrogen to carbon monoxide oxidation reaction over copper-titanium dioxide catalysts. Both interstitial and substitutional nitrogen are observed on the surface, but the interstitial nitrogen is the dominant nitrogen species, which are confirmed by XPS analysis. The enhancement of the reaction rate could be attributed to the improved copper dispersion, which was facilitated by the addition of nitrogen. Cu^{+} is abundant copper species on the surface, but we propose to correlate the reaction rate with the value of ($[Cu^{+}]/[O]_{surf}$) while considering the vanity around active copper species.

CHAPTER 6

EFFECT OF TITANIUM DIOXIDE PHASES ON COPPER-NITROGEN-TITANIUM DIOXIDE CATALYZED CARBON MONOXIDE OXIDATION

6.1 INTRODUCTION

Titanium dioxide (TiO_2) is widely used as a catalyst support in various catalytic processes because of its low cost and high chemical stability. Three crystalline phases, namely anatase, rutile, and brookite, have been extensively studied for their applications in chemical and physical sciences. Anatase and brookite are stable at low temperature and could transform to rutile at a higher temperature. However, synthesis studies mostly focused on anatase and rutile phases because they are more chemically active as supports as compared with brookite.

Metals (including copper and precious metals) doped TiO_2 catalysts have been studied for numerous industrial applications, such as selective hydrogenation reaction, water gas shift reaction, and carbon monoxide (CO) oxidation. Regarding the Cu-TiO_2 catalysts, studies focused on catalysts synthesis and optimizing reaction conditions, while aiming to increase the interaction between copper and supports. Researchers identified that the TiO_2 crystalline phase could tune the activity performance differently. In-situ infrared studies suggested different reaction mechanisms of CO oxidation over CuO supported on rutile or anatase phase of TiO_2 [171]. The difference could be explained that rutile phase of TiO_2 interacts weakly, therefore rutile TiO_2 lacked the highest activity [105].

At the same time, non-metal doping TiO_2, such as carbon, boron, and nitrogen doped TiO_2 catalysts have been extensively studied in photocatalysis to increase the activity in visible light range. Densities of states (DOS) calculation results indicated the substitutional doping of nitrogen was the most effective structure compared with other non-metals (including C, F, P, or S) doped TiO_2. This is due to its p states contributed to the band gap narrowing by mixing with O 2p states [172]. The presence of nitrogen atoms in the lattice greatly decreases the formation energy for oxygen vacancies based on density functional theory (DFT) calculations [173]. The energy cost of creating oxygen vacancies on N doped TiO_2 is 0.6 eV, which is much lower than that of pure TiO_2 (4.2 eV). Theoretical calculation explains why more oxygen vacancies were reported on nitrogen modified TiO_2 than pure TiO_2. In addition, this was confirmed by real-time transmission electron microscopy (TEM) [174]. The large decrease of formation energy of oxygen vacancy also suggests that oxygen vacancies are most probably induced by the N-doping of TiO_2 [175]. Experimentally, nitrogen modified TiO_2 demonstrated the enhanced activity in a variety of photocatalytic reactions, such as photodegradations of acetaldehyde (CH_3CHO) [176].

We conducted the investigation of CO oxidation over Cu-N-TiO_2 catalysts, which used different phases of TiO_2 (anatase and rutile). A series of characterization techniques were employed to understand the composition and chemical states of copper, existential state of nitrogen, and oxygen species on the Cu-N-TiO_2 catalysts. Furthermore, the effect of phases on surface properties and CO oxidation activity was interpreted.

6.2 CARBON MONOXIDE OXIDATION ACTIVITY

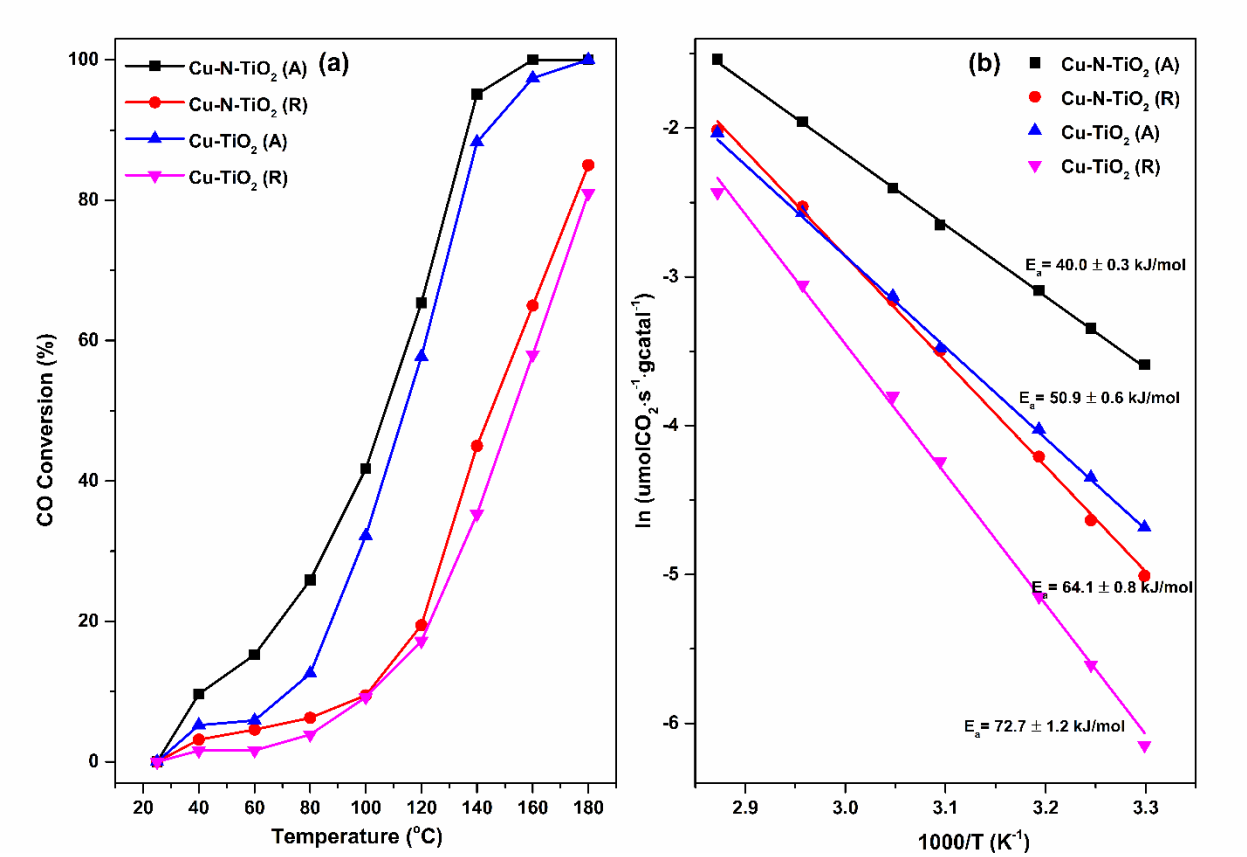

Figure 6.1 Catalytic performance of copper-based catalysts in carbon monoxide oxidation. (a) Light-off curves, (b) Arrhenius plots, Test condition: 1%CO/20%O_2/ Helium, flow rate 30 mL/min.

Cu-N-TiO_2 (A & R) and Cu-TiO_2 (A & R) samples were evaluated for the CO oxidation reaction to compare the effects of TiO_2 phases. Light-off curves (shown in Figure 6.1 (a)) demonstrated that the phases of TiO_2 affected the activity performance. As it sugggested the Cu-N-TiO_2 (A) had a much better catalytic performance than Cu-N-TiO_2 (R). Cu-N-TiO_2 (A) achieved T_{50} at 107 ^oC and achieved full CO conversion when the reaction temperature reached 180 ^oC. Meanwhile, the CO oxidation over Cu-N-TiO_2 (R) reached 50 % conversion at 143 ^oC, which is higher than Cu-N-TiO_2 (A), and only 85 % of CO converted to CO_2 at 180 ^oC. Cu-TiO_2 (A & R) samples were employed as reference. The light-off results indicated that Cu-N-TiO_2 (A) exhibited

better catalytic performance than Cu-TiO_2 (A). The same trend applied to Cu-N-TiO_2 (R) and Cu-TiO_2 (R). This result is in consistent with the result in Chapter 5, which illustrated that the nitrogen modification facilitated the catalytic performance of Cu-TiO_2 catalysts. Additionally, light-off results indicated that the Cu-TiO_2 (A) performed better than Cu-TiO_2 (R). As all four catalysts were synthesized under the same conditions, the impact of copper loading and calcination conditions were eliminated. Therefore, the phases of TiO_2, anatase and rutile, would be significant factors that led to the different catalytic performance.

Furthermore, reaction rate and activation energy over presented four catalysts were measured to evaluate their performance. Figure 6.1 (b) exhibited the activation energy, Cu-N-TiO_2 (A) catalyst had the lowest activation energy as 40.0 ± 0.3 kJ/mol. In comparison with Cu-N-TiO_2 (R), Cu-N-TiO_2 (A) presented a 37.5 % lower activation energy than Cu-N-TiO_2 (R). In the meantime, CO oxidation reaction rate at 60 ^oC of Cu-N-TiO_2 (A) was determined as 0.11 $\mu mol \cdot s^{-1} \cdot gcatal^{-1}$, and it was 0.06 $\mu mol \cdot s^{-1} \cdot gcatal^{-1}$ for Cu-N-TiO_2 (R). This result indicated that the reaction rate over Cu-N-TiO_2 (A) is two times higher than Cu-N-TiO_2 (R), which demonstrated that the anatase phase improved the catalytic performance. Comparing the Cu-N-TiO_2 with Cu-TiO_2 catalysts, relatively lower activation energy and faster reaction rate were obtained on Cu-N-TiO_2 catalysts. These results further confirmed the positive effect of nitrogen. Overall, based on the light-off curves, activation energy, and reaction rate, it suggested that the anatase phase TiO_2 was able to promote the CO oxidation reaction over copper-titanium catalysts.

6.3 CHARACTERIZATION OF Cu-N-TiO_2 CATALYSTS

6.3.1 PHYSICAL PROPERTIES

To investigate the physical properties of Cu-N-TiO_2 and Cu-TiO_2 catalysts, characterizations were carried out through ICP-AES, BET, N_2O titration, and Raman spectroscopy.

Table 6.1 Physical properties of Cu-N-TiO_2 and Cu-TiO_2 catalysts.

Samples	Surface Area ($m^2/g \cdot catal$)	ICP (%) [b]	Dispersion (%) [c]	Surface Area of Cu atom (m^2/g) [c]	Ratio of E_g/A_{1g}
Cu-N-TiO_2 (A)	144	8.8	34.4	223.1	--
Cu-TiO_2 (A)	123	9.4	29.4	190.9	--
N-TiO_2 (A)	131	--	--	--	2.16
TiO_2 (A) [a]	143	--	--	--	3.33
Cu-N-TiO_2 (R)	45	9.0	27.6	179.4	--
Cu-TiO_2 (R)	43	8.6	25.8	167.3	--
N-TiO_2 (R)	13	--	--	--	1.11
TiO_2 (R) [a]	15	--	--	--	1.27

[a] As-received TiO_2 calcined at 550 ^oC for 15 hours. [b] Determined by Inductive Coupled Plasma. [c] Copper dispersion measured by N_2O titration.

ICP tests were performed to evaluate the amount of Cu loading and shown in Table 6.1. The results indicated that the copper loading is around 9.0 wt% among all four catalysts. It suggested that the amount of copper species would not be impacted by nitrogen modification as well as the different TiO_2 phases. In terms of surface area, anatase based catalysts have much higher surface area than those of rutile-based catalysts. This could be attributed to the TiO_2 supports themselves.

As shown in Table 6.1, the surface area of anatase TiO_2 is much greater than rutile TiO_2. Upon the addition of nitrogen to TiO_2 supports, the surface area slightly decreased due to the calcination process. Cu-N-TiO_2 (A) and Cu-N-TiO_2 (R) gained a larger surface area comparing with the unloaded supports. It suggested that the addition of copper species was beneficial in terms of surface area, and copper species were well dispersed on the surface. By applying the N_2O titration, copper dispersion and Cu atoms surface area were measured. As shown in Table 6.1, all catalysts have high Cu dispersion and large surface area of Cu atoms. Generally, anatase TiO_2 supported Cu catalysts presented greater Cu dispersion and Cu atoms surface area than rutile TiO_2 supported catalysts. Herein, results from ICP, N_2O titration, and BET surface area revealed the presence of highly dispersed copper species. Meanwhile, these results suggested that the anatase phase of TiO_2 would increase the surface area, copper dispersion and could eventually result in a better catalytic performance.

Raman spectrometer was applied to gain further understanding of the structure change after the introduction of nitrogen and copper. As shown in Figure 6.2, TiO_2 (A) spectra exhibited five typical bands around 166, 196, 398, 516 and 640 cm^{-1}, which represent vibration models as $E_g(1)$, $E_g(2)$, B_{1g}, A_{1g}, and $E_g(3)$, respectively [13]. Meanwhile, three typical bands at 237, 447, and 611 cm^{-1}, which represent B_{1g}, E_g, and A_{1g}, respectively, were observed over TiO_2 (R) [13]. The addition of nitrogen resulted in the decrease of band intensity, indicating the overall titanium dioxide lattice structure was maintained. The decrease of band intensity may be explained by the disorder of oxygen sublattice due to the addition of nitrogen atom. The introduction of copper further decreased the peak intensity. CuO crystal has the characteristic band located around 300 cm^{-1}, corresponding to the single A_g mode [177]. In our case, we only observed a very weak bump at 300 cm^{-1}. Therefore, we would suggest that copper oxides were highly dispersed on the surface.

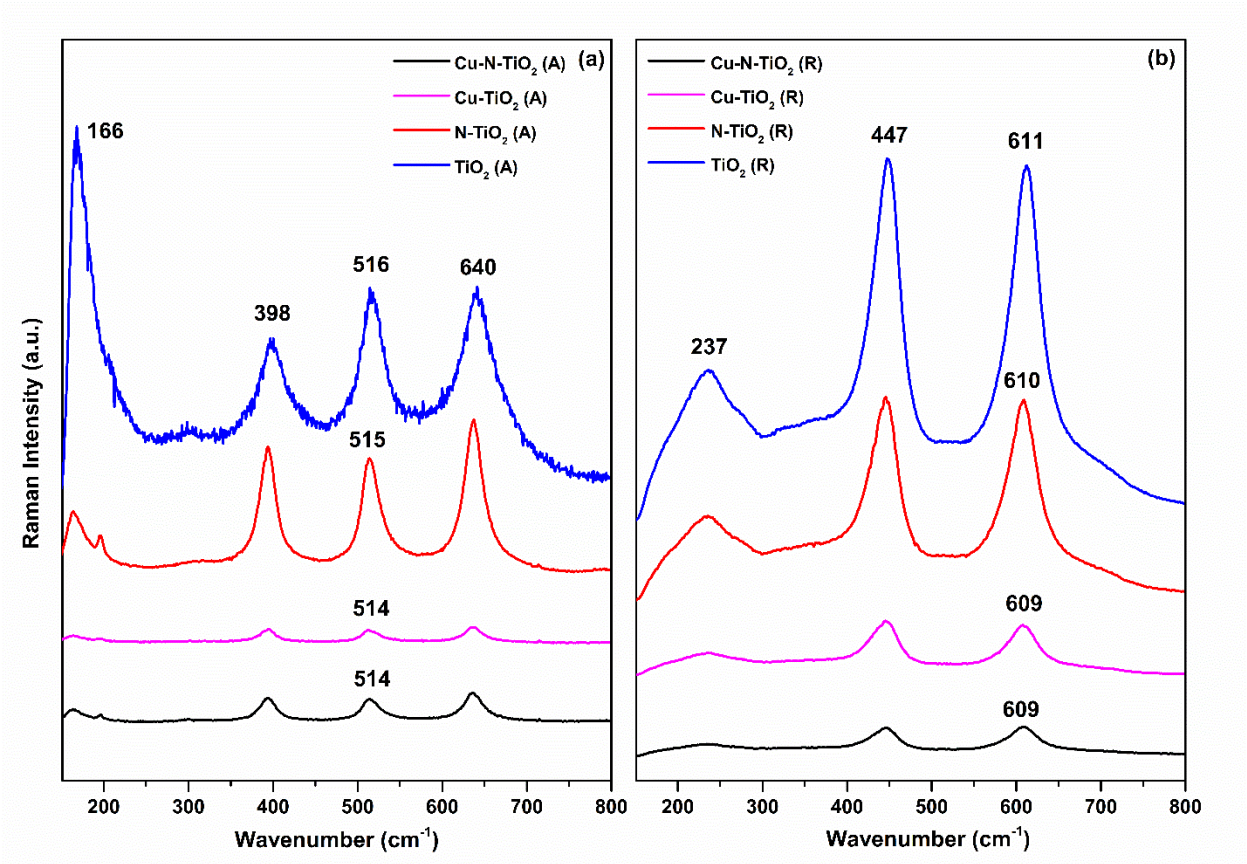

Figure 6.2 Raman spectra profiles of different TiO_2 supports and catalysts: (a) TiO_2 (A) based samples, (b) TiO_2 (R) based samples.

The introduction of copper also resulted in the Raman shift. The A_{1g} mode shifted from 516 to 514 cm^{-1} for Cu-N-TiO_2 (A), and from 611 to 609 cm^{-1} for Cu-N-TiO_2 (R). This slight shift of the peaks indicated the interaction between copper species with N-TiO_2 supports.

It has been reported that the frequency and intensity of the E_g mode could be affected when the oxygen ions in the structure were lost from the crystalline structure [133, 178]. Because of this, we calculated the ratio of E_g/A_{1g} for TiO_2 and N-TiO_2 supports. As shown in Table 6.1, the ratio of E_g/A_{1g} decreased when nitrogen was introduced for both N-TiO_2 (A) and N-TiO_2 (R). A greater decrease of this ratio indicated that oxygen vacancies were generated on the surface after the calcination process. The results presented that the values of E_g/A_{1g} were 3.33 and 2.16 for TiO_2

(A) and N-TiO_2 (A), respectively. The ratio decreased by 35 % from TiO_2 (A) support to the nitrogen modified N-TiO_2 (A) support. In the meantime, the values of E_g/A_{1g} for TiO_2 (R) and N-TiO_2 (R) were 1.27 and 1.11, respectively. This ratio only decreased by 12.5 %, which is much lower than anatase TiO_2. Therefore, Raman spectra results suggested that more oxygen vacancies were obtained on the surface of N-TiO_2 (A) support.

6.3.2 CHEMICAL STATES ANALYSIS

X-ray photon spectroscopy (XPS) was employed to analyze the surface composition, investigate the presence of nitrogen, reveal the oxidation state of copper species, and elucidate the types of oxygen species.

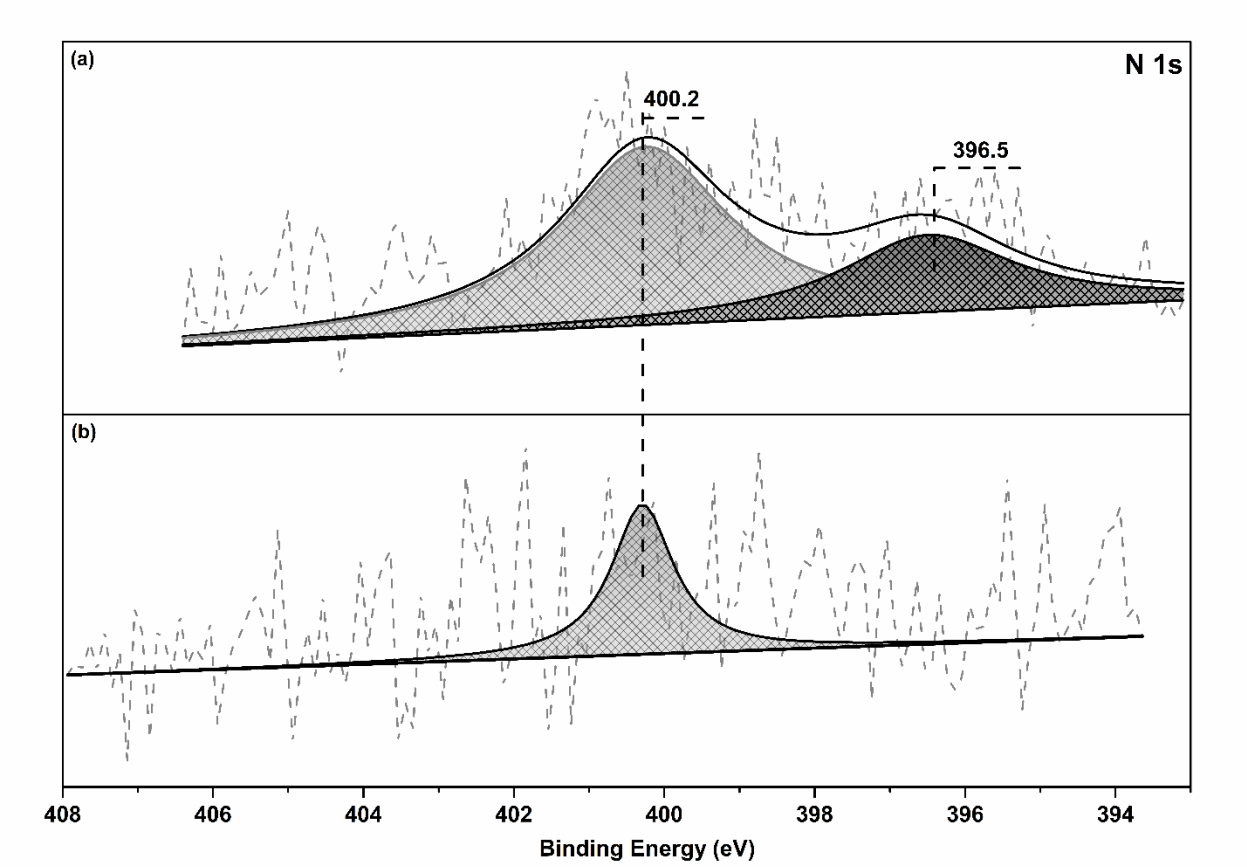

Figure 6.3 XPS N 1s profiles for (a) N-TiO_2 (A) support, (b) N-TiO_2 (R) support.

N1s XPS spectra were collected for both N-TiO_2 (A) and N-TiO_2 (R) supports and shown in Figure 6.3. The results confirmed that the nitrogen was successfully anchored to the supports. Quantitative analysis revealed that the amount of introduced nitrogen were 1.6 % and 0.6 % for N-TiO_2 (A) and N-TiO_2 (R), respectively. Less amount of nitrogen anchored on N-TiO_2 (R) could be attributed to the better thermal stability of the rutile phase than the anatase phase. Peak deconvolutions of N 1s spectra revealed two different peaks for N-TiO_2 (A), while only one peak was detected on N-TiO_2 (R). The peak at 396.5 eV could be assigned as substitutional nitrogen located at an oxygen lattice site [165, 166]. N 1s peaks at 400.2 - 400.3 eV can be attributed to interstitial nitrogen species, which occupied the space among Ti and O atoms [165, 166]. The percentages of interstitial nitrogen and substitutional nitrogen species were 69.1 % and 30.9 % on N-TiO_2 (A). The morphology of anatase TiO_2 support would be affected by interstitial nitrogen and consequently facilitated the copper dispersion on the surface. The substitutional nitrogen could potentially create oxygen vacancies, which agreed with the Raman results.

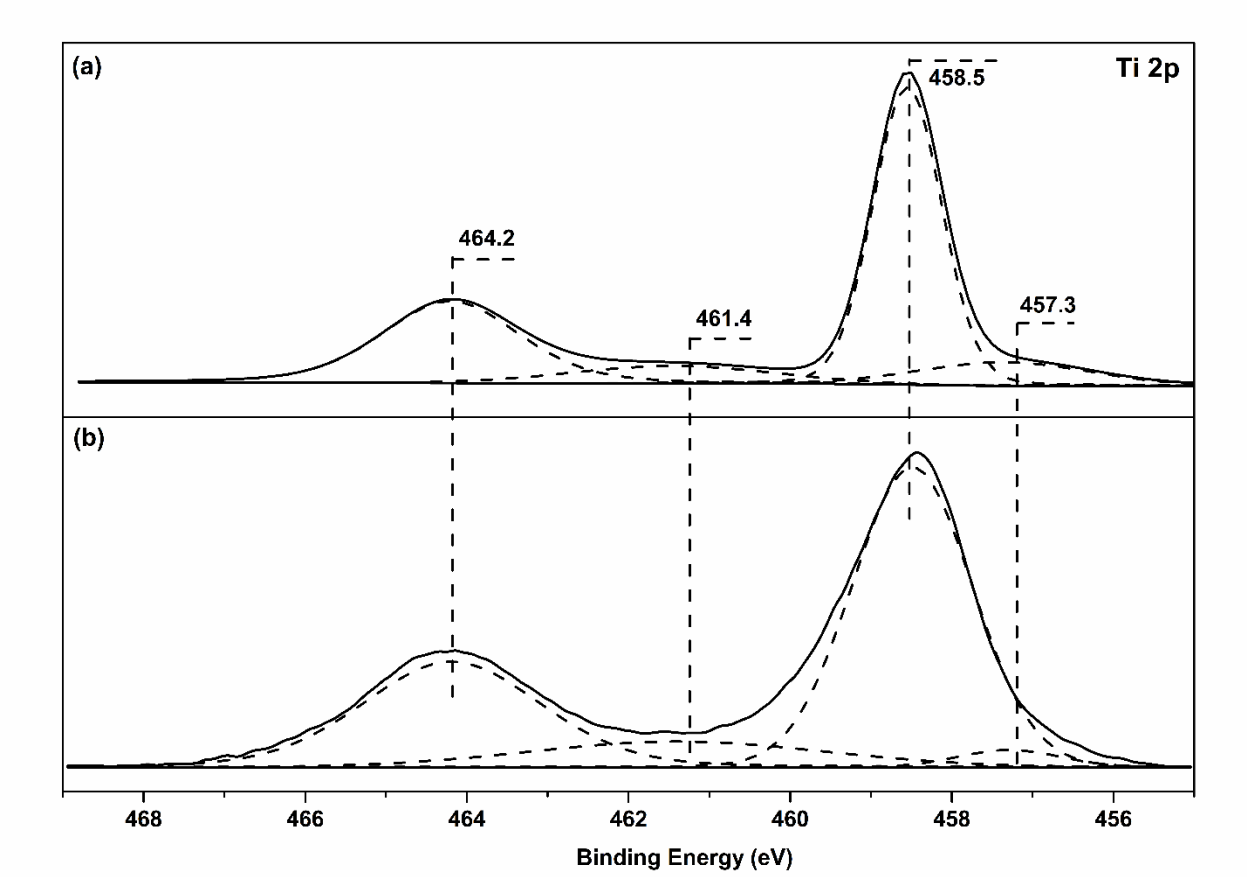

Figure 6.4 XPS Ti 2p profiles of (a) N-TiO_2 (A) support, (b) N-TiO_2 (R) support.

Ti 2p XPS spectra of N-TiO_2 supports were shown in Figure 6.4. Four peaks after the deconvolution analysis were presented for both N-TiO_2 (A) and N-TiO_2 (R). Peaks located at 458.5 eV and 464.2 eV are typical binding energy of Ti^{4+} [151, 152]. The peak appeared at 457.3 eV was assignable to titanium species with the oxidation state between +3 and +4, which were correlated with titanium in a distorted lattice located between TiO_2 and TiN phases [179]. The peak at 461.4 eV could be corresponded to Ti^{3+} species [153]. The appearance of non-Ti^{4+} indicated that the possible replacement of oxygen atoms occurred by nitrogen atoms. Ti^{3+} is in an unstable state and has a significant influence on the catalytic property of the catalyst because the Ti^{3+} can diffuse to the Cu-Ti interface to reduce Cu^{2+} to Cu^{+} or stabilize Cu^{+} species [105, 180]. Therefore, the introduced nitrogen led to the formation of Ti^{3+} by replacing oxygen atoms, and further facilitated

the reduction of Cu^{2+} to Cu^{+}. We calculated the percentage summation of peaks at 457.3 eV and 461.4 eV, and it decreased in the order of N-TiO_2 (A) (18.3 %) > N-TiO_2 (R) (14.1 %). This indicated that N-TiO_2 (A) had much abundant Ti^{3+} species than N-TiO_2 (R). Additionally, the ratio between the amount of oxygen atoms and titanium atoms (O/Ti) was calculated based on XPS analysis. The ratio values are 2.05 and 2.38 for N-TiO_2 (A) and N-TiO_2 (R). The lower ratio indicated more oxygen atoms were potentially replaced by nitrogen to create oxygen vacancies. Overall, it is clear that the anatase TiO_2 was easier to be impacted by nitrogen than the rutile TiO_2. Moreover, it confirmed that oxygen vacancies presented on N-TiO_2 (A) support.

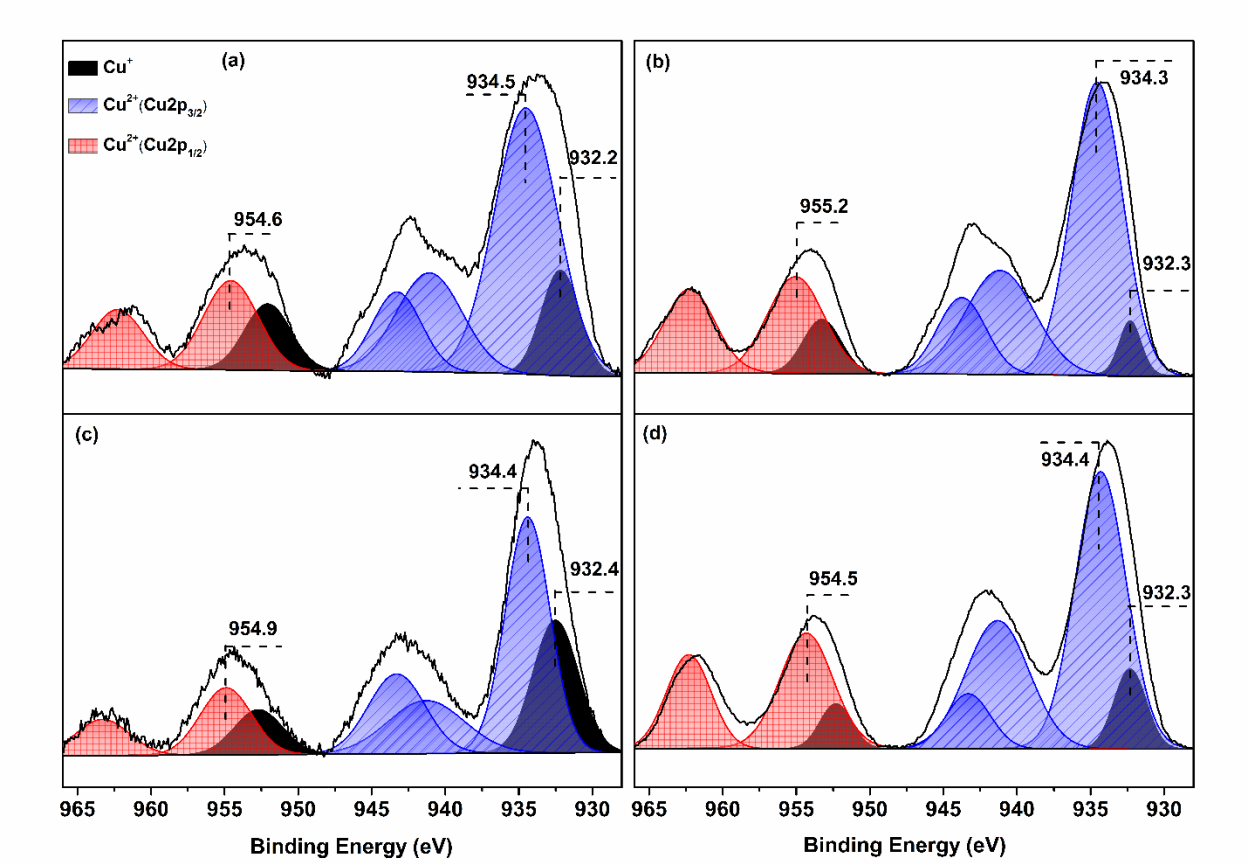

Figure 6.5 XPS Cu 2p spectra over (a) Cu-N-TiO_2 (A), (b) Cu-N-TiO_2 (R), (c) Cu-TiO_2 (A), and (d) Cu-TiO_2 (R).

XPS was also applied to reveal the oxidation state of copper species as copper species played the role of the active site in the reaction. XPS Cu 2p spectra were shown in Figure 6.5. The profiles revealed three different types of copper states existing on the surface for all four catalysts. The existence of Cu^{2+} was evidenced by the typical Cu $2p_{3/2}$ binding energy located at 934.3 - 934.5 eV and two intensive shake-up satellites in the range of 938 - 946 eV [136]. Meanwhile, the typical Cu $2p_{1/2}$ which was also attributed to Cu^{2+}, was confirmed by the peaks located at 954.6 - 955.0 eV and its shake-up satellites in the range of 960 - 966 eV. The existence of Cu^{+} was confirmed by 932.2 - 932.4 eV and its shake-up satellite peak located at 952.7 - 952.9 eV [20]. The formation of Cu^{+} may be due to the electronegativity of Cu being greater than Ti. Thus, the electron can donate to Cu^{2+}. Another explanation could be that the Cu-O-Ti band formed by the oxygen of CuO occupies the vacancy may result in the generation of Cu^{+}. Comparing Figure 6.5 (a), (c) with (b), (d), the results indicated that Cu^{+} is much more abundant for anatase TiO_2 supported catalysts than rutile TiO_2 supported catalysts. Herein, anatase TiO_2 was able to facilitate the formation of Cu^{+}, which is in agreement with previous XPS investigations on N-TiO_2 supports. To quantify the relative concentration of Cu^{+}, the ratio of Cu^{+} to the entire copper species was calculated. The results indicated that Cu-N-TiO_2 (A) presented 28.9 % of Cu^{+}, while Cu-N-TiO_2 (R) contained 17.6 % Cu^{+}. As reported, among copper oxides catalysts for CO oxidation, Cu^{+} has been considered as the active species [104,130]. Therefore, the abundance of Cu^{+} on Cu-N-TiO_2 (A) dramatically improved its catalytic performance. Meanwhile, Cu-TiO_2 (A) presented more Cu^{+} but worse CO oxidation activity than Cu-N-TiO_2 (A), consequently other surface species could also have an impact on the reaction.

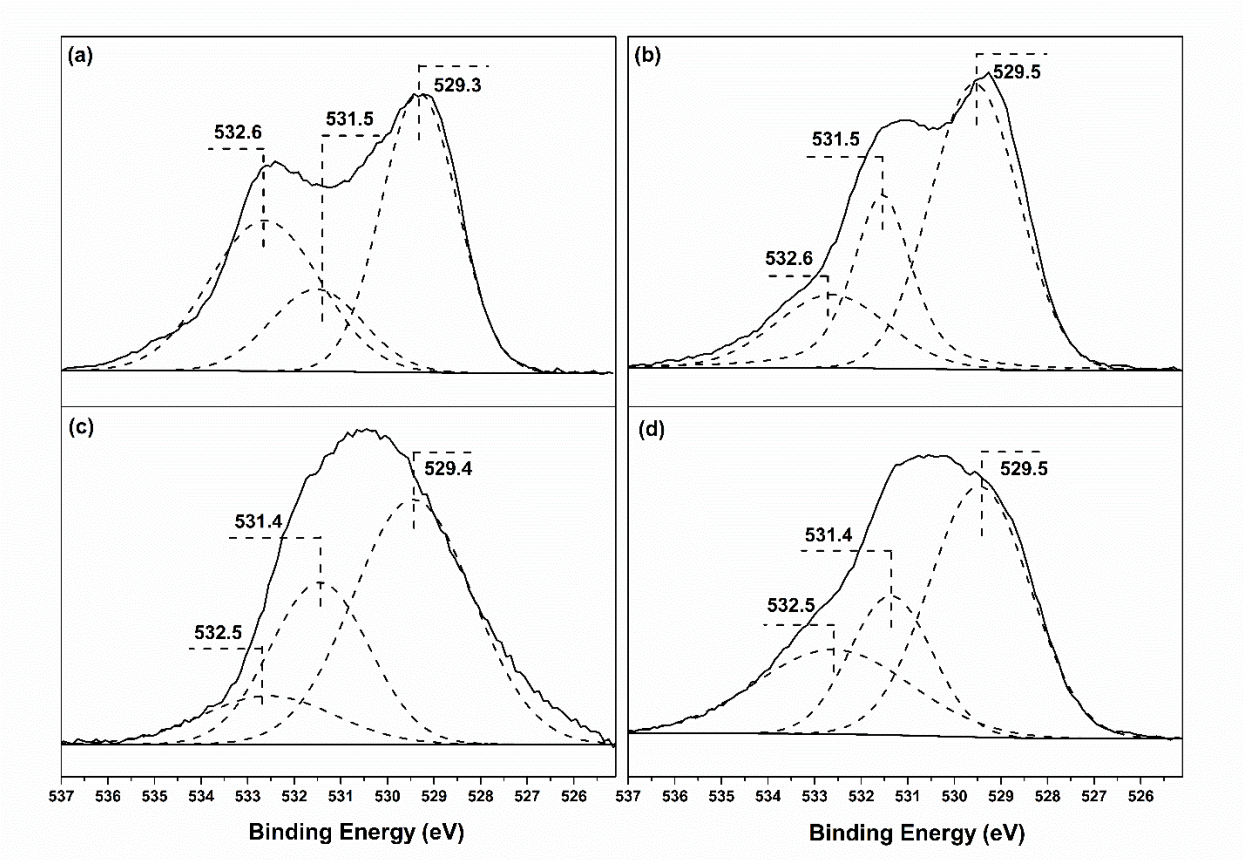

Figure 6.6 XPS O 1s spectra over (a) Cu-N-TiO_2 (A), (b) Cu-N-TiO_2 (R), (c) Cu-TiO_2 (A), and (d) Cu-TiO_2 (R).

Not only the copper species, but also oxygen species were existed on the surface and could affect the reaction. In order to study the surface oxygen species, the XPS O 1s spectra were recorded and shown in Figure 6.6. The deconvolution analysis of O 1s spectra revealed three different types of oxygen species, namely, lattice oxygen ($[O]_{latt}$) in TiO_2 represented by peaks at 529.3 - 529.4 eV, surface active oxygen ($[O]_{surf}$) identified by peaks at 531.5 eV and adsorbed oxygen species ($[O]_{ads}$) at 532.6 eV [137]. Regarding the $[O]_{surf}$, it is well known that the high $[O]_{surf}$ concentration is beneficial for the activity of catalytic oxidation [18]. So, the ratio of $[O]_{surf}$ / ($[O]_{latt}$ + $[O]_{surf}$ + $[O]_{ads}$) was calculated to compare the abundance of $[O]_{surf}$ on each catalyst. The ratio for Cu-N-TiO_2 (A) and Cu-N-TiO_2 (R) are 16.7 % and 27.18 %. However, Cu-TiO_2 (A) has

30.8 % of $[O]_{surf}$, which is greater than Cu-TiO_2 (R) (25.6 %). The comparison between Cu-N-TiO_2 (A) and Cu-TiO_2 (A) catalysts indicated the introduction of nitrogen decreased the surface oxygen species on anatase TiO_2. Whereas the amount of $[O]_{surf}$ slightly increased for rutile TiO_2 after nitrogen doping. These results seem on the contrary to our light-off results, because Cu-N-TiO_2 (A) carried the least amount of $[O]_{surf}$ and presented the best catalytic performance. Accordingly, both Cu^+ and surface oxygen species should be taken into consideration when evaluating the catalytic CO conversion.

6.3.3 REDOX PROPORTIES

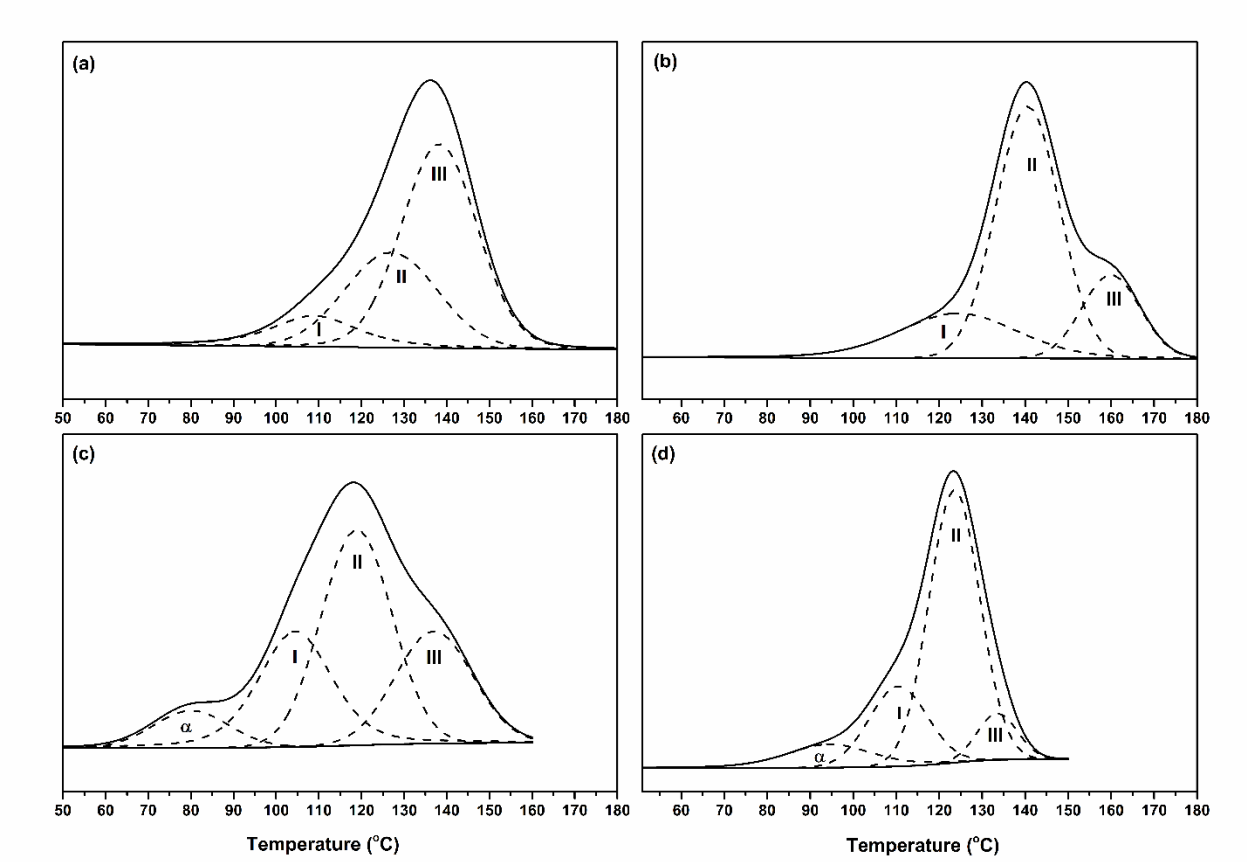

Figure 6.7 H_2-TPR profiles of (a) Cu-TiO_2 (A), (b) Cu-TiO_2 (R), (c) Cu-N-TiO_2 (A), and (d) Cu-N-TiO_2 (R).

Table 6.2 H_2-TPR deconvolution analysis and H_2 consumption results.

Sample	Peak α		Peak I		Peak II		Peak III	
	T (°C)	H_2 Consumption (μmol/g) (%)	T (°C)	H_2 Consumption (μmol/g) (%)	T (°C)	H_2 Consumption (μmol/g) (%)	T (°C)	H_2 Consumption (μmol/g) (%)
Cu-N-TiO_2 (A)	80	185.8 (12.1)	104	549.0 (35.7)	119	672.3 (43.7)	137	132.7 (8.5)
Cu-N-TiO_2 (R)	94	136.6 (10.3)	113	272.4 (20.6)	124	816.2 (60.8)	133	109.3 (8.3)
Cu-TiO_2 (A)	--	--	108	171.2 (12.0)	126	443.9 (31.2)	136	808.1 (56.8)
Cu-TiO_2 (R)	--	--	124	336.7 (27.2)	141	620.0 (50.1)	160	280.5 (22.7)

Hydrogen-Temperature Programmed Reduction (H_2-TPR) was applied to study the surface redox properties. As shown in Figure 6.7 (a) and (b), the reduction process started at around 80 °C and completed around 180 °C for Cu-TiO_2 catalysts. Three reduction peaks were observed from deconvolution results, regardless of the phases of TiO_2 support. The reduction of pure copper (II) oxide and copper (I) oxide usually occurred in a higher temperature range. When copper oxides supported on titanium dioxide, the interaction between copper oxides and titanium dioxide support would contribute to the reduction occurred in much lower temperature range. Peak I and Peak II were assigned to step reduction ($Cu^{2+} \rightarrow Cu^{+} \rightarrow Cu^{0}$) of copper (II) oxides. Peak III could be assigned to the reduction of crystalline CuO or copper species that has strong interaction with the support [132]. Regarding the Cu-N-TiO_2 (A) and Cu-N-TiO_2 (R) catalysts, additional Peak α was detected, which is unique for Cu-N-TiO_2 catalysts. This is related to highly dispersed copper species on the surface [22]. Therefore, nitrogen modification facilitated copper dispersion.

The hydrogen consumption in each step was calculated and presented in Table 6.2. Cu-N-TiO_2 (A) consumed 1539.8 μmol hydrogen per gram catalyst, which is 13.3 % higher than Cu-N-TiO_2 (R). Moreover, Cu-N-TiO_2 (R) presented more hydrogen consumption at a higher temperature range. 70 % hydrogen consumption of Cu-N-TiO_2 (R) resulted from higher temperatures (higher than 120 ^oC). It could help to understand why Cu-N-TiO_2 (A) had better catalytic performance in low temperature range. For the catalysts without nitrogen, the results indicated that hydrogen consumption increased from 1237.2 μmol/g over Cu-TiO_2 (R) to 1423.2 μmol/g over Cu-TiO_2 (A). The majority of hydrogen consumption over Cu-TiO_2 (R) occurred at high temperature. With more low temperature related hydrogen consumption over Cu-N-TiO_2 (A) and Cu-TiO_2 (A), it suggested the anatase TiO_2 would accelerate CO conversion, which is in line with light-off and XPS results.

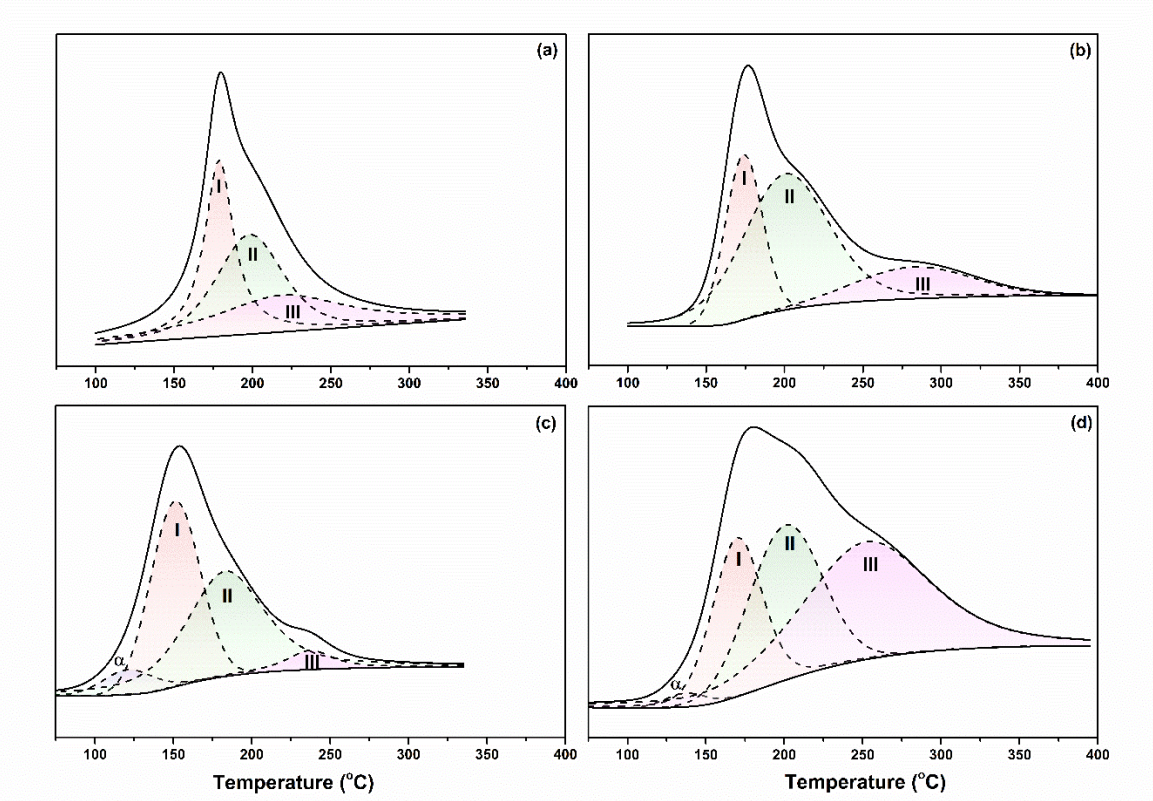

Figure 6.8 CO-TPSR profiles of (a) Cu-TiO_2 (A), (b) Cu-TiO_2 (R), (c) Cu-N-TiO_2 (A), and (d) Cu-N-TiO_2 (R).

When we applied H_2-TPR to study different copper species on the surface, each type of copper species would be stabilized by the interaction between copper and surface oxygen species. Therefore, we applied the CO-TPSR to study the types and concentrations of surface oxygen species by monitoring the formation of carbon dioxide from Cu-TiO_2 and Cu-N-TiO_2 catalysts. Similar to what we observe in H_2-TPR, the occurrences of three peaks over Cu-TiO_2 catalysts and four peaks over Cu-N-TiO_2 catalysts were identified and shown in Figure 6.8. Peak α that was located at low temperature, was detected on Cu-N-TiO_2 (A) and Cu-N-TiO_2 (R). Peak α was crucial to the high activity of nitrogen modified catalysts in contrast with the non-nitrogen catalysts in the low temperature range. This is because the low temperature oxygen species are easier to be activated during the reaction. CO-TPSR results agreed with the H_2-TPR results that nitrogen modification was able to promote the reaction. In the meantime, there is 6.1 % of overall CO consumption over Cu-N-TiO_2 (A) was attributed to the peak α, which was higher than 1.4 % CO consumption on Cu-N-TiO_2 (R) catalyst. Clearly, anatase TiO_2 supports were able to provide more active species on the surface, which eventually facilitated the CO conversion.

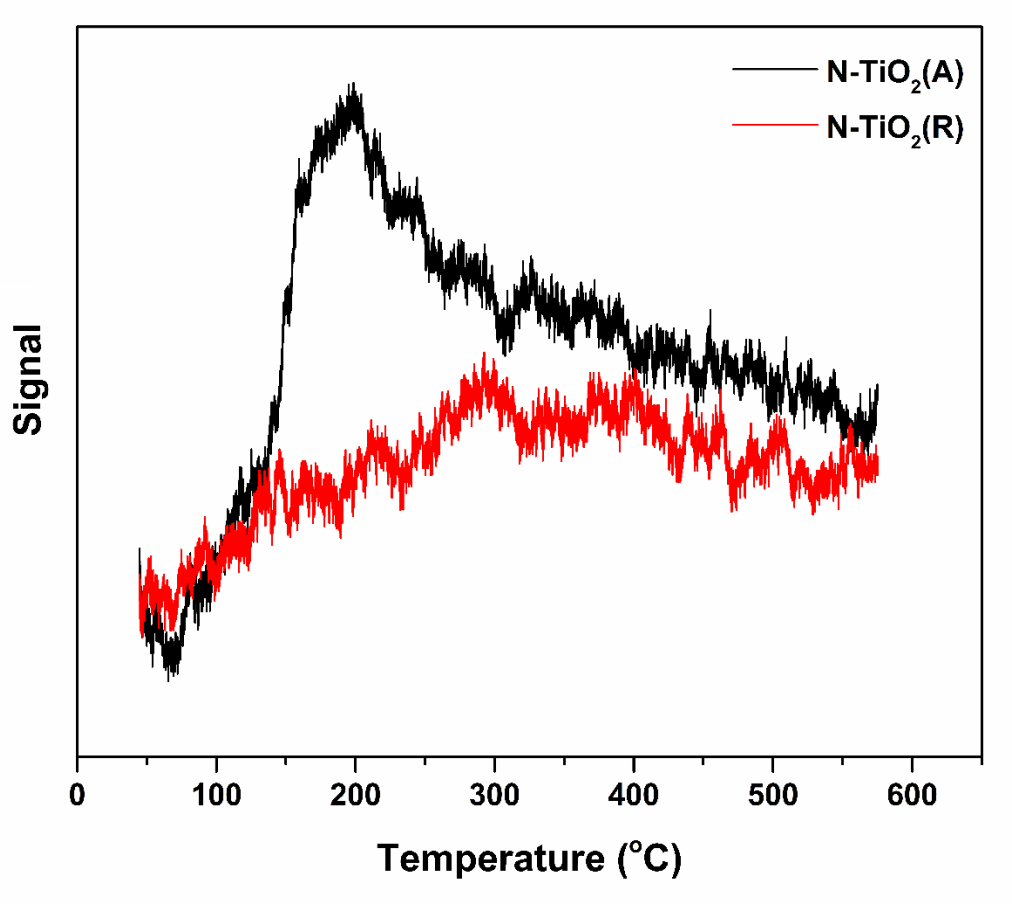

Figure 6.9 O_2-TPR profiles of N-TiO_2 supports.

The addition of nitrogen could affect the structure of titanium dioxides. This change would result in the formation of oxygen vacancies on the surface. The oxygen-temperature programmed reaction (O_2-TPR) experiment was performed on the supports to identify the ability to consume oxygen. The oxygen consumption could be attributed to the oxidation of Ti^{3+} species and oxygen vacancies. Figure 6.9 compared the O_2-TPR profiles of N-TiO_2 supports. A distinct peak located at 200 ^oC was obtained on N-TiO_2 (A), while it was not recorded on N-TiO_2 (R). Additionally, the oxygen consumption over N-TiO_2 (A) was two times higher than that of the N-TiO_2 (R). This indicated the presence of more Ti^{3+} and oxygen vacancies on N-TiO_2 (A), which is consistent with

the XPS and Raman spectra results. It could explain why Cu-N-TiO_2 (A) demonstrated better activity performance.

6.3.4 IN-SITU DRIFTS

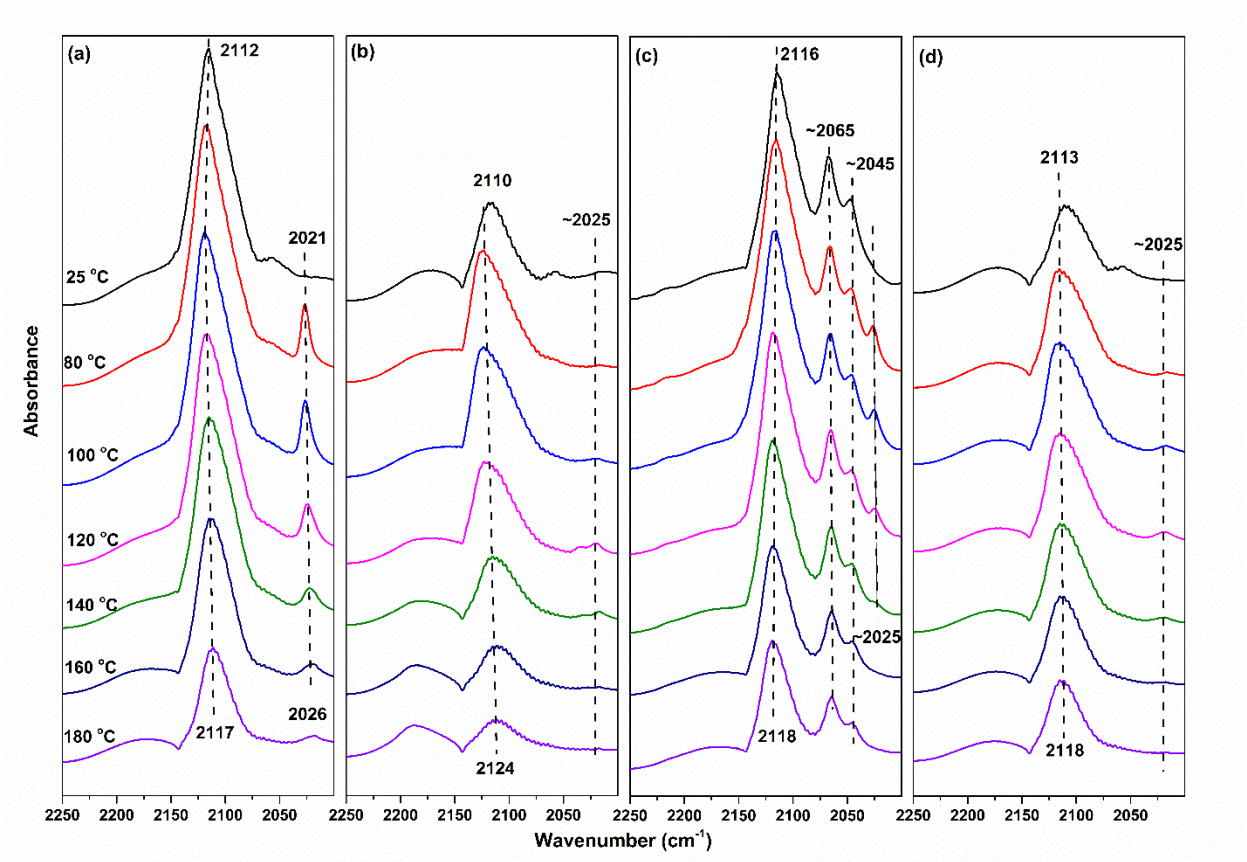

Figure 6.10 In-situ DRIFTS profiles over copper-based catalysts: (a) Cu-TiO_2 (A), (b) Cu-TiO_2 (R), (c) Cu-N-TiO_2 (A), and (d) Cu-N-TiO_2 (R), Test condition: 10% CO, balanced in Helium.

CO adsorption was recorded via in-situ DRIFTS and shown in Figure 6.10 to study the effects of support on copper species. It allowed us to identify the oxidation state of copper species. For all Cu-TiO_2 and Cu-N-TiO_2 catalysts, the band around 2110 cm^{-1} confirmed the existence of Cu^+ [140]. The peaks of CO adsorption confirmed the presence of Cu^+ on the surface, which matched with the XPS profile. The intensity of this band is much stronger on anatase TiO_2 supported catalysts. This is because more amount of Cu^+ was identified by XPS over anatase TiO_2 catalysts.

It could also be interpreted as less amount of O_{surf} on the surface gave more space for CO to adsorb. For anatase TiO_2 samples, the band around 2025 cm^{-1} was observed. This band could be assigned to the Cu^0-CO. As the temperature increased, this peak decreased until its disappearance because CO was reacted with surface oxygen species. Two bands around 2063 cm^{-1} and 2045 cm^{-1} were exclusively presented on Cu-N-TiO_2 (A). They might be assigned to the CO adsorbed on Cu^0, while these bands were not recorded on Cu-TiO_2 (A). Therefore, they could be attributed to the structure characteristic bands only presented on N-TiO_2 (A).

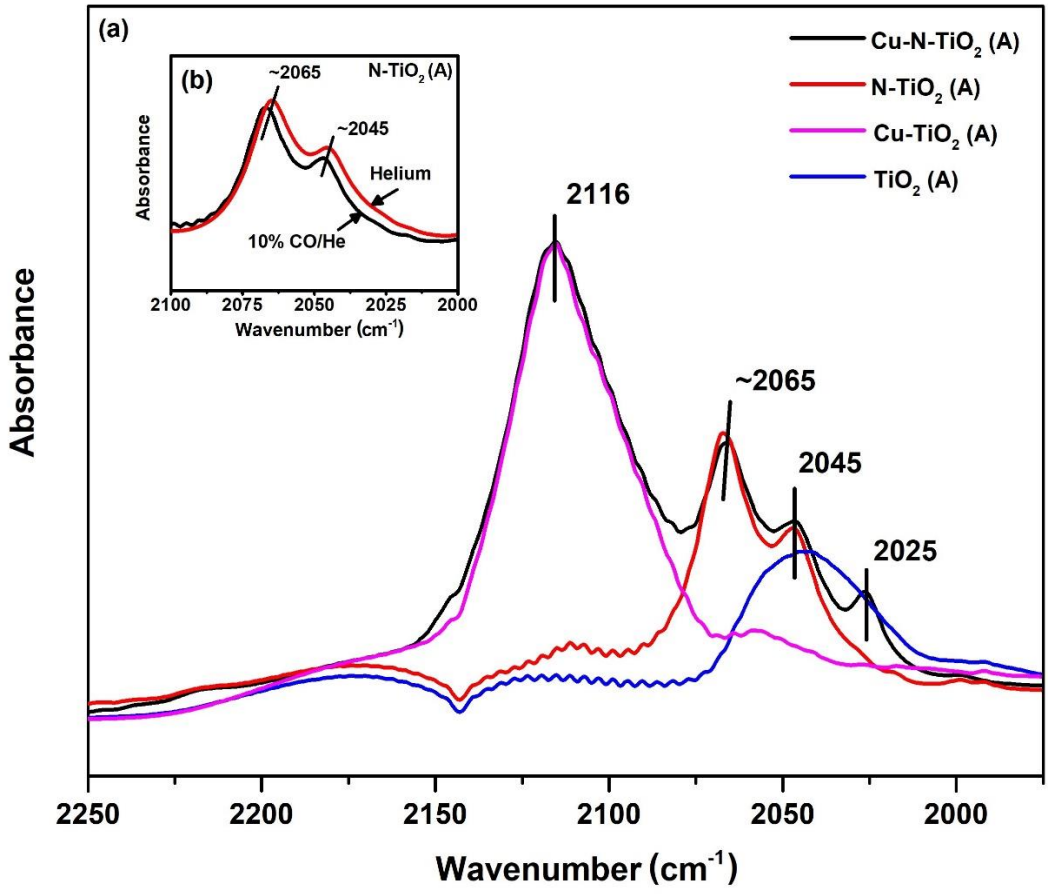

Figure 6.11 (a) In-situ DRIFTS profiles of anatase TiO_2 based supports and catalysts. Test condition: 10% CO, balanced in Helium; (b) In-situ DRIFTS profiles of N-TiO_2 (A) tested in different conditions, Test condition: pure Helium and 10% CO, balanced in Helium.

In order to understand those two bands, which located at 2045 cm^{-1} and 2063 cm^{-1} on Cu-N-TiO_2 (A) catalyst, the same mixture gases were applied to investigate the CO adsorption behavior on the anatase supports. The comparison of anatase TiO_2 based supports and catalysts were recorded and shown in Figure 6.11 (a). Based on the results, the bands located at 2045 cm^{-1} and 2063 cm^{-1} bands were also recorded on N-TiO_2 (A) support. This suggested that both bands could be related to the N-TiO_2 (A) support itself. Furthermore, pure Helium was employed instead of 10 % CO/Helium to study if previous mentioned two bands are correlated to CO adsorption on the surface. As shown in Figure 6.11 (b), similar bands location and intensity were recorded under both pure Helium and 10 % CO/Helium conditions. The results suggested that the bands at 2045 cm^{-1} and 2063 cm^{-1} came from the N-TiO_2(A) support, they were not correlated to CO adsorption.

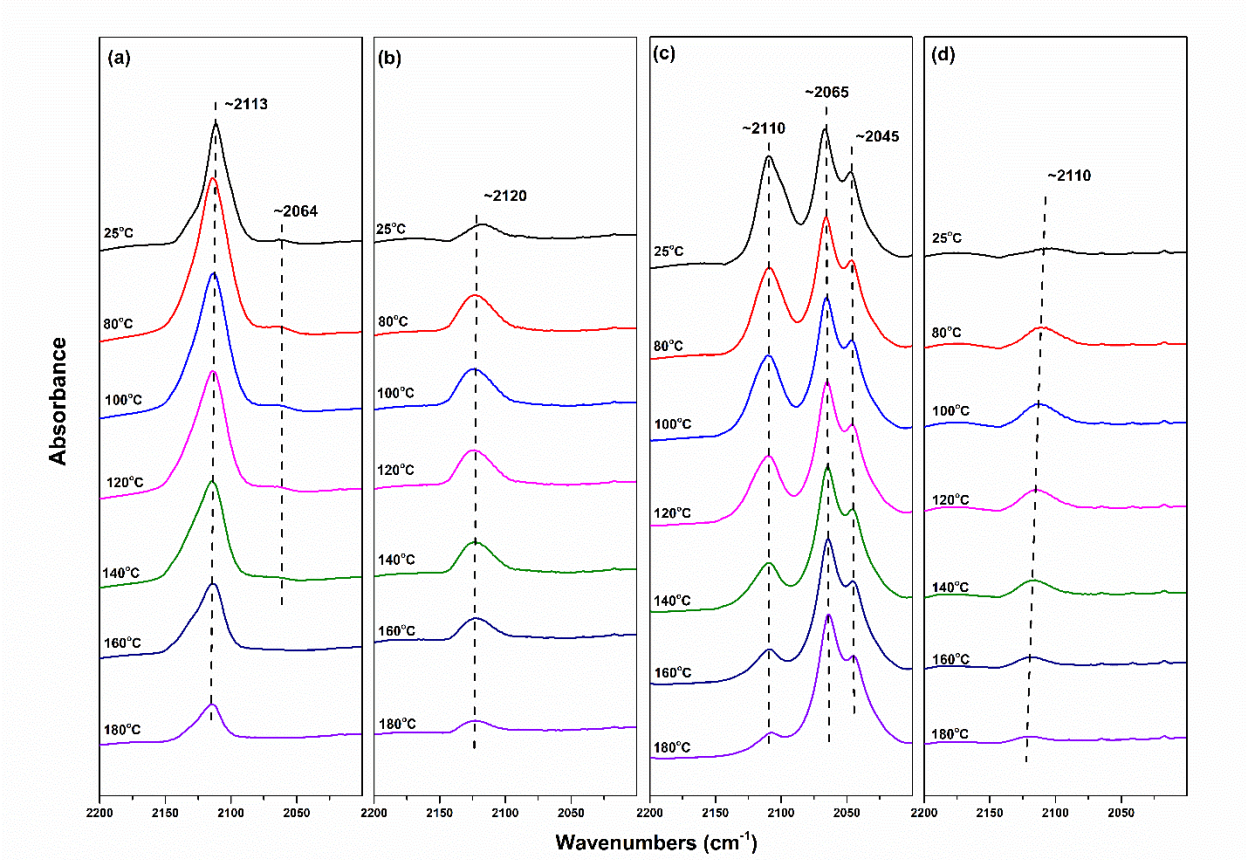

Figure 6.12 In-situ DRIFTS profiles of: (a) Cu-TiO_2 (A), (b) Cu-TiO_2 (R), (c) Cu-N-TiO_2 (A), and (d) Cu-N-TiO_2 (R) Test condition: 1% CO, 20% O_2 balanced in Helium.

To monitor how the surface species interacted with reactant gases, we carried out in-situ DRIFTS study of CO and O_2 co-adsorption, as shown in Figure 6.12. The in-situ DRIFTS was recorded with the temperature range between 25 ^oC and 180 ^oC. Similar to Figure 6.10, the band around 2110 cm^{-1} was attributed to Cu^+-CO band. However, the peak intensity at 2110 cm^{-1} was weaker than the intensity of the same peak in Figure 6.10. It is because of the lower concentration of CO that was used as the reactant gas. In addition, it was also possibly caused by the O_2 molecules that adsorbed on the surface and occupied oxygen vacancies. Furthermore, the CO adsorption was blocked [133]. With the increase of temperature, the intensity of Cu^+-CO raised up to the maximum at 100 ^oC and then started to decrease. At 180^oC, the intensity of peak at 2110 cm^{-1} of Cu-N-TiO_2

(A) is weaker than that of Cu-N-TiO_2 (R), indicating more CO had been reacted with O_2. This agreed with light-off results that Cu-N-TiO_2 (A) had better activity than Cu-N-TiO_2 (R).

6.4 SUMMARY

To evaluate the effect of TiO_2 phases on the CO oxidation reaction, it is critical to understand how the phases impact the surface properties of as-designed catalysts. This would eventually be beneficial for getting a deep insight into the property-activity relationship.

To exclude the interference factors toward the comparison of surface properties, all catalysts were pre-treated at 200 ^oC with Helium to remove all moisture and other volatile impurities. In this way, only surface oxygen species and copper species remained, which offered access to investigate how the phases of TiO_2 affect surface properties and catalytic performance. Raman spectroscopy suggested that copper oxides were highly dispersed on the surface, and more oxygen vacancies were obtained on the surface of N-TiO_2 (A) support. Unique substitutional nitrogen was identified in anatase TiO_2 support, which suggested that nitrogen atoms replaced the oxygen atoms and created oxygen vacancies. The XPS results revealed the presence of copper (II) and copper (I) species on all Cu-TiO_2 and Cu-N-TiO_2 catalysts. The supports extensively influenced the concentration of different types of copper species. Cu-N-TiO_2 (A) presented 28.9 % of copper (I) while Cu-N-TiO_2 (R) contained 17.6 % copper(I). Clearly, N-TiO_2 (A) facilitated the formation of copper (I) species in the synthesis process. In addition, surface oxygen species are beneficial for the catalytic oxidation and are the most abundant species on the surface along with copper species. XPS results demonstrated that the $[O]_{surf}$ concentration for Cu-N-TiO_2 (A) and Cu-N-TiO_2 (R) are 16.7 % and 27.18 %, respectively. This is in contrast with the light-off results. Therefore, it is essential to consider the balance between surface oxygen species and copper (I) species to interpret the surface property and catalytic performance relationship. To properly illustrate the relation

between copper (I) and surface oxygen species, the ratio between them was defined as $[Cu^{+}]/[O]_{surf}$. The values were 1.73 and 0.83 for Cu-N-TiO_2 (A) and Cu-N-TiO_2 (R), respectively. This ratio of Cu-TiO_2 (A) and Cu-TiO_2 (R) were 1.22 and 0.73. The $[Cu^{+}]/[O]_{surf}$ ratio values are in great agreement with the light-off and reaction rate.

In brief, the promotion effect of anatase phase TiO_2 on CO oxidation over copper and nitrogen modified TiO_2 catalysts was illustrated. Enhanced catalytic performance could be attributed to the improved copper dispersion and generated oxygen vacancies, which could stabilize copper species and activate O_2 to join the reaction. A ratio of $[Cu^{+}]/[O]_{surf}$ was put forward to declare the surface property-activity relationship.

CHAPTER 7

CONCLUSIONS AND PERSPECTIVES

7.1 CONCLUSIONS

Copper titanium dioxide (Cu-TiO_2) catalysts are robust and efficient for a variety of chemical production processes. Because of low cost and comparable activity to precious metal-based catalysts, Cu-TiO_2 has been studied for carbon monoxide oxidation. This dissertation focused on the development of four different strategies to tune the surface properties and built the property-activity relationship while considering the spectator species. Tuning the surface concentration of hydroxyl group, the effect of pretreatment and the addition of nitrogen were used to study P25 TiO_2. The phase effect from different TiO_2 phase (anatase vs. rutile) was applied to further study the promotion effect from the addition of nitrogen. The combination of the oxidation state of copper and surface oxygen species is considered a reliable approach to balance the active and spectator species on the surface. Most importantly, the reaction rate in CO oxidation is correlated with the value of $[Cu^{+}]/[O]_{surf}$.

Cu-TiO_2 catalysts presenting varies amounts of hydroxyl groups were synthesized through a unique one-step impregnation method without further calcination. Cu-TiO_2-pH7 catalyst prevailed Cu-TiO_2-pH14 in terms of reaction rate for CO oxidation. Catalysts characterization results demonstrated the improved copper dispersion, while less amount of Cu (I) species was presented on the surface of Cu-TiO_2-pH7. However, surface Cu (I) species have been proposed as the active species toward CO oxidation. It is reasonable to consider the surroundings next to Cu (I) species and include other species to interpret the property-activity relationship. Therefore, we calculated the ratio between Cu (I) species and hydroxyl groups, which was proved to correlate well with the

activity performance. Our results suggested that the activity can not only be determined by the surface abundance of copper (I) species but also the ratio between copper (I) and surface hydroxyl groups needs to be tuned for optimized CO conversion.

To investigate the effect of pretreatment conditions, Cu-TiO_2 catalysts were prepared through the same impregnation method with further calcination in reductive, oxidative, and inert gases. Activation energy and characterization results indicated pre-reduced Cu-TiO_2-H_2 promoted the CO oxidation compared with other pretreatments, facilitated the reduction of copper to form more Cu (I) species on Cu-TiO_2-H_2. Additionally, pre-oxidized Cu-TiO_2-O_2 exhibited the worst catalytic performance and presented fewer Cu (I) species along with more surface oxygen species than Cu-TiO_2-H_2. Therefore, the ratio between Cu (I) species and surface oxygen species was defined as $[Cu^+]/[O]_{surf}$ and applied to evaluate the combined action.

Cu-N-TiO_2 catalyst was prepared to study the effect of nitrogen on the surface properties and CO oxidation reaction. Urea and TiO_2 were used as precursors to synthesize N-TiO_2 support. Copper was loaded via same impregnation method without further calcination. The improvement of reaction rate in terms of TOF and activation energy were obtained over the Cu-N-TiO_2 catalyst. The characterization results indicated a similar amount of Cu (I) species on both Cu-N-TiO_2 and Cu-TiO_2 catalysts, while improved copper dispersion on Cu-N-TiO_2. Both interstitial and substitutional nitrogen are observed on the surface, and the interstitial nitrogen is the dominant nitrogen species. The introduced nitrogen promoted the N-TiO_2 support to generate oxygen vacancies, reduce the adsorption of surface oxygen species, and therefore increase the ratio of ($[Cu^+]/[O]_{surf}$).

Cu-N-TiO_2 catalysts were synthesized with different phases of TiO_2 (anatase and rutile) to understand the impact of TiO_2 phases on the surface properties and catalytic performance. Cu-N-

TiO_2 (A) presented a 37.5 % lower activation energy and a two times higher reaction rate than Cu-N-TiO_2 (R). Characterization results revealed the presence of highly dispersed copper species and oxygen vacancies on Cu-N-TiO_2 (A). Unique substitutional nitrogen was identified in anatase TiO_2 support. The substitutional nitrogen was suggested to replace the oxygen atoms, therefore resulted in the increase of oxygen vacancies. Abundance of Cu (I) species and lack of oxygen species were obtained on Cu-N-TiO_2 (A) attribute to the presence of Ti^{3+} and oxygen vacancies in the N-TiO_2 (A) supports.

7.2 PERSPECTIVES

Kinetic studies, especially microkinetic study, would clarify the role of copper and supports in CO oxidation. Systematic IR studies and collaborated DFT calculation would be applied for the future efforts to improve understandings on reaction mechanism.

The strong metal support interaction (SMSI) plays a vital role to increase the activity and selectivity in heterogeneous catalysis. Meanwhile temperature controls the occurrence of metal-oxide support. It is important to understand the structural evolution of our Cu-TiO_2 catalysts under in-situ conditions. X-ray absorption near edge structure (XANES) and near ambient pressure X-ray photoelectron spectroscopy (NAP-XPS) would be implemented to future studies.

This dissertation mainly focused on using urea as the nitrogen sources to synthesize N-TiO_2 catalysts. Meanwhile, the surface nitrogen concentration was around 1.0 wt %. Given there are other nitrogen sources available, it is worthy to investigate if other nitrogen sources would make it possible to increase the nitrogen concentration. Therefore, the reaction rate in CO oxidation would be further improved.

The essential of non-metal modified titanium dioxide is the increase of oxygen vacancies on the surface. Given hydrogen and boron modified titanium dioxide has been extensively studied for

photocatalysis, it is useful to investigate the applications of hydrogen and boron modified TiO_2 as supports to improve copper dispersion.

Single atom catalysts have been proved to an efficient approach to reduce metal usage and improve catalytic performance in heterogenous catalysis. Future studies would focus on the development of copper single-atom catalyst. When the goals of comparable activity and stability are achieved, it is expected to further increase of benefits of using copper based catalysts for CO oxidation.

LIST OF REFERENCES

[1] E. L. Muetterties, and J. Stein, *Chem. Rev.*, 1979, 79, 479-490.

[2] X. Xie, Y. Li, Z. Q. Liu, M. Haruta, and W. Shen, *Nature*, 2009, 458, 746-749.

[3] H. J. Freund, G. Meijer, M. Scheffler, R. Schlögl, and M. Wolf, *Angew. Chem. Int. Edit.*, 2011, 50, 10064-10094.

[4] F. Cai, S. Shan, L. Yang, B. Chen, J. Luo, and C.J. Zhong, *Sci. China Chem.*, 2015, 58, 14-28.

[5] N. Drenchev, E. Ivanova, M. Mihaylov, and K. Hadjiivanov, *Phys. Chem. Chem. Phys.*, 2010, 12, 6423-6427.

[6] B. Qiao, A. Wang, X. Yang, L. F. Allard, Z. Jiang, Y. Cui, J. Liu, J. Li, and T. Zhang, *Nat. Chem.*, 2011, 3, 634.

[7] G. M. Lari, E. Nowicka, D. J. Morgan, S. A. Kondrat, and G. J. Hutchings, *Phys. Chem. Chem. Phys.*, 2015, 17, 23236-23244.

[8] G. Turnes Palomino, P. Fisicaro, S. Bordiga, A. Zecchina, E. Giamello, and C. Lamberti, *J. Phys. Chem. B*, 2000, 104, 4064-4073

[9] B. Seyfi, M. Baghalha, and H. Kazemian, *Chem. Eng. J.*, 2009, 148, 306-311

[10] M. Ozawa, *J. Alloys Compd.*, 2006, 408-412, 1090-1095.

[11] L. Nie, D. Mei, H. Xiong, B. Peng, Z. Ren, X. I. P. Hernandez, A. DeLaRiva, M. Wang, M. H. Engelhard, L. Kovarik, and A. K. Datye, *Science*, 2017, 358, 1419-1423.

[12] V. Ulrich, C. Froese, B. Moroz, P. Pyrjaev, E. Gerasimov, I. Sinev, B. R. Cuenya, M. Muhler, V. Bukhtiyarov, and W. Grünert, *Appl. Catal. B*, 2018, 237, 1021-1032.

[13] A.J. Appleby, F.R. Foulkes, *Fuel Cell Handbook*, Van Nostrand Reinhold, New York, 1989.

[14] W. Vielstich, T. Iwasita, in: G. Ertl, H. Knözinger, J. Weitkamp, *Handbook of Heterogeneous Catalysis*, Weinheim, 1997.

[15] A. Wootsch, C. Descorme, and D. Duprez, *J. Catal.*, 2004, 225, 259-266.

[16] R. A. Lemons, *J. Power Sources*, 1990, 29, 251-264.

[17] L. Cao, W. Liu, Q. Luo, R. Yin, B. Wang, J. Weissenrieder, M. Soldemo, H. Yan, Y. Lin, Z. Sun, and C. Ma, *Nature*, 2019, 565, 631-635.

[18] J. Lu, J. Wang, Q. Zou, D. He, L. Zhang, Z. Xu, S. He, and Y. Luo, *ACS Catal.*, 2019, 9, 3, 2177-2195.

[19] F. Jiao, J. Li, X. Pan, J. Xiao, H. Li, H. Ma, M. Wei, Y. Pan, Z. Zhou, M. Li, S. Miao, J. Li, Y. Zhu, D. Xiao, T. He, J. Yang, F. Qi, Q. Fu, and X. Bao, *Science*, 2016, 351, 1065-1068.

[20] Q. Fu, H. Saltsburg, and M. Flytzani-Stephanopoulos, *Science*, 2003, 301, 935-938.

[21] X. P. Fu, L. W. Guo, W. W. Wang, C. Ma, C. J. Jia, K. Wu, R. Si, L. D. Sun, and C. H. Yan, *J. Am. Chem. Soc.*, 2019, 141, 4613-4623.

[22] F. Studt, F. Abild-Pedersen, Q. Wu, A. D. Jensen, B. Temel, J. D. Grunwaldt, and J. K. Nørskov, *J Catal.*, 2012, 293, 51-60.

[23] B. L. M. Hendriksen, and J. W. M. Frenken, *Phys. Rev. Lett.*, 2002, 89, 046101.

[24] R. M. Al Soubaihi, K. M. Saoud, and J. Dutta, *Catalysts*, 2018, 8, 660.

[25] Y. Y. Yeo, L. Vattuone, and D. A. King, *J. Chem. Phys.*, 1997, 106, 392-401.

[26] M. D. Ackermann, T. M. Pedersen, B. L. M. Hendriksen, O. Robach, S. C. Bobaru, I. Popa, C. Quiros, H. Kim, B. Hammer, S. Ferrer, and J. W. M. Frenken, *Phys. Rev. Lett.*, 2005, 95, 255505.

[27] L. Grabow, Y. Xu, and M. Mavrikakis, *Phys. Chem. Chem. Phys.*, 2006, 8, 3369-3374.

[28] A. von Oertzen, A. S. Mikhailov, H. H. Rotermund, and G. Ertl, *J. Phys. Chem. B*, 1998, 102, 4966-4981.

[29] P. J. Berlowitz, C. H. Peden, and D. W. Goodman, *J. Phys. Chem.*, 1988, 92, 18, 5213-5221.

[30] A. D. Logan, and M. T. Paffett, *J. Catal.*, 1992, 133, 179-190.

[31] J. Szanyi, and D. W. Goodman, *J. Phys. Chem.*, 1994, 98, 11, 2972-2977.

[32] H. Uetsuka, K. Watanabe, H. Ohnuma, and K. Kunimori, *Surf. Sci.*, 1997, 377, 765-769.

[33] J. Szanyi, W. K. Kuhn, and D. W. Goodman, *J. Phys. Chem.*, 1994, 98, 11, 2978-2981.

[34] Y. Lian, W. Yang, C. Zhang, H. Sun, Z. Deng, W. Xu, L. Song, Z. Ouyang, Z. Wang, J. Guo, and Y. Peng, *Angew. Chem. Int. Ed.*, 2020, 59, 286-294.

[35] D. A. Outka, and R. J. Madix, *Surf. Sci.*, 1987, 179, 351-360.

[36] J. M. Gottfried, K. J. Schmidt, S. L. M. Schroeder, and K. Christmann, *Surf. Sci.*, 2003, 525, 197-206.

[37] B. K. Min, A. R. Alemozafar, D. Pinnaduwage, X. Deng, and C. M. Friend, *J. Phys. Chem. B*, 2006, 110, 19833-19838.

[38] J. Gong, R. A. Ojifinni, T. S. Kim, J. D. Stiehl, S. M. McClure, J. M. White, and C. B. Mullins, *Top. Catal.*, 2007, 44, 57-63.

[39] H. Y. Su, M. M. Yang, X. H. Bao, and W. X. Li, *J.Phys. Chem. C*, 2008, 112, 17303-17310.

[40] M. Bowker, M. A. Barteau, and R. J. Madix, *Surf. Sci.*, 1980, 92, 528-548.

[41] J. V. Barth, and T. Zambelli, *Surf. Sci.*, 2002, 513, 359-366.
[42] G. Yi, H. Yang, B. Li, H. Lin, K. I. Tanaka, and Y. Yuan, *Catal. Today*, 2010, 157, 83-88.

[43] T. Sueyoshi, T. Sasaki, and Y. Iwasawa, *Surf. Sci.*, 1995, 343, 1-16.

[44] B. Eren, C. Heine, H. Bluhm, G. A. Somorjai, and M. Salmeron, *J. Am. Chem. Soc.*, 2015, 137, 11186-11190.

[45] J. Szanyi, and D. W. Goodman, *Catal Lett.*, 1993, 21, 165-174.

[46] B.C. Gates, *Top. Catal.*, 2000, 14, 173-180.

[47] M. M. Schubert, S. Hackenberg, A. C. Van Veen, M. Muhler, V. Plzak, and R. J. Behm, *J. Catal.*, 2001, 197, 113-122.

[48] D. Andreeva, I. Ivanov, L. Ilieva, J. W. Sobczak, G. Avdeev, and K. Petrov, *Top. Catal.*, 2007, 44, 173-182.

[49] M. A. Centeno, T. Ramírez Reina, S. Ivanova, O. H. Laguna, and J. A. Odriozola, *Catalysts*, 2016, 6, 158.

[50] K. Oberlander, *Applied Industrial Catalysis*, Academic Press, New York, 1984.

[51] K. Wefers, *Alumina Chemicals: Science and Technology Hand-book*, The American Ceramic Society, Ohio, 1990.

[52] M. Trueba, and S. P. Trasatti, *Eur. J. Inorg. Chem.*, 2005, 17, 3393-3403

[53] R. H. Nibbelke, M. A. J. Campman, J. H. B. J. Hoebink, and G. B. Marin, *J. Catal.*, 1997, 171, 358-373.

[54] S. N. Pavlova, V. A. Sadykov, V.A. Razdobarov, and E. A. Paukshtis, *J. Catal.*, 1996, 161, 507-516.

[55] D. Widmann, Y. Liu, F. Schüth, and R. J. Behm, *J. Catal.*, 2010, 276, 292-305

[56] S. Soled, *Science*, 2015, 350, 1171-1172.

[57] D. J. Kaul, R. Sant, and E. E. Wolf, *Chem. Eng. Sci.*, 1987, 42, 1399-1411.

[58] J. L. Margitfalvi, I. Borbáth, M. Hegedűs, S. Gőbölös, and K. Lázár, *J. Catal.*, 2010, 196, 200-204.

[59] N. Almana, S. P. Phivilay, P. Laveille, M. N. Hedhili, P. Fornasiero, K. Takanabe, and J. M. Basset, *J. Catal.*, 2016, 340, 368-375.

[60] J. N. Park, A. J. Forman, W. Tang, J. Cheng, Y. S. Hu, H. Lin, and E. W. McFarland, *Small*, 2008, 4, 1694-1697.

[61] K. Qian, L. Luo, H. Bao, Q. Hua, Z. Jiang, and W. Huang, *Catal. Sci. Technol.*, 2013, 3, 679-687.

[62] S. A. Mock, S. E. Sharp, T. R. Stoner, M. J. Radetic, E. T. Zell, and R. Wang, *J. Colloid Interf. Sci.*, 2016, 466, 261-267.

[63] P. Bera, A. Gayen, M. S. Hegde, N. P. Lalla, L. Spadaro, F. Frusteri, and F. Arena, *J. Phys. Chem. B*, 2003, 107, 6122-6130.

[64] S. Zhang, X. S. Li, B. Chen, X. Zhu, C. Shi, and A. M. Zhu, *ACS Catal.*, 2014, 4, 3481-3489.

[65] H. H. Liu, Y. Wang, A. P. Jia, S. Y. Wang, M. F. Luo, and J. Q. Lu, *Appl. Surf. Sci.*, 2014, 314, 725-734.

[66] U. Oran, and D. Uner, *Appl. Catal. B*, 2004, 54, 183-191.

[67] E. M. Slavinskaya, R. V. Gulyaev, A. V. Zadesenets, O. A. Stonkus, V. I. Zaikovskii, Y. V. Shubin, S. V. Korenev, and A. I. Boronin, *Appl. Catal. B*, 2015, 166, 91-103.

[68] D. Widmann, R. Leppelt, and R. J. Behm, *J. Catal.*, 2007, 251, 437-442.

[69] Y. Ma, X. Wang, Y. Jia, X. Chen, H. Han, and C. Li, *Chem. Rev.*, 2014, 114, 9987-10043.

[70] M. Valden, S. Pak, X. Lai, and D. W. Goodman, *Catal. Lett.*, 1998, 56, 7-10.

[71] G. R. Bamwenda, S. Tsubota, T. Nakamura, and M. Haruta, *Catal. Lett.*, 1997, 44, 83-87.

[72] K. Taira, K. Nakao, K. Suzuki, and H. Einaga, *Environ. Sci. Technol.*, 2016, 50, 9773-9780.

[73] D. Widmann, and R. J. Behm, *Angew. Chem. Int. Ed.*, 2011, 50, 10241-10245.

[74] J. Li, G. Lu, G. Wu, D. Mao, Y. Guo, Y. Wang, and Y. Guo, *Catal. Sci. Technol.*, 2014, 4, 1268-1275.

[75] L. Di, D. Duan, X. Zhang, B. Qi, and Z. Zhan, *IEEE T. Plasma Sci.*, 2016, 44(11), 2692-2698.

[76] L. Liu, and A. Corma, *Chem. Rev.*, 2018, 118, 4981-5079.

[77] S.J. Tauster, S. C. Fung, and R. L. Garten, *J. Am. Chem. Soc.*, 1978, 100, 170-175.

[78] K. Tanabe, *Catal. Today*, 1990, 8, 1-11.

[79] C. J. Pan, M. C. Tsai, W. N. Su, J. Rick, N. G. Akalework, A. K. Agegnehu, S. Y. Cheng, and B. J. Hwang, *J. Taiwan Inst. Chem. E*, 2017, 74, 154-186.

[80] D. E. Resasco, R. S. Weber, S. Sakellson, M. McMillan, and G. L. Haller, *J. Phys. Chem.*, 1988, 92, 189-193.

[81] B. C. Beard, and P. N. Ross, *J. Phys. Chem.*, 1986, 90, 6811-6817.

[82] A. Sasahara, C. L. Pang, and H. Onishi, *J. Phys. Chem. B*, 2006, 110, 13453-13457.

[83] T. Ioannides, and X. E. Verykios, *J. Catal.*, 1996, 161, 560-569.

[84] O. Dulub, W. Hebenstreit, and U. Diebold, *Phys. Rev. Lett.*, 2000, 84, 3646.

[85] H. R. Sadeghi, and V. E. Henrich, *J. Catal.*, 1988, 109, 1-11.

[86] I. X. Green, W. Tang, M. Neurock, and J. T. Yates, *Science*, 2011, 333, 736-739.

[87] A. Prestianni, A. Martorana, F. Labat, I. Ciofini, and C. Adamo, *J. Mol. Struc. -THEOCHEM*, 2009, 903(1-3), pp.34-40.

[88] Z. P. Liu, P. Hu, and A. Alavi, *J. Am. Chem. Soc.*, 2002, 124, 14770-14779.

[89] S. T. Zhang, C. M. Li, H. Yan, M. Wei, D. G. Evans, and X. Duan, *J. Phys. Chem. C*, 2014, 118, 7, 3514-3522.

[90] G. Wu, N. Guan, and L. Li, *Catal. Sci. Technol.*, 2011, 1, 601-608.

[91] M. Ozawa, H. Toda, O. Kato, and S. Suzuki, *Appl. Catal. B*, 1996, 8, 123-140.

[92] W. E. Garner, F. S. Stone, and P. F. Tiley, *P. Roy. Soc. A-Math Phy.*, 1952, 211, 472-489.

[93] T. J. Jennings, F. S. Stone, *Adv. Catal*., 1957, 9, 441-451.

[94] B. White, M. Yin, A. Hall, D. Le, S. Stolbov, T. Rahman, N. Turro, and S. O'Brien, *Nano Lett.*, 2006, 6, 2095-2098.

[95] H. Wan, Z. Wang, J. Zhu, X. Li, B. Liu, F. Gao, L. Dong, and Y. Chen, *Appl. Catal. B*, 2008, 79, 254-261.

[96] T. J. Huang, and D. H. Tsai, *Catal. Lett.*, 2003, 87, 173-178.

[97] G.G. Jernigan and G.A. Somorjai, *J. Catal.*, 1994, 147, 567-577.

[98] C. S. Chen, J. H. You, J. H. Lin, and Y. Y. Chen, *Catal. Commun.*, 2008, 9, 2381-2385.

[99] M. F. Luo, J. M. Ma, J. Q. Lu, Y. P. Song, and Y. J. Wang, *J. Catal.*, 2007, 246, 52-59.

[100] W. Liu, and M. Flytzani-Stephanopoulos, *J. Catal*., 1995, 153, 304-316.

[101] W. Liu, and M. Flytzani-Stephanopoulos, *J. Catal.*, 1995,153, 317-332.

[102] S. A. Mock, E. T. Zell, S. T. Hossain, R. G. Wang, *ChemCatChem*, 2018, 10, 311-319.

[103] M. Lykaki, E. Pachatouridou, S. A. Carabineiro, E. Iliopoulou, C. Andriopoulou, N. Kallithrakas-Kontos, S. Boghosian, and M. Konsolakis, *Appl. Catal. B*, 2018, 230, 18-28.

[104] C. S. Chen, T. C. Chen, C. C. Chen, Y. T. Lai, J. H. You, T. M. Chou, C. H. Chen, and J. F. Lee, *Langmuir*, 2012, 28, 9996-10006.

[105] M. Y. Kang, H. J. Yun, S. Yu, W. Kim, N. D. Kim, and J. Yi, *J. Mol. Catal. A-Chem.*, 2013, 368, 72-77.

[106] H. Knözinger, and K. Kochloefl, *Heterogeneous Catalysis and Solid Catalysts in Ullmann's Encyclopedia of Industrial Chemistry*, Wiley-VCH, Weinheim, 2002.

[107] S. Albertin, 2017, '*Preparation, characterization and testing of model catalysts for CO oxidation and CO_2 hydrogenation'*, master's thesis, Lund University, Lund.

[108] W. M. Irvine, *Langmuir-Hinshelwood Mechanism. In: Gargaud M. et al. (eds) Encyclopedia of Astrobiology*. Springer, Berlin, Heidelberg, 2011.

[109] K. J. Laidler, and J. H. Meiser, *Physical Chemistry*, Benjamin/Cummings, 1982.

[110] W. M. Irvine, *Eley-Rideal Mechanism. In: Gargaud M. et al. (eds) Encyclopedia of Astrobiology*. Springer, Berlin, Heidelberg, 2011.

[111] M. E. Domagala, and C. T. Campbell, *Catal. Lett.*, 1991, 9, 65-70.

[112] K. I. Choi, and M. A. Vannice, *J. Catal.*, 1991, 131, 22-35.

[113] X. Liu, T. Duan, Y. Sui, C. Meng, and Y. Han, *RSC Adv.*, 2014, 4, 38750-38760.

[114] J. Q. Lu, C. X. Sun, N. Li, A. P. Jia, and M. F. Luo, *Appl. Surf. Sci.*, 2013, 287, 124-134.

[115] Y. Wang, G. Wu, M. Yang, and J. Wang, *J. Phys. Chem. C*, 2013, 117, 8767-8773.

[116] B. Z. Sun, W. K. Chen, and Y. J. Xu, *J. Chem. Phys.*, 2010, 133, 154502.

[117] S. PalDey, S. Gedevanishvili, W. Zhang,and F. Rasouli, *Appl. Catal. B*, 2005, 56, 241-250.

[118] M. Ojeda, B. Z. Zhan, and E. Iglesia, *J. Catal.*, 2012, 285, 92-102.

[119] P. Munnik, P. E. de Jongh, and K. P. de Jong, *Chem. Rev.*, 2015, 115, 6687-6718.

[120] B. A. Mehrabadi, S. Eskandari, U. Khan, R. D. White, and J. R. Regalbuto, *A review of preparation methods for supported metal catalysts. In Advances in Catalysis*. Academic Press, Cambridge, Massachusetts, 2017.

[121] T. Kida, T. Oka, M. Nagano, Y. Ishiwata, and X. G. Zheng, *J. Am. Ceram. Soc*, 2007, 90, 107-110.

[122] C. J. G. Van Der Grift, A. F. H. Wielers, B. P. J. Jogh, J. Van Beunum, M. De Boer, M. Versluijs-Helder, and J. W. Geus, *J. Catal.*, 1991, 131, 178-189.

[123] M. Boudart, *Chem. Rev.*, 1995, 95, 661-666.

[124] S. Kozuch, and J. M. Martin, *ACS Catal.*, 2012, 2, 2787-2794.

[125] G. G. Jernigan, and G. A. Somorjai, *J. Catal.*, 1994, 147, 567-577.

[126] S. Royer, and D. Duprez, *ChemCatChem*, 2011, 1, 24-65.

[127] G. J. Wu, N. J. Guan, and L. D. Li, *Catal. Sci. Technol.*, 2011, 1, 601-608.

[128] Z. L. Yan, H. M. Yang, J. Ouyang, and A. D. Tang, *Chem. Eng. J.*, 2017, 316, 1035-1046.

[129] L. Clarizia, D. Spasiano, I. D. Somma, R. Marotta, R. Andreozzi, and D. D. Dionysiou, *Int. J. Hydrogen Energy*, 2014, 39, 16812-16831.

[130] A. F. Zedan, N.K. Allam, and S. Y. AlQaradawi, *Catalysts*, 2017, 7, 129.

[131] D. A. Svintsitskiy, A. P. Chupakhin, E. M. Slavinskaya, O. A. Stonkus, A. I. Stadnichenko, S. V. Koscheev, and A. I. Boronin, *J. Mol. Catal. A*, 2013, 368, 95-106.

[132] D. Liu, Y. Fernandez, O. Ola, S. Mackintosh, M. Maroto-Valer, C.M.A. Parlett, A.F. Lee, and J. C.S. Wu, *Catal. Commun.*, 2012, 25, 78-82.

[133] L. H. Dong, Y. X. Tang, B. Li, L. Y. Zhou, F. Z. Gong, H. X. He, B. Z. Sun, C. J. Tang, F. Gao, and L. Dong, *Appl. Catal. B*, 2016, 180, 451-462.

[134] G. Avgouropoulos, T. Ioannides, and H. Matralis, *Appl. Catal. B*, 2005, 56, 87-93.

[135] D. N. Bui, S. Z. Kang, L. Qin, X. Q. Li, and J. Mu, *Appl. Surf. Sci.*, 2013, 266, 288-293.

[136] X. Yao, Q. Yu, Z. Ji, Y. Lv, Y. Cao, C. Tang, F. Gao, L. Dong, and Y. Chen, *Appl. Catal. B*, 2013, 130, 293-304.

[137] V. P. Santos, S. A. C. Carabineiro, J. J. W. Bakker, O. S. G. P. Soares, X. Chen, M. F. R. Pereira, J. J. M. Orfao, J. L. Figueiredo, J. Gascon, and F. Kapteijn, *J. Catal.*, 2014, 309, 58-65.

[138] L. Li, J. Yan, T. Wang, Z. Zhao, J. Zhang, J. Gong, and N. Guan, *Nat. Commun.*, 2015, 6, 5881.

[139] L. H. Dong, L. J. Liu, Y. Y. Lv, J. Zhu, H. Q. Wan, B. Liu, F. Gao, X. S. Wang, L. Dong, Y. Chen, *J. Mol. Catal. A*, 2012, 265, 87-94.

[140] S. D. Senanayake, N. A. Pappoe, T. D. Nguyen-Phan, S. Luo, Y. Y. Li, W. Q. Xu, Z. Y. Liu, K. Mudiyanselage, A. C. Johnston-Peck, A. L. FrenkeleI, I. Heckler, D. Stacchiola, and J. A. Rodriguez, *Surf. Sci.*, 2016, 652, 206-212.

[141] AM. Hernández-Giménez, D. Lozano-Castelló, and A. Bueno-López, *Appl. Catal. B*, 2014, 148, 406-414.

[142] Z. Liu, Z. Wu, X. Peng, A. Binder, S. Chai, and S. Dai, *J. Phys. Chem. C*, 2014, 118, 27870-27877.

[143] G. Li, L. Li, D. Jiang, Y. Li, and J. Shi, *Nanoscale*, 2015, 7, 5691-5698.

[144] A. Litke, Y. Su, I. Tranca, T. Weber, E. Hensen, and J. P. Hofmann, *J. Phys. Chem. C*, 2017, 121, 7514-7524.

[145] R. N. S. H. Magalhães, F. S. Toniolo, V. T. D. Silva, and M. Schmal, *Appl. Catal. A*, 2010, 388, 216-224.

[146] J. Y. Zheng, T-K Van, A. U. Pawar, C. W. Kim, and Y. S. Kang, *RSC Adv.*, 2014, 4, 18616-18620.

[147] S. S. Sun, D. S. Mao, J. Yu, Z. Q. Yang, G. Z. Lu, and Z. Ma, *Catal. Sci. Technol.*, 2015, 5, 3166-3181.

[148] M. Zhang, Z. Jin, J. Zhang, Z. Zhang, and H. Dang, *J. Mol. Catal. A-Chem.*, 2005, 225, 59-63.

[149] L. C. Wang, L. He, Y. M. Liu, Y. Cao, H. Y. He, K. N. Fan, and J. H. Zhuang, *J. Catal.*, 2009, 264, 145-153.

[150] R. Si, J. Raitano, N. Yi, L. Zhang, S. W. Chan, M. Flytzani-Stephanopoulos, *Catal. Today*, 2012, 180, 68-80.

[151] M. S. P. Francisco, V. R. Mastelaro, P. A. Nascente, and A. O. Florentino, *J. Phys. Chem. B*, 2001, 105, 43, 10515-10522.

[152] B. Y. Jia, L. Y. Duan, C. L. Ma, and C. M. Wang, *Chin. J. Chem.*, 2007, 25, 553-557.

[153] J. Lynch, C. Giannini, J. K. Cooper, A. Loiudice, I. D. Sharp, and R. Buonsanti, *J. Phys. Chem. C*, 2015, 119, 7443-7452.

[154] J. Gao, C. Jia, L. Zhang, H. Wang, Y. Yang, S. F. Hung, Y. Y. Hsu, and B. Liu, *J. Catal.*, 2016, 341, 82-90.

[155] X. Zou, S. Qi, J. Xu, Z. Suo, L. An, and F. Li, *J. Nat. Gas Chem.*, 2010, 19, 307-312.

[156] S. J. Tauster, S. C. Fung, R. L. Garten, *J. Am. Chem. Soc.*, 1978, 100, 170-175.

[157] J. Huang, S. Wang, Y. Zhao, X. Wang, S. Wang, S. Wu, S. Zhang, and W. Huang, *Catal. Commun.*, 2006, 7, 1029-1034.

[158] Y. Lin, S. Yang, Y. Liu, S. Zhang, H. Wang, H. Yu, and F. Peng, *Int. J. Hydrogen Energy*, 2017, 42, 19942-19950.

[159] G. Liu, H. G. Yang, J. Pan, Y. Q. Yang, G. Q. Lu, and H. M. Cheng, *Chem. Rev.*, 2014, 114, 9559-9612.

[160] R. Asahi, T. Morikawa, H. Irie, and T. Ohwaki, *Chem. Rev.*, 2014, 114, 9824-9852.

[161] S. G. Kumar, and L. G. Devi, *J. Phys. Chem. A*, 2011, 115, 13211-13241.

[162] G. Barolo, S. Livraghi, M. Chiesa, M. C. Paganini, and E. Giamello, *J. Phys. Chem. C*, 2012, 116, 20887-20894.

[163] Y. Sakatani, J.Nunoshige, H. Ando, K. Okusako, H. Koike, T. Takata, J. N. Kondo, M. Hara, and K. Domen, *Chem. Lett.*, 2003, 32, 1156-1157.

[164] O. Frank, M. Zukalova, B. Laskova, J. Kürti, J. Koltai, and L. Kavan, *Phys. Chem. Chem. Phys.*, 2012, 14, 14567-14572.

[165] C. Feng, Y. Wang, J. Zhang, L. Yu, D. Li, J. Yang, and Z. Zhang, *Appl. Catal. B*, 2012, 113, 61-71.

[166] J. Wang, D. N. Tafen, J. P. Lewis, Z. Hong, A. Manivannan, M. Zhi, M. Li, and N. Wu, *J. Am. Chem. Soc.*, 2009, 131, 12290-12297.

[167] S. A. Ansari, M. M. Khan, M. O. Ansari, M. H. Cho, *New J. Chem.*, 2016, 40, 3000-3009.

[168] D. Scarano, S. Boridga, C. Lamberti, G. Spoto, G. Ricchiardi, A. Zecchina, C. O. Arean, *Surf. Sci.*, 1998, 411, 272-285.

[169] C. Garlisi, J. Szlachetko, C. Aubry, D. L. Fernandes, Y. Hattori, C. Paun, M. V. Pavliuk, N. S. Rajput, E. Lewin, and J. Sá, G. Palmisano, *J. Catal.*, 2017, 353, 116-122.

[170] F. H. M. Dekker, M. C. Dekker, A. Bliek, F. Kapteijn, and J. A. Moulijn, *Catal. Today*, 1994, 20, 409-422.

[171] Y. Tang, L. Dong, C. Deng, M. Huang, B. Li, and H. Zhang, *Catal. Commun.*, 2016, 78, 33-36.

[172] R. Y. O. J. I. Asahi, T. A. K. E. S. H. I. Morikawa, T. Ohwaki, K. Aoki, and Y. Taga, *Science*, 2001, 293, 269-271.

[173] C. Di Valentin, G. Pacchioni, A. Selloni, S. Livraghi, and E. Giamello, *J. Phys. Chem. B*, 2005, 109, 11414-11419.

[174] E. Sutter, P. Sutter, E. Fujita, J. Muckerman, Abstracts of the European Materials Research Society Spring Meeting, Nice, France, 2006, p. M-14.

[175] C. Di Valentin, E. Finazzi, G. Pacchioni, A. Selloni, S. Livraghi, M. C. Paganini, and E. Giamello, *Chem. Phys.*, 2007, 339, 44-56.

[176] D. Li, H. Haneda, S. Hishita, and N. Ohashi, *N. Mater. Sci. Eng. B*, 2005, 117, 67-75.

[177] H. Hagemann, H. Bill, E. Walker, and M. François, *Solid State Commun.*, 1990, 73, 447-451.

[178] T. C. Lu, L. B. Lin, X. T. Zu, S. Zhu, L. M. Wang, *Nucl. Instrum. Methods Phys. Res. B*, 2004, 218, 111-116.

[179] Z. Zhang, X. Wang, J. Long, Q. Gu, Z. Ding, and X. Fu, *J. Catal.*, 276, 201-214.

[180] W. Yang, L. Li, Y. Fang, Y. Shan, J. Xu, H. Shen, Y. Yu, Y. Guo, and H. He, *Catal. Sci. Technol.*, 2020, 10, 1661-1674.